Measurements of inclusive and differential cross sections for the Higgs boson production and decay to four-leptons in proton-proton collisions at √s = 13 TeV at CMS

Qianying GUO

(Beihang University and Institute of High Energy Physics, Beijing)

On behalf of CMS Collaboration

The 9th China LHC Physics Workshop (CLHCP2023)

Overview

- **Fiducial cross section measurement** [JHEP08(2023)040] in $H \rightarrow ZZ^* \rightarrow 4l$ channel with 138fb^{-1} of Run II samples with latest objects calibration
- Extend the measurement with respect to the previous Run II analysis [EPJC81(2021)488]
- **Inclusive fiducial** cross section measurement
- **Differential fiducial** cross section measurements
  - Revised binning and extended set of variables (4 ⇛ **32**)
  - Compared with POWHEG, **MADGRAPH5**, and NNLOPS predictions
  - **1D measurements**
    - Production observables
    - Decay observables
      - Matrix-Element discriminants
  - **2D measurements**
    - Enhance sensitivity to specific phase space regions
- **Interpretations**
  - Higgs boson trilinear self-coupling κ_λ
  - Higgs boson couplings modifier κ_b, κ_c

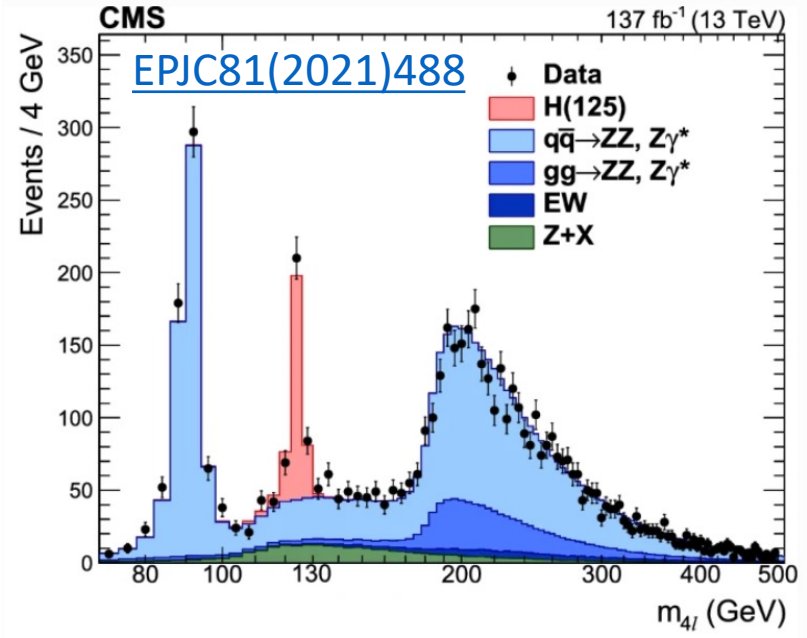

Overview

- **Fiducial cross section measurement** [JHEP08(2023)040] in $H \rightarrow ZZ^* \rightarrow 4l$ channel with 138fb^{-1} of Run II samples with latest objects calibration
- Extend the measurement with respect to the previous Run II analysis [EPJC81(2021)488]
- **Inclusive fiducial** cross section measurement
- **Differential fiducial** cross section measurements

Requirements for the $H \rightarrow ZZ \rightarrow 4\ell$ fiducial phase space	
Lepton kinematics and isolation	
Leading lepton p_T	$p_T > 20\,\text{GeV}$
Sub-leading lepton p_T	$p_T > 10\,\text{GeV}$
Additional electrons (muons) p_T	$p_T > 7(5)\,\text{GeV}$
Pseudorapidity of electrons (muons)	$\lvert\eta\rvert < 2.5\ (2.4)$
Sum of scalar p_T of all stable particles within $\Delta R < 0.3$ from lepton	$< 0.35 p_T$
Event topology	
Existence of at least two same-flavor OS lepton pairs, where leptons satisfy criteria above	
Inv. mass of the Z_1 candidate	$40 < m_{Z_1} < 120\,\text{GeV}$
Inv. mass of the Z_2 candidate	$12 < m_{Z_2} < 120\,\text{GeV}$
Distance between selected four leptons	$\Delta R(\ell_i, \ell_j) > 0.02$ for any $i \neq j$
Inv. mass of any opposite sign lepton pair	$m_{\ell^+\ell'^-} > 4\,\text{GeV}$
Inv. mass of the selected four leptons	$105 < m_{4\ell} < 160\,\text{GeV}$

Its definition matches closely the experimental acceptance after the reconstruction-level selection.

Fiducial Cross Section of 4l channel

- Number of events of different final state *f* and different year *y* in the given bin *i* are expressed as a function of 4l invariable mass

$$
\begin{aligned}
N_{\text{obs}}^{f,i,y}(m_{4\ell}) &= N_{\text{fid}}^{f,i,y}(m_{4\ell}) + N_{\text{nonfid}}^{f,i,y}(m_{4\ell}) + N_{\text{nonres}}^{f,i,y}(m_{4\ell}) + N_{\text{bkg}}^{f,i,y}(m_{4\ell}) \\
&= \sum_{j}^{\text{genBin}} \epsilon_{i,j}^{f,y} \left(1 + f_{\text{nonfid}}^{f,i,y}\right) \sigma_{\text{fid}}^{f,j,y} \, \mathcal{L} \, \mathcal{P}_{\text{res}}^{f,y}(m_{4\ell}) \\
&\quad + N_{\text{nonres}}^{f,i,y} \, \mathcal{P}_{\text{nonres}}^{f,y}(m_{4\ell}) + N_{\text{bkg}}^{f,i,y} \, \mathcal{P}_{\text{bkg}}^{f,i,y}(m_{4\ell}).
\end{aligned}
$$

Signal process	$\mathcal{A}_{\text{fid}}$	ϵ	f_{nonfid}	$(1+f_{\text{nonfid}})\epsilon$
ggH (POWHEG)	0.408 ± 0.001	0.619 ± 0.001	0.053 ± 0.001	0.652 ± 0.001
VBF	0.448 ± 0.001	0.632 ± 0.002	0.043 ± 0.001	0.659 ± 0.002
WH	0.332 ± 0.001	0.616 ± 0.002	0.077 ± 0.001	0.664 ± 0.002
ZH	0.344 ± 0.002	0.626 ± 0.003	0.083 ± 0.002	0.678 ± 0.003
$t\bar{t}H$	0.320 ± 0.002	0.614 ± 0.003	0.179 ± 0.003	0.725 ± 0.005

JHEP08(2023)040

- Fiducial + non-fiducial resonances signal contribution:
  - Shape is described by double-sided Crystal Ball function.
  - Normalization is proportional to the fiducial cross section.
- Non-resonant signal contribution
  - Arises from WH, ZH ttH where one of the leptons from Higgs is lost or not selected.
  - Modeled by Landau distribution
  - Treated as background

Results of Inclusive Fiducial Cross Section

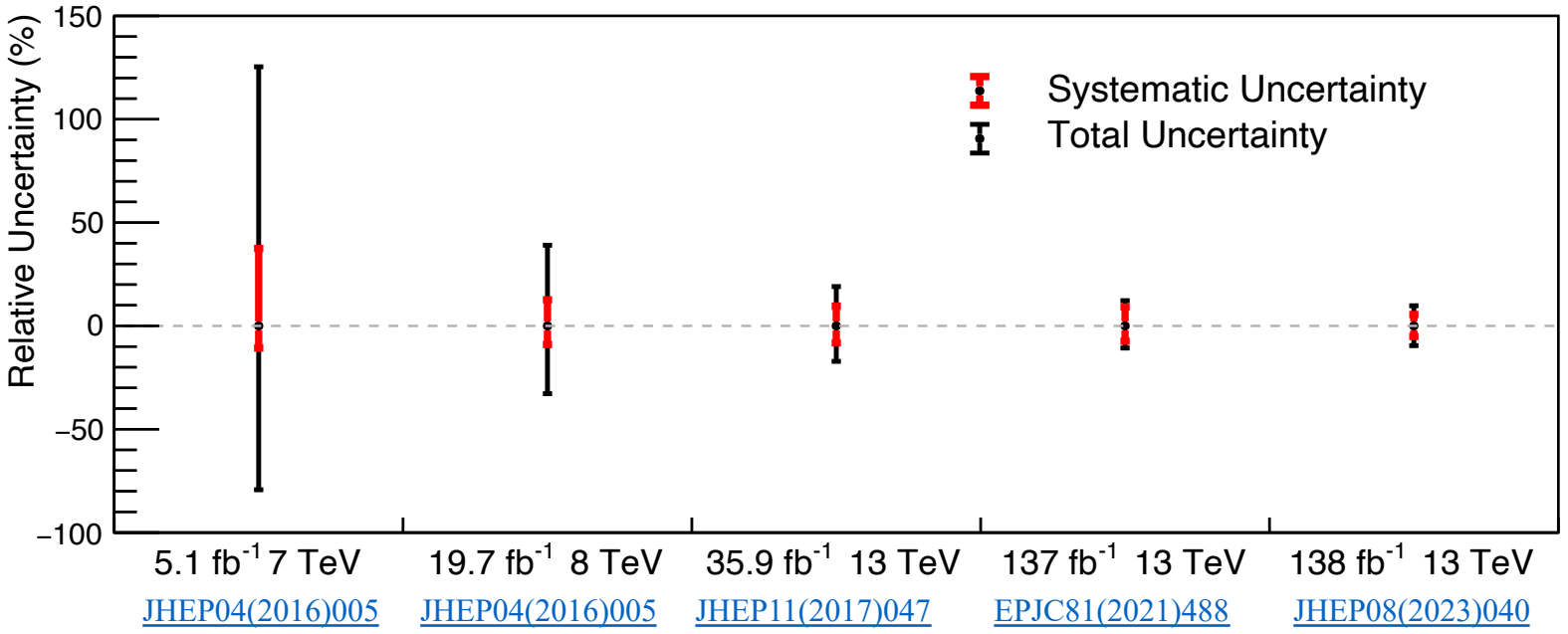

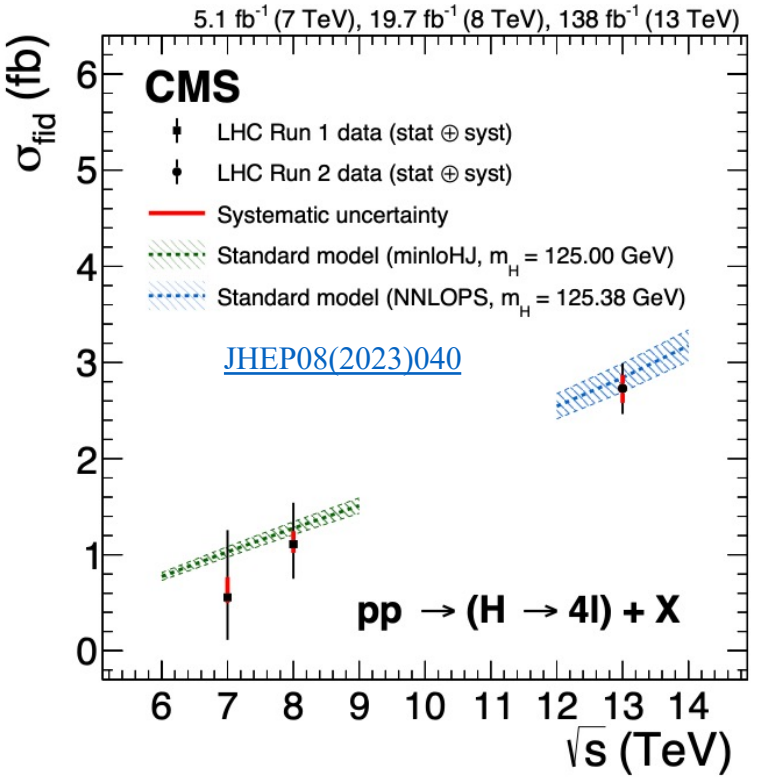

$$\sigma^{\text{fid}} = 2.73 \pm 0.22\,(\text{stat}) \pm 0.15\,(\text{syst})\ \text{fb}$$
$$= 2.73 \pm 0.22\,(\text{stat}) \pm 0.12\ (\text{electrons}) \pm 0.05\ (\text{lumi}) \pm 0.05\ (\text{bkg}) \pm 0.03\ (\text{muons})\ \text{fb}$$

Fiducial cross section as a function of center of mass

- Systematic uncertainty dominated by
  - Electrons-related nuisances,
  - Especially electron reconstruction efficiency

Results of Inclusive Fiducial Cross Section

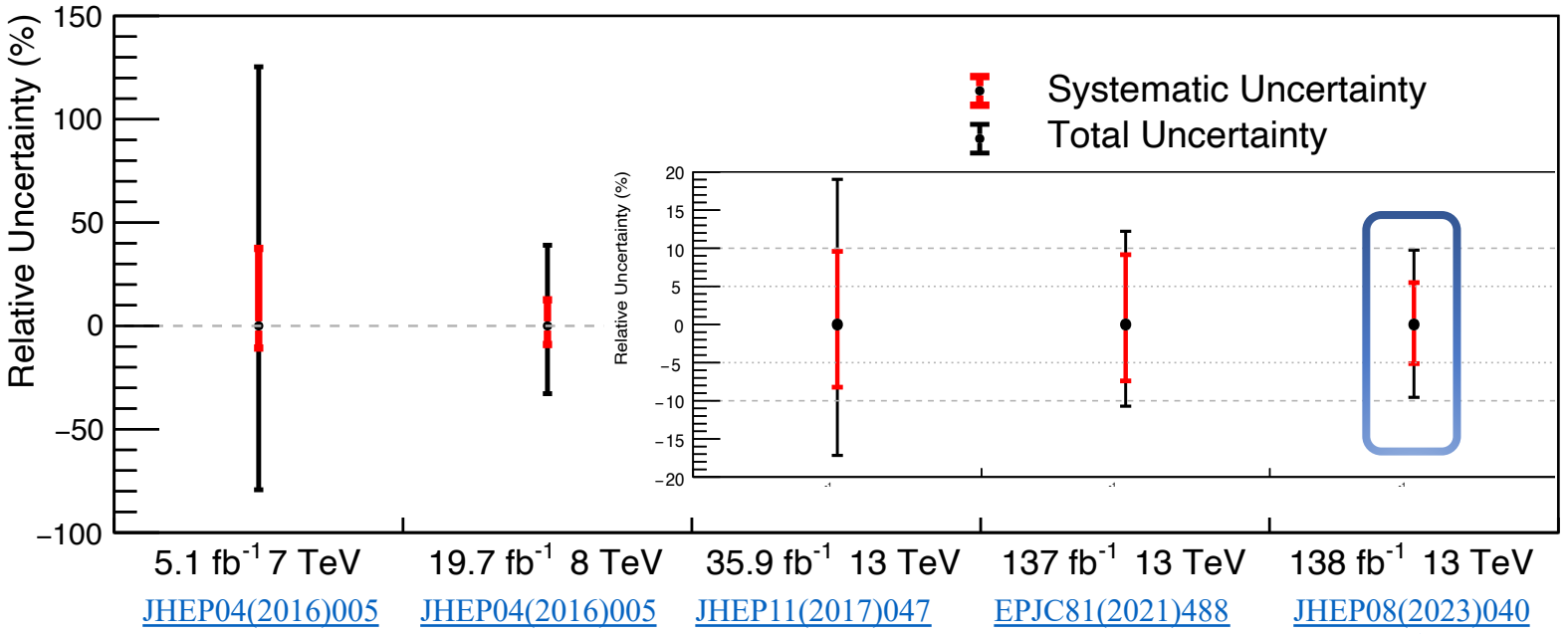

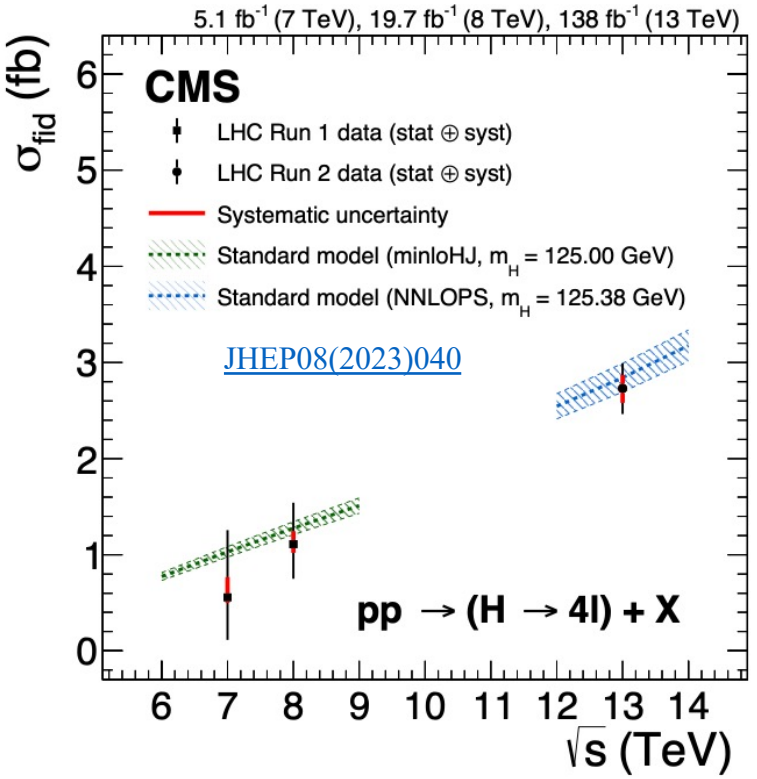

10% precision

$$\sigma^{\text{fid}} = 2.73 \pm 0.22\,(\text{stat}) \pm 0.15\,(\text{syst})\ \text{fb}$$
$$= 2.73 \pm 0.22\,(\text{stat}) \pm 0.12\ (\text{electrons}) \pm 0.05\ (\text{lumi}) \pm 0.05\ (\text{bkg}) \pm 0.03\ (\text{muons})\ \text{fb}$$

Fiducial cross section as a function of center of mass

- Systematic uncertainty dominated by
  - Electrons-related nuisances,
  - Especially electron reconstruction efficiency
- **Reduction of the systematic component** due to the reduction of the main lepton nuisances

Results of Inclusive Fiducial Cross Section

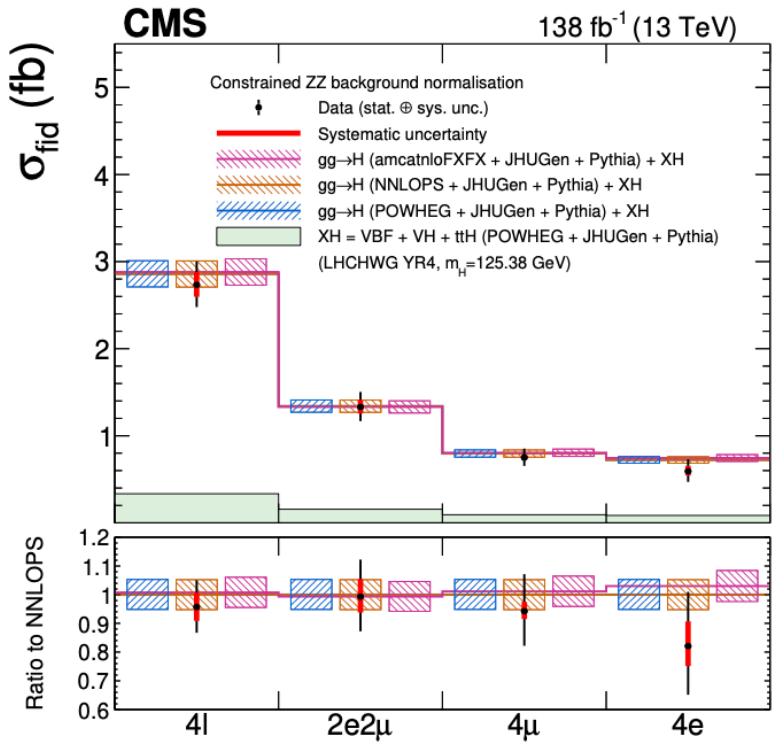

$\sigma^{\text{fid}} = 2.73 \pm 0.22(stat) \pm 0.15(syst)\text{fb}$

Irreducible background

normalization taken from MC simulation

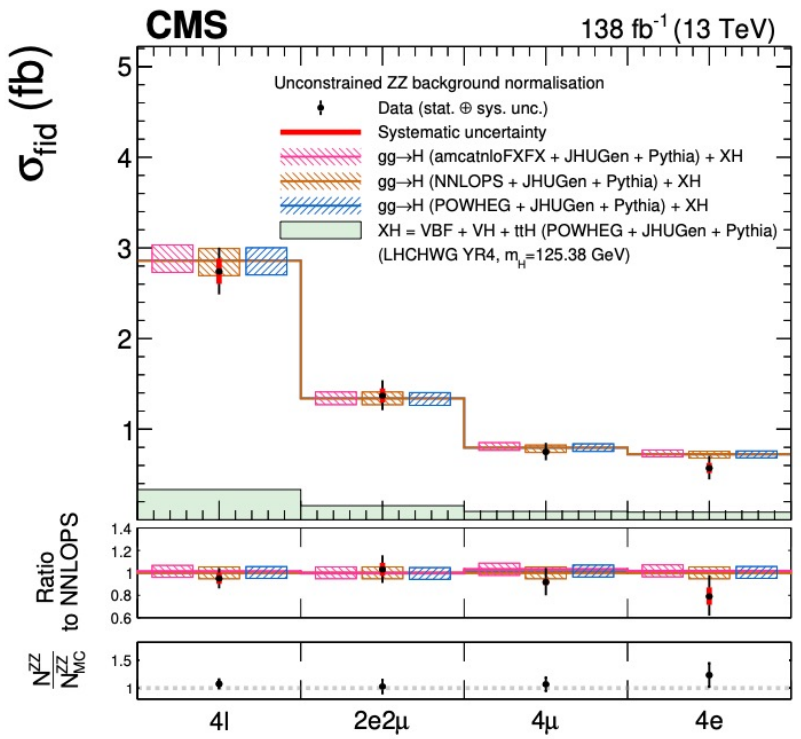

$\sigma^{\text{fid}} = 2.74^{+0.24}_{-0.23}(\text{stat})^{+0.14}_{-0.11}(\text{syst})\text{fb}$

Irreducible background

normalization ZZ floating in the fit

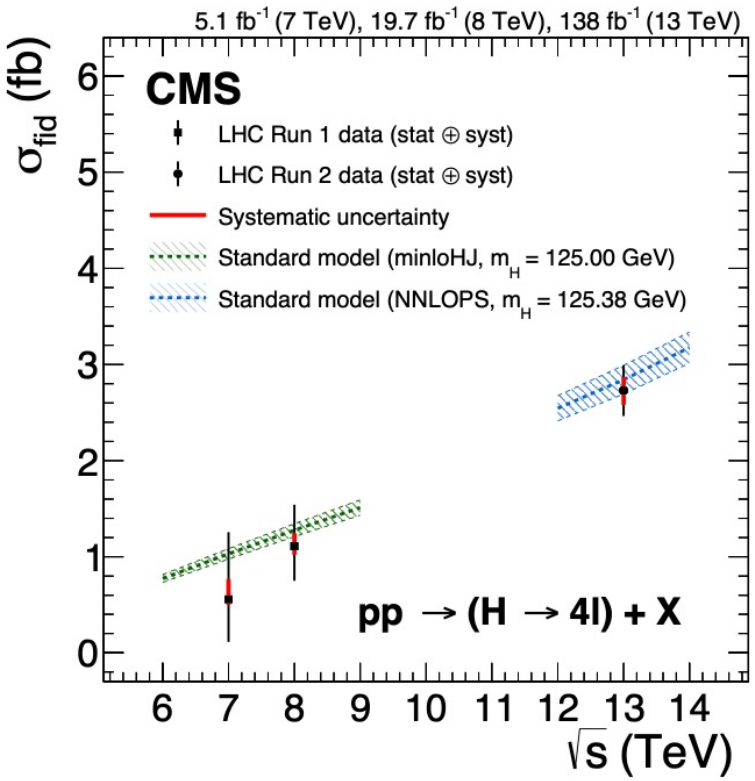

Fiducial cross section as a function of center of mass

JHEP08(2023)040

- Remove the impact of nuisances on ZZ normalization
- Being sensitive to BSM effects in the background

Differential Fiducial Cross Section

- Higgs **production** observables (13):

$$\begin{array}{ccccc} \boldsymbol{p_T^H} & \boldsymbol{|y_H|} & \boldsymbol{N_{jets}} & \boldsymbol{p_T^{j1}} & \\ p_T^{j2} & m_{jj} & |\Delta\eta_{jj}| & \Delta\phi_{jj} & \\ p_T^{Hj} & m_{Hj} & p_T^{Hjj} & \mathcal{T}_B & \mathcal{T}_C \end{array}$$

- Higgs **decay** observables (13):

$$\begin{array}{ccccccc} m_{Z1} & m_{Z2} & \Phi & \Phi_1 & \cos\theta & \cos\theta_1 & \cos\theta^* \\ \mathcal{D}_{0-}^{\mathrm{dec}} & \mathcal{D}_{cp}^{\mathrm{dec}} & \mathcal{D}_{0h+}^{\mathrm{dec}} & \mathcal{D}_{\Lambda 1}^{\mathrm{dec}} & \mathcal{D}_{\Lambda 1}^{\mathrm{Z}\gamma,\mathrm{dec}} & \mathcal{D}_{int}^{\mathrm{dec}} & \end{array}$$

- **Double** differential observables (6):

$$\begin{array}{cc} m_{Z1} \text{ vs } m_{Z2} & N_{jets} \text{ vs } p_T^H \\ p_T^{j1} \text{ vs } p_T^{j2} & \mathcal{T}_C \text{ vs } p_T^H \\ p_T^{Hj} \text{ vs } p_T^H & |y^H| \text{ vs } p_T^H \end{array}$$

1D Differential Cross Section --- Production

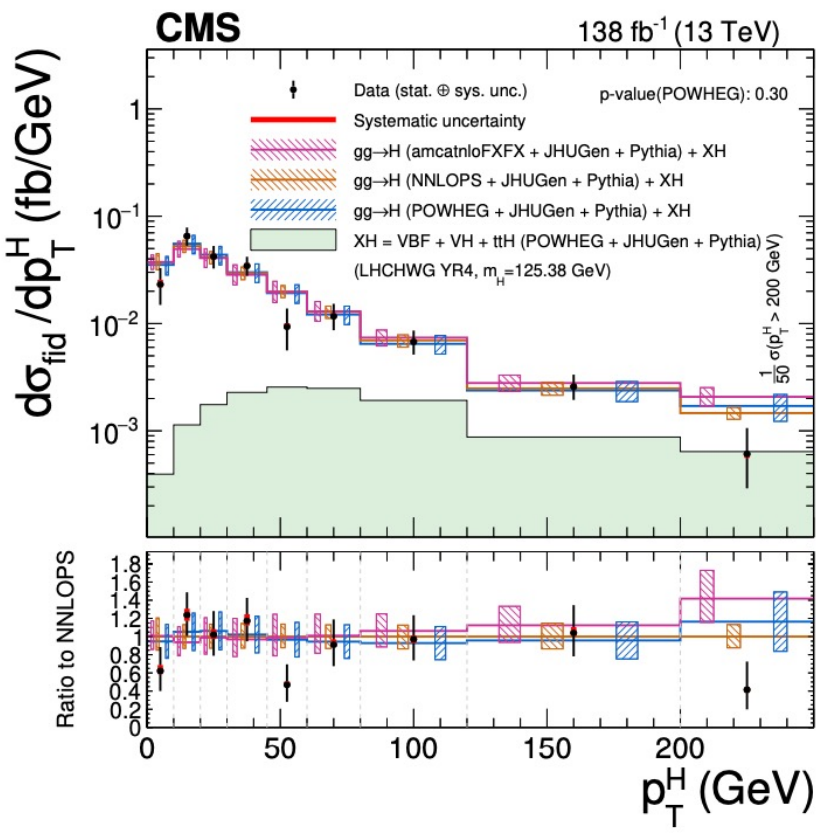

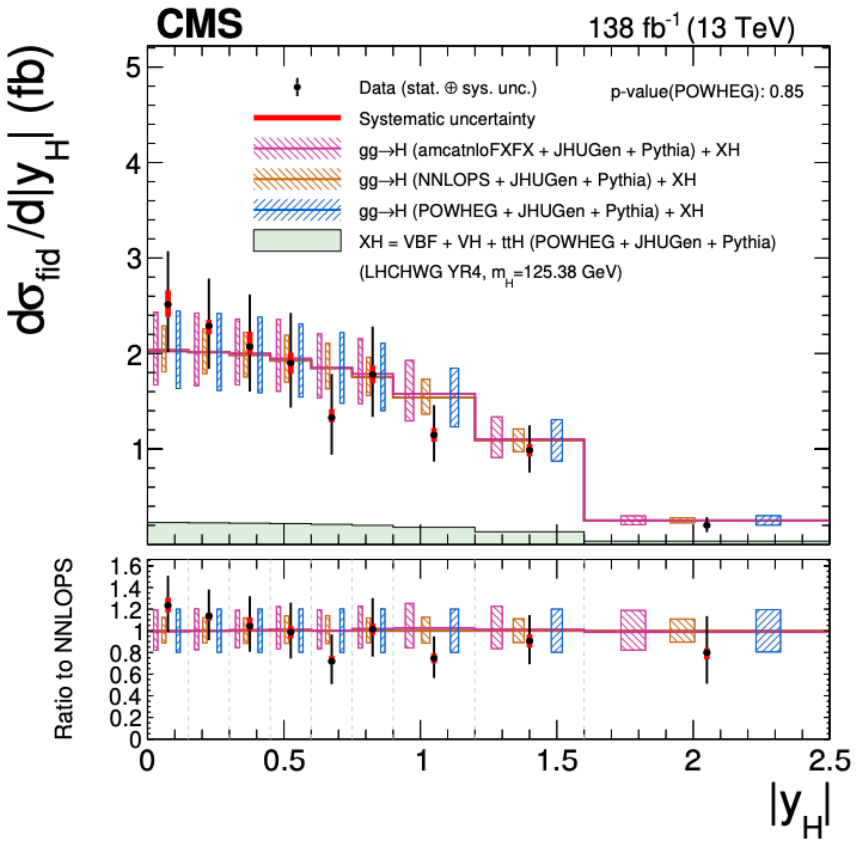

- Differential observables of **Higgs boson kinematics** JHEP08(2023)040
  - P_T^H: probes the perturbative QCD modelling of this production mechanism
  - $|y^H|$: sensitive to the gluon fusion production mechanism and PDFs
- Average precision of 35%

1D Differential Cross Section --- Production

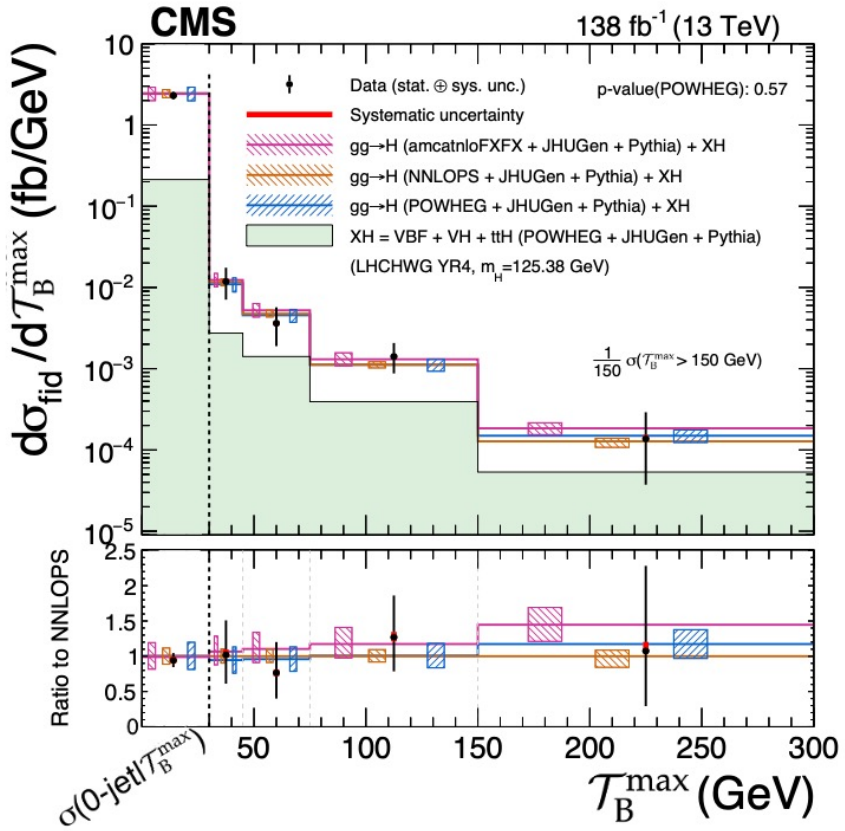

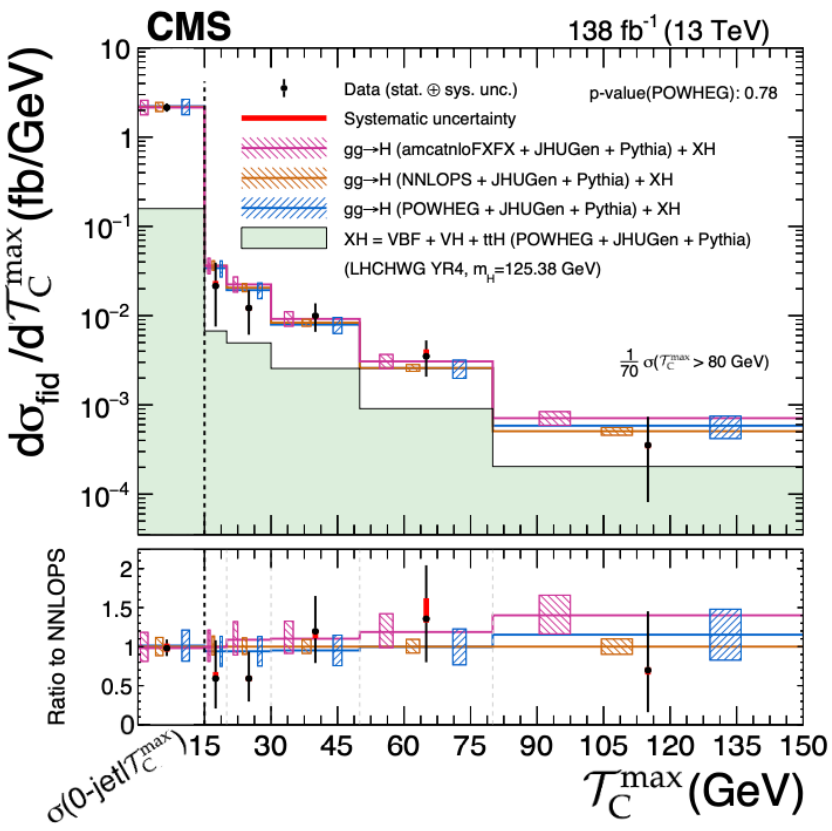

- Differential observables of **Jet activity**
  - Jet rapidity-weighted observables

JHEP08(2023)040

$$\mathcal{T}_B^{max} = \max_j (m_T^j e^{-|y_j - y_H|})$$

$$\mathcal{T}_C^{max} = \max_j \left(\frac{\sqrt{E_j^2 - p_{z,j}^2}}{2\cosh(y_j - y_H)}\right)$$

  - Maximum is taken among all jets and events with $\mathcal{T}_B \leq 30$ GeV and $\mathcal{T}_C \leq 15$ GeV make the 0-jet bin
  - The advantage of such observables is that they can be ***factorized and resumed*** allowing for ***precise theory predictions***.

1D Differential Cross Section --- Decay

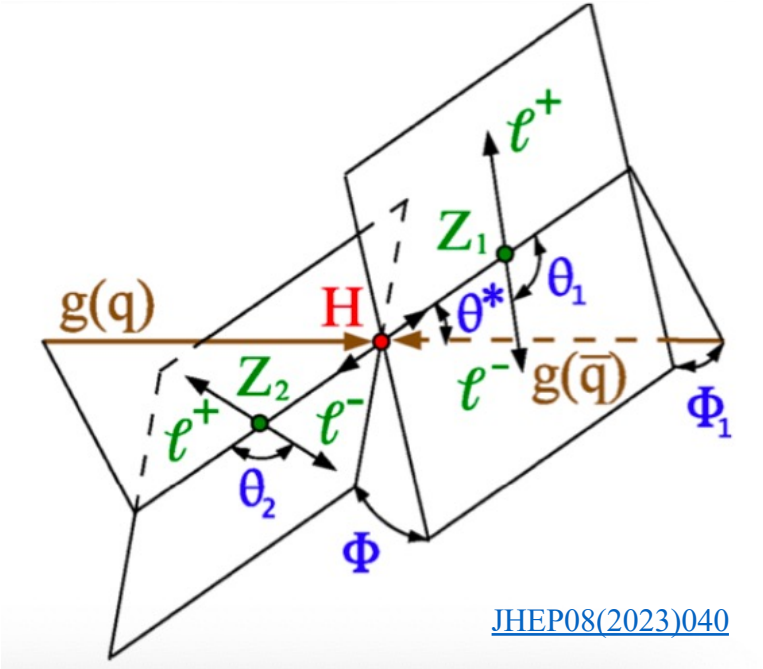

JHEP08(2023)040

- Differential observables of **Higgs decay**
  - Angular observables: Φ Φ_1 $\cos\theta$ $\cos\theta_1$ $\cos\theta^*$
  - Describe angle between the plane of Higgs, Z_1, Z_2 decay and the beam direction
  - Sensitive to the spin and charge conjugation and parity properties of the Higgs

1D Differential Cross Section --- Decay

- Higgs **Decay** in 4l final states could be characterized by the following seven parameters:
  - m_{Z1}, m_{Z2}
  - Φ , Φ_1 , $\cos\theta$, $\cos\theta_1$, $\cos\theta^*$

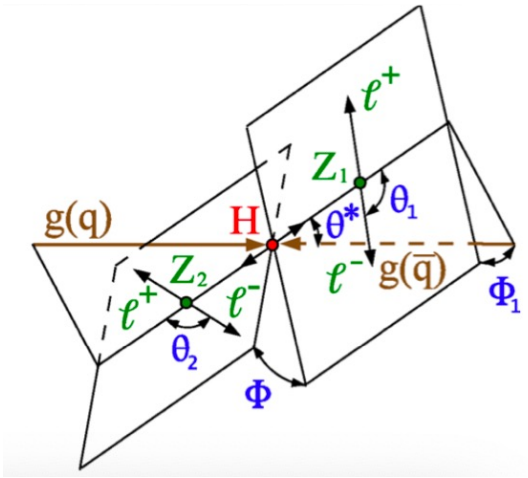

☆ $\mathcal{D}_{0-}^{\mathbf{dec}}$ $\mathcal{D}_{0h+}^{\mathbf{dec}}$ $\mathcal{D}_{\Lambda 1}^{\mathbf{dec}}$ $\mathcal{D}_{\Lambda 1}^{\mathbf{Z\gamma,dec}}$ | $\mathcal{D}_{cp}^{\mathbf{dec}}$ $\mathcal{D}_{int}^{\mathbf{dec}}$

1D Differential Cross Section --- Decay

- Higgs **Decay** in 4l final states could be characterized by the following seven parameters:
  - m_{Z1}, m_{Z2}
  - Φ , Φ_1 , $\cos\theta$, $\cos\theta_1$, $\cos\theta^*$

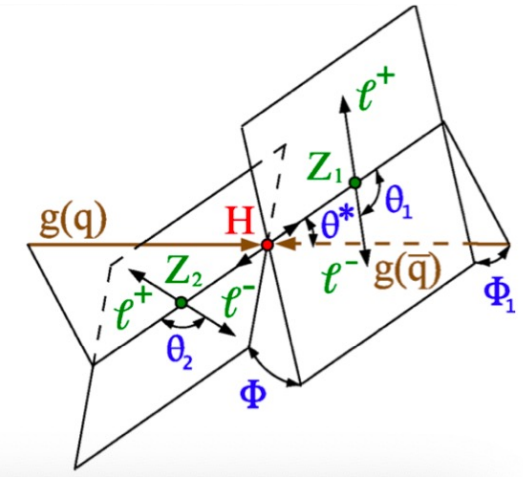

☆ $\mathcal{D}_{0-}^{dec}$ $\mathcal{D}_{0h+}^{dec}$ $\mathcal{D}_{\Lambda 1}^{dec}$ $\mathcal{D}_{\Lambda 1}^{Z\gamma,dec}$ | $\mathcal{D}_{cp}^{dec}$ $\mathcal{D}_{int}^{dec}$

- HVV scattering amplitude of a spin-0 boson H and two spin-one gauge bosons

$$A(HV_1V_2) = \frac{1}{v}\left[a_1^{VV} + \frac{k_1^{VV} q_{V1}^{VV} + k_2^{VV} q_{V2}^2}{(\Lambda_1^{VV})^2} + \frac{k_3^{VV}(q_{V1}+q_{V2})^2}{(\Lambda_Q^{VV})^2}\right] m_{V1}^2 \epsilon_{V1}^* \epsilon_{V2}^* + a_2^{VV} f_{\mu\nu}^{*(1)} f^{*(2),\mu\nu} + a_3^{VV} f_{\mu\nu}^{*(1)} \tilde{f}^{*(2),\mu\nu}$$

CP even
- SM-like spin-zero 0^+: $a_1^{ZZ}=a_1^{WW}=2$
- Higher order spin-zero 0_h^+: a_2

CP odd
- Pseudoscalar spin-zero 0^-: a_3

Scales of BSM physics

- Observables sensitive to HVV anomalous couplings using kinematics of leptons in decay

$$\mathcal{D}_{\text{alt}} = \frac{\mathcal{P}_{\text{sig}}(\vec{\Omega})}{\mathcal{P}_{\text{sig}}(\vec{\Omega}) + \mathcal{P}_{\text{alt}}(\vec{\Omega})} \qquad \mathcal{D}_{\text{int}} = \frac{\mathcal{P}_{\text{int}}(\vec{\Omega})}{2 \cdot \sqrt{\mathcal{P}_{\text{sig}}(\vec{\Omega}) \cdot \mathcal{P}_{\text{alt}}(\vec{\Omega})}},$$

	$\mathcal{D}_{\text{alt}}$				$\mathcal{D}_{\text{int}}$	
	Coupling					
	a_3	a_2	κ_1	$\kappa_2^{Z,\gamma}$	a_3	a_2
Discriminant	$\mathcal{D}_{0-}$	$\mathcal{D}_{0h+}$	$\mathcal{D}_{\Lambda 1}$	$\mathcal{D}_{\Lambda 1}^{Z,\gamma}$	$\mathcal{D}_{\text{CP}}$	$\mathcal{D}_{\text{int}}$

1D Differential Cross Section --- Decay

- Higgs **Decay** in 4l final states could be characterized by the following seven parameters:
  - m_{Z1}, m_{Z2}
  - Φ , Φ_1 , $\cos\theta$, $\cos\theta_1$, $\cos\theta^*$

☆ $\mathcal{D}_{0-}^{dec}$ $\mathcal{D}_{cp}^{dec}$ | $\mathcal{D}_{0h+}^{dec}$ $\mathcal{D}_{int}^{dec}$ | $\mathcal{D}_{\Lambda 1}^{dec}$ $\mathcal{D}_{\Lambda 1}^{Z\gamma,dec}$

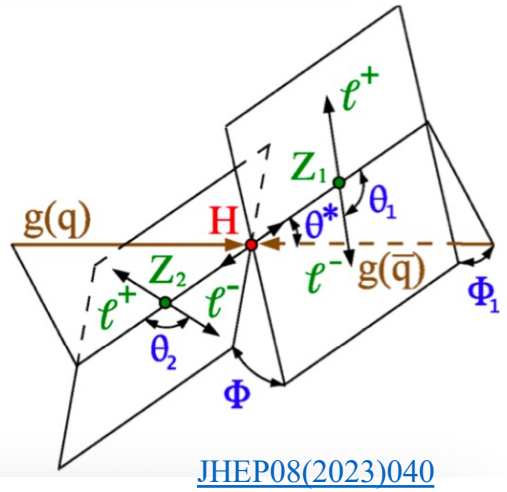

JHEP08(2023)040

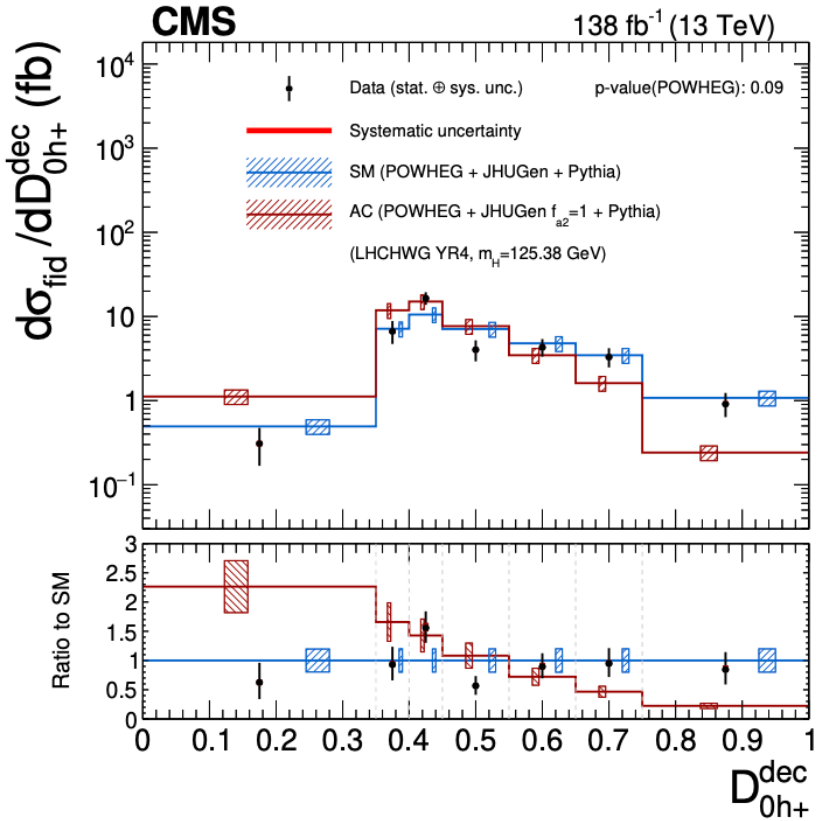

- Higher order spin-zero 0_h^+ a_2: sensitive to possible BSM contributions from heavy H bosons

- 13 Differential cross sections of decay are also measured in the **same-flavor** and **different flavor** final states.
- Its final state is sensitive to ***interference effects***

1D Differential Cross Section --- Decay

- Higgs **Decay** in 4l final states could be characterized by the following seven parameters:
  - m_{Z1}, m_{Z2}
  - Φ , Φ_1 , $\cos\theta$, $\cos\theta_1$, $\cos\theta^*$

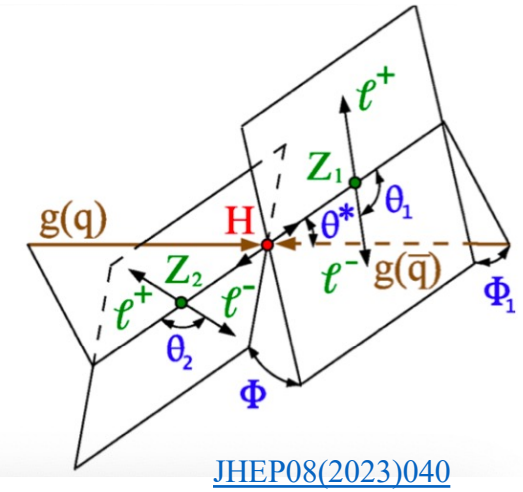

JHEP08(2023)040

☆ $\mathcal{D}_{0-}^{dec}$ $\mathcal{D}_{cp}^{dec}$ | $\mathcal{D}_{0h+}^{dec}$ $\mathcal{D}_{int}^{dec}$ | $\mathcal{D}_{\Lambda 1}^{dec}$ $\mathcal{D}_{\Lambda 1}^{Z\gamma,dec}$

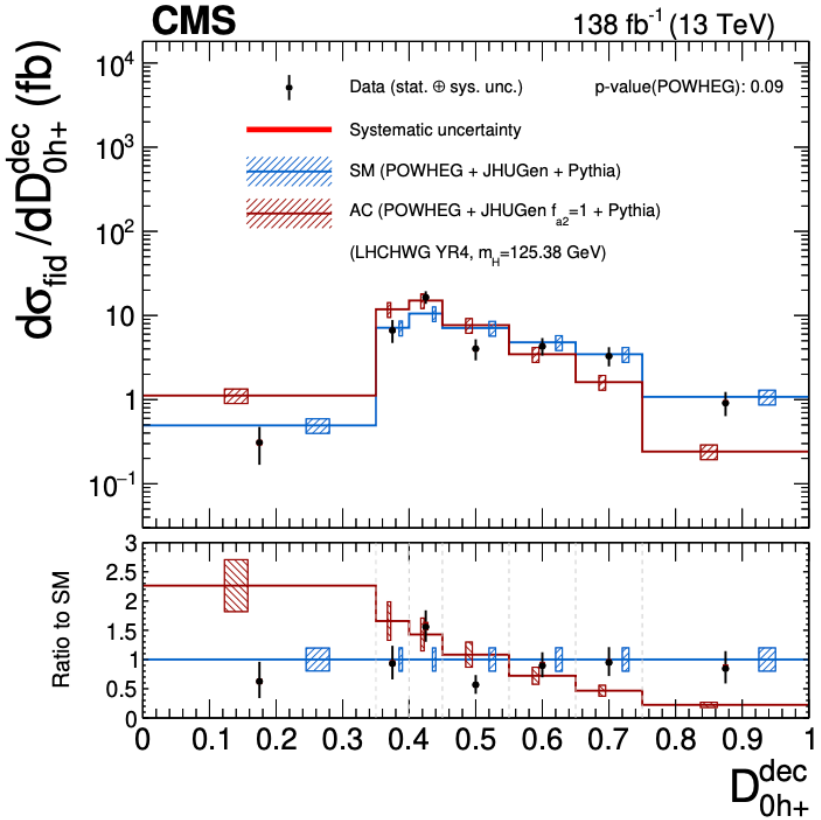

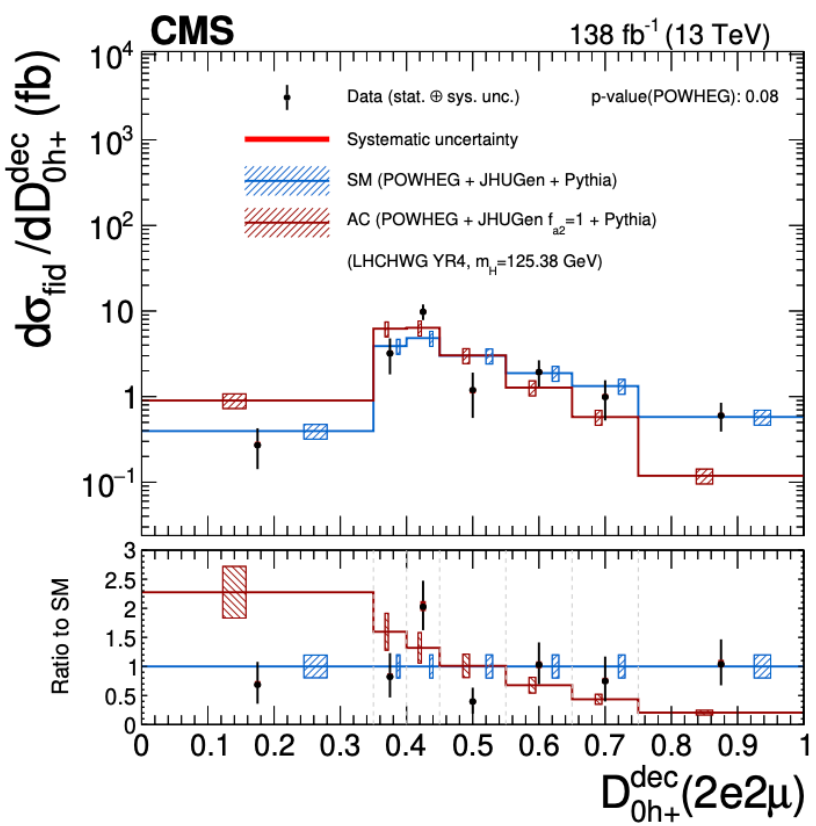

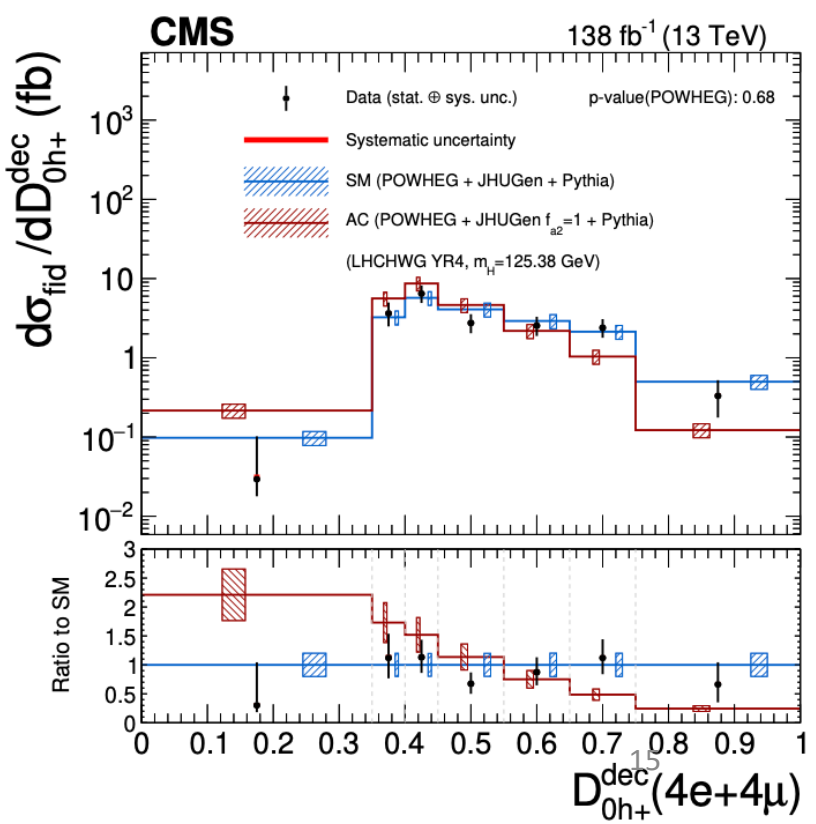

Constraints on the H boson self-coupling

Probing κ_λ via single-Higgs decay

- Differential XS measurement as a function of p_T^H ⇨ extract limits on H boson self coupling.

production decay

$$\mu_i^f = \mu_i \times \mu^f = \frac{\sigma^{NLO}}{\sigma_{SM}^{NLO}} \frac{BR(H\to ZZ)}{BR^{SM}(H\to ZZ)} = \frac{1+\kappa_\lambda C_{1,i}+\delta Z_H}{(1-(\kappa_\lambda^2-1)\delta Z_H)(1+C_{1,i}+\delta Z_H)} \times \left[1 + \frac{(\kappa_\lambda-1)(C_1^{\Gamma ZZ}-C_1^{\Gamma tot})}{1+(\kappa_\lambda-1)C_1^{\Gamma tot}}\right]$$

- Cross sections of different production mechanisms of H boson is parameterized as a function of

$$\kappa_\lambda = \lambda_3/\lambda_3^{SM}$$

- The corresponding observed (expected) excluded κ_λ range at 95% CL

$$-5.4(-7.6) < \kappa_\lambda < 14.9(17.7)$$

JHEP08(2023)040

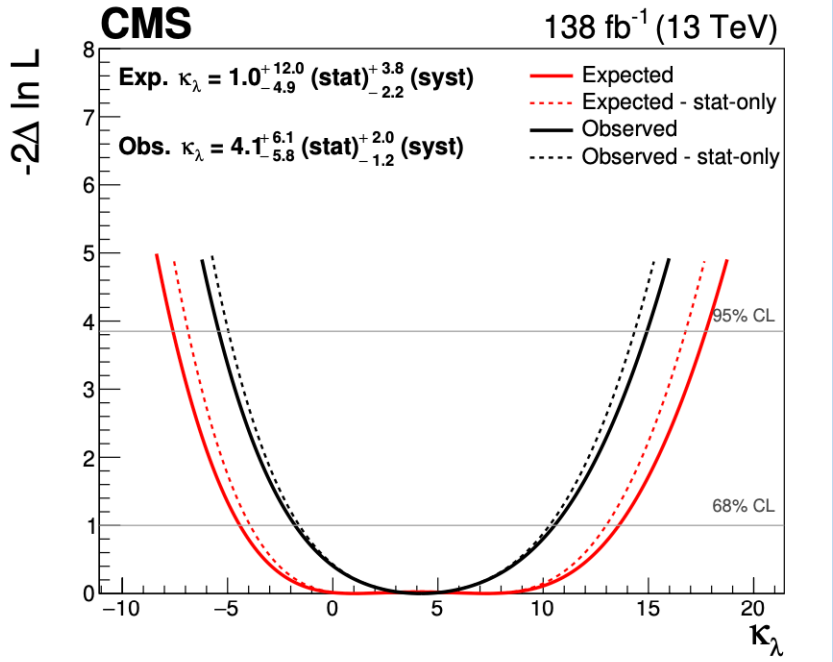

Constraints on Higgs boson couplings modifier

Probing κ_b, κ_c via p_T^H differential cross section

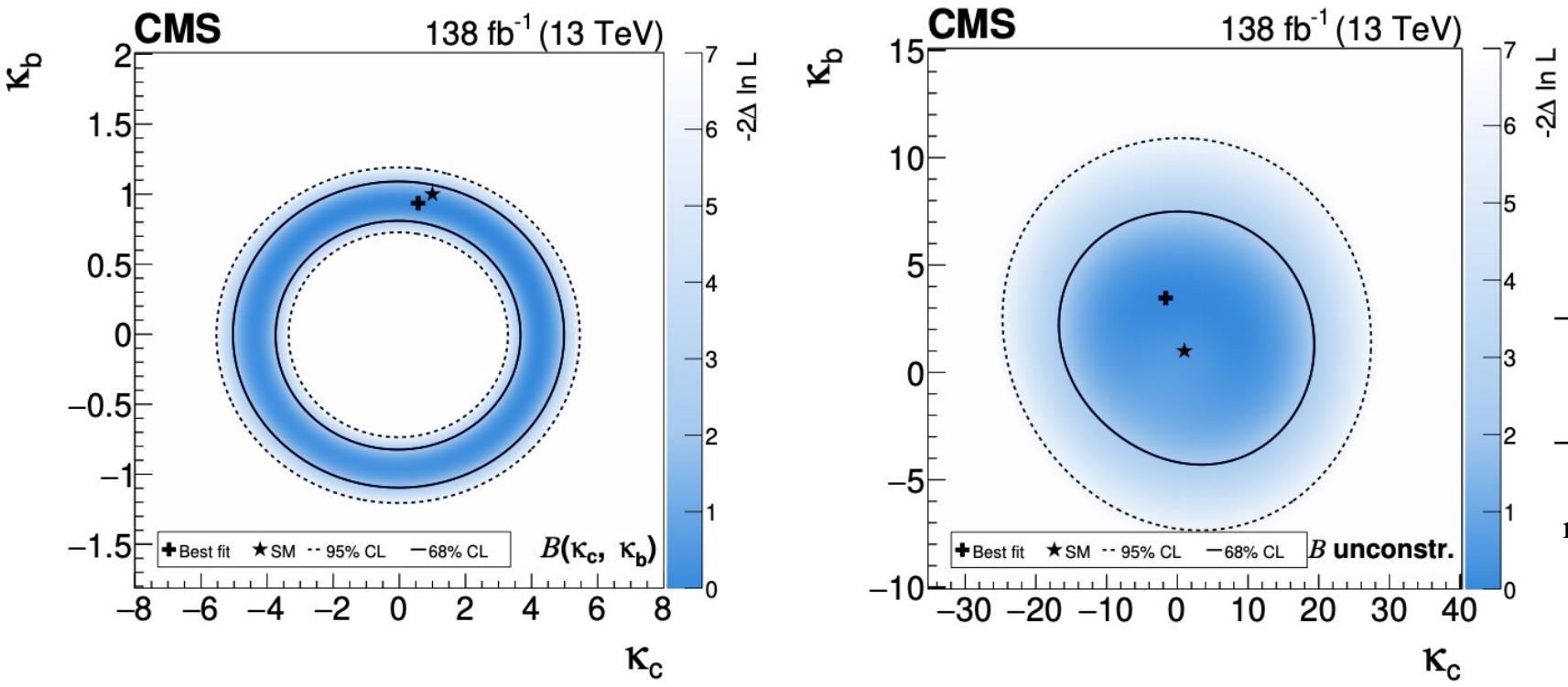

		Full Run2 Ultra Legacy Floating κ_b κ_c	
JHEP08(2023)040		**Observed** 95% confidence interval	**Expected** 95% confidence interval
Shape-Only	κ_b	[-5.6, 8.9]	[-5.5, 7.4]
	κ_c	[-20, 23]	[-19, 20]
Shape+ normalization	κ_b	[-1.1, 1.1]	[-1.3, 1.2]
	κ_c	[-5.3, 5.2]	[-5.7, 5.7]

- Simultaneous fit for coupling modifier κ_b, κ_c assuming
  - (left) coupling dependence of the branching fractions (*shape+normalization*)
  - (right)branching fractions implemented as nuisance parameters with no prior constraint (*shape-only*)
- Observed and expected 95% confidence intervals for the Yukawa coupling modifiers

Summary

- Measurements of Higgs boson cross section in four-lepton final state at $\sqrt{s} = 13TeV$ using data sample corresponding to an integrated luminosity of 138 fb^{-1}
  - The **inclusive fiducial cross section** measured is $\sigma^{fid} = 2.73 \pm 0.22(stat) \pm 0.15(syst)$ fb.
  - **Differential** cross sections as a function of **32 observables** are measured, including one and **two dimension observables**, which involves the
    - H boson production and **HZZ decay**, jet related observables, and observables sensitive to spin and CP quantum numbers
    - Complete coverage of the whole phase space
  - The measurement of fiducial cross section in bins of the transverse momentum is reinterpreted to set constraints to
    - **H boson self-coupling** (κ_λ)
    - **Couplings to bottom and charm quarks** (κ_b, κ_c)
- All results are consistent, within their uncertainties, with the expectations for the Standard Model H boson.

Thanks for your listening!

Backup

Introduction

➢Standard model

- Describe elementary particles and interactions
- Introduce Higgs mechanism in1960s
- Predict a scalar field responsible for mass origin

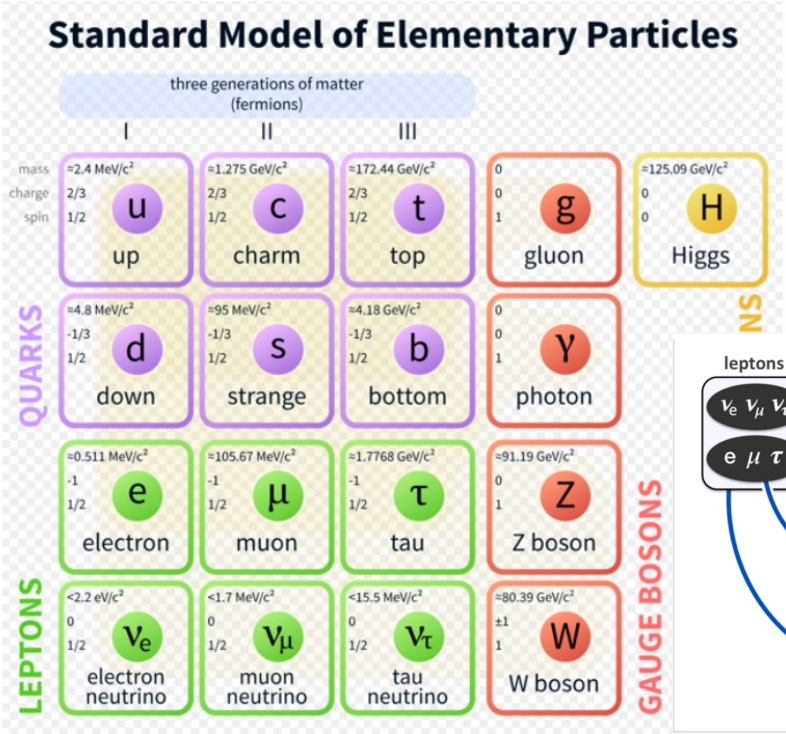

➢Higgs boson

- Particle corresponding to excitation of the predicted scalar field
- Key to verify the current understanding of boson/fermion mass generation
- A new probe to new physics after its experimental observation
- Crucial to measure its properties

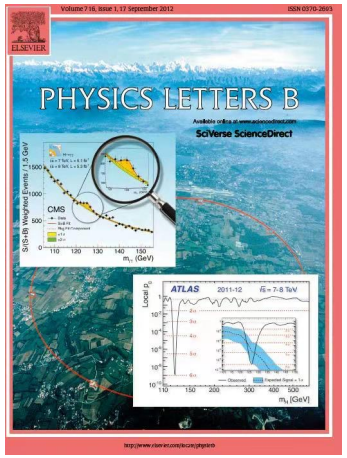

Observed in 2012

Experimental measurements

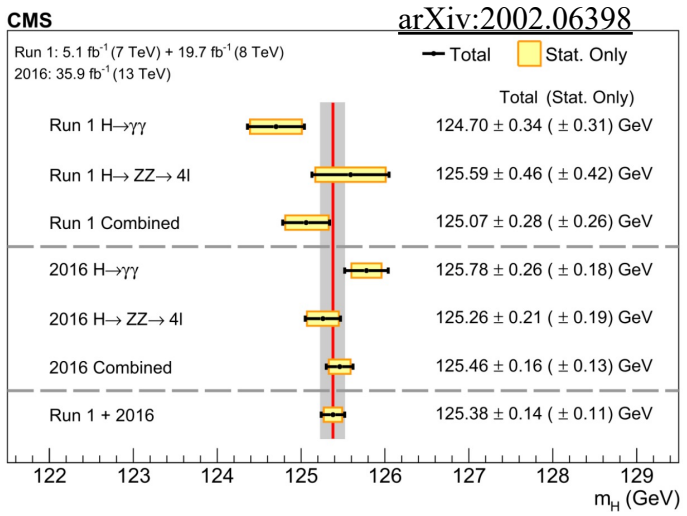

arXiv:2002.06398

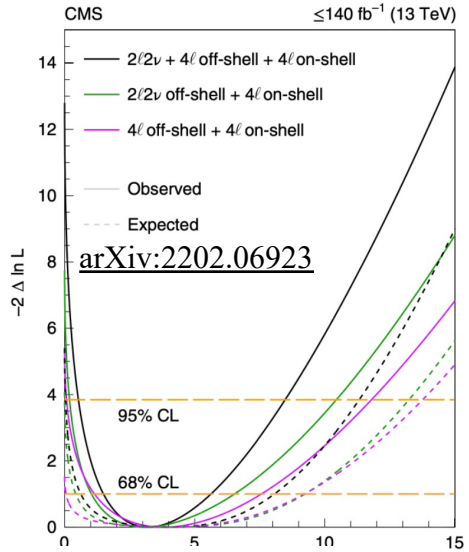

arXiv:2202.06923

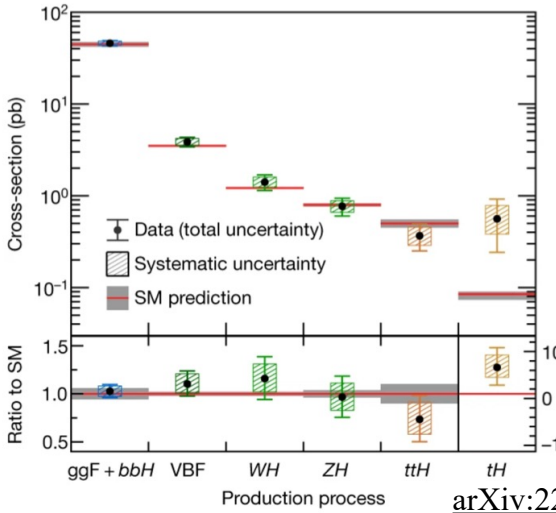

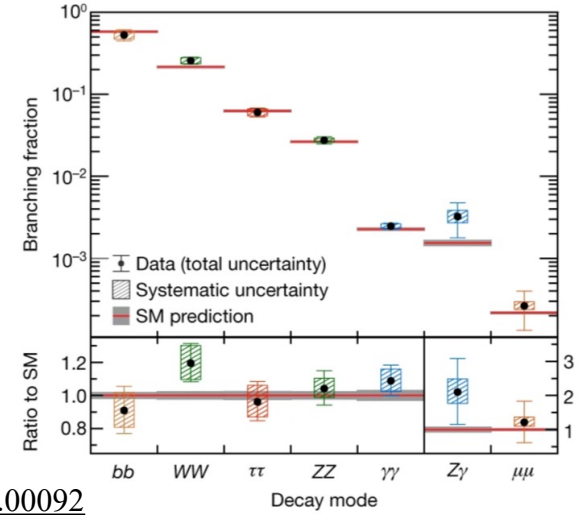

arXiv:2207.00092

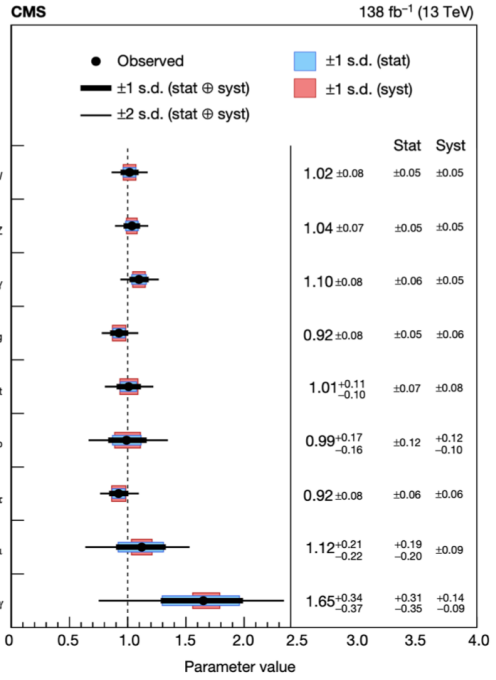

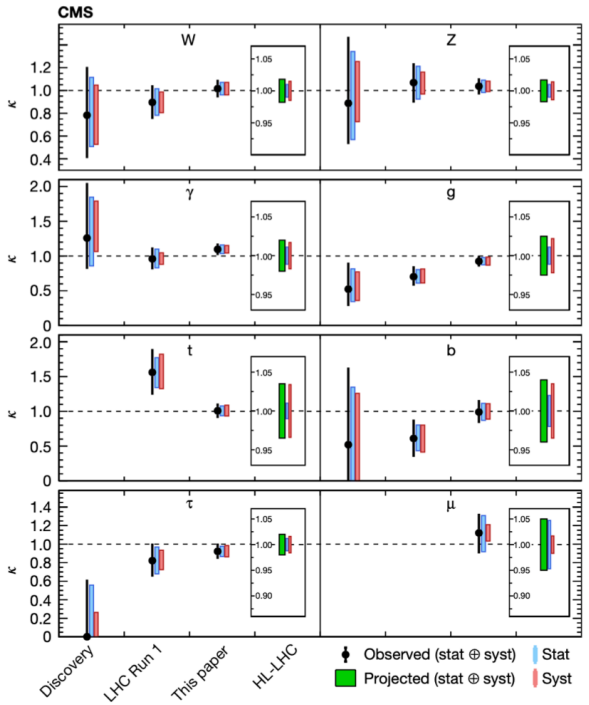

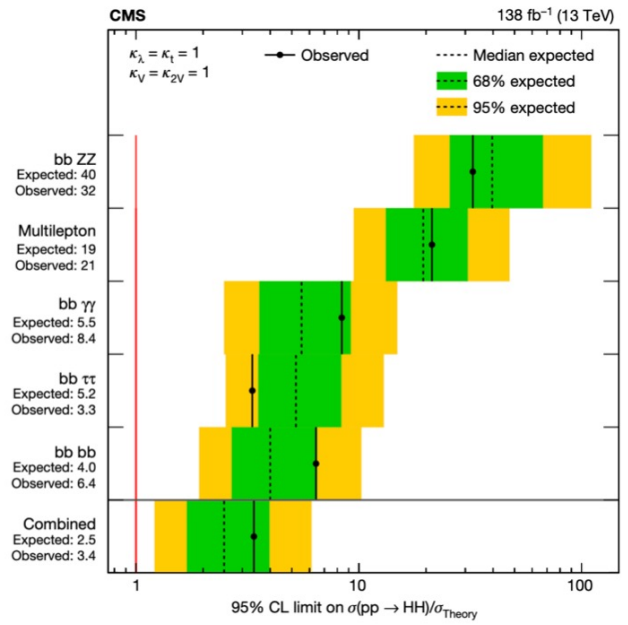

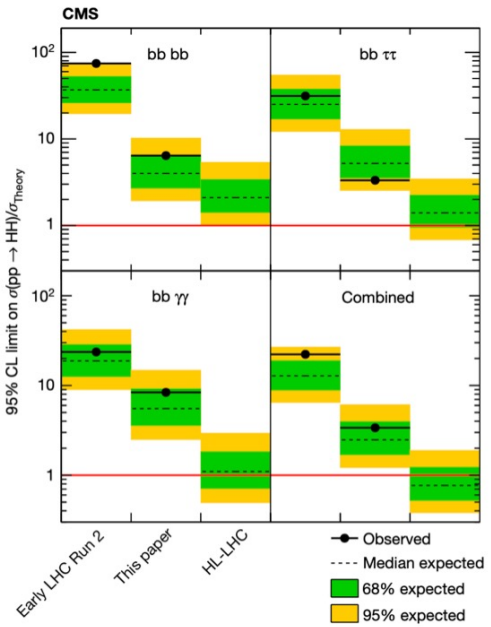

arXiv:2207.00043

Higgs production at LHC

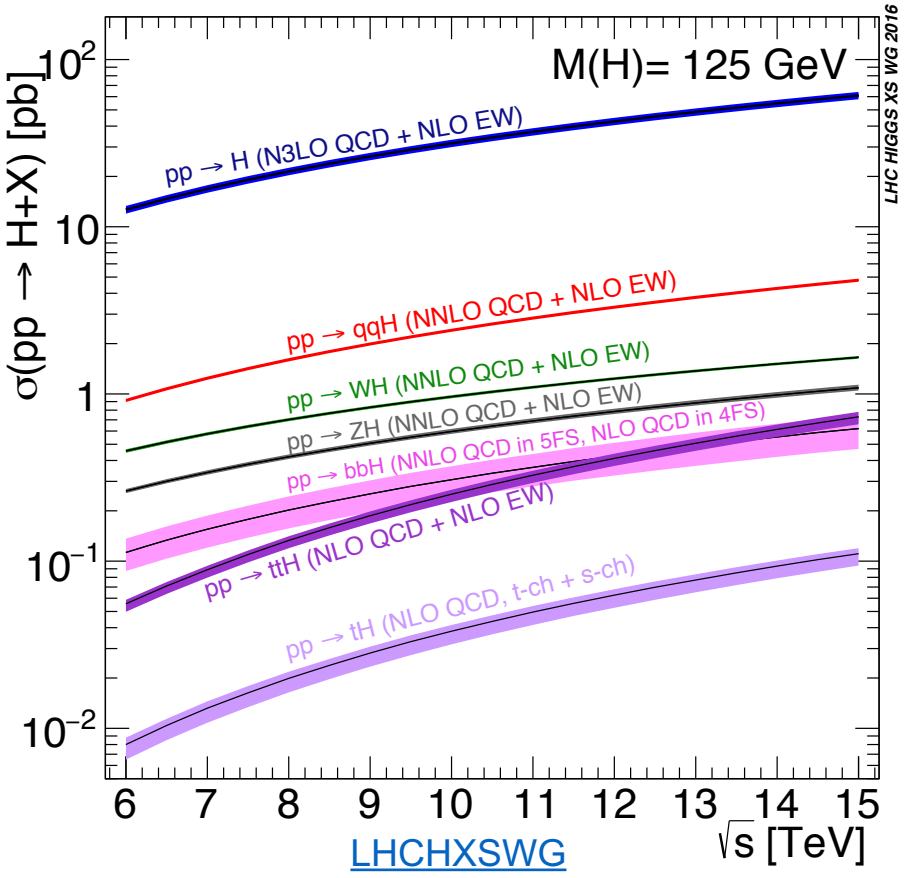

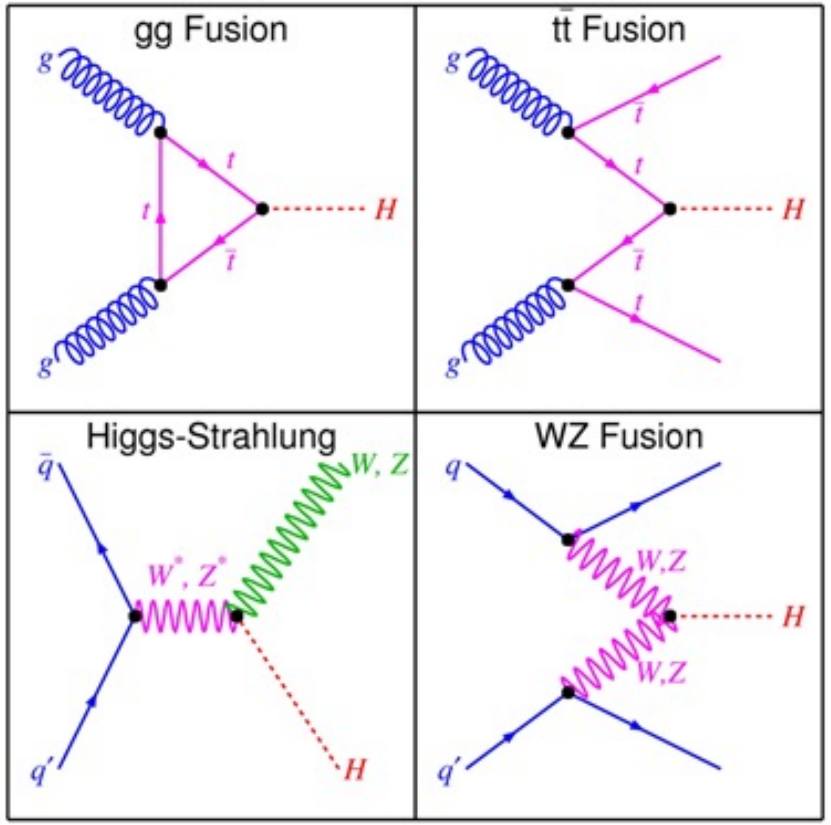

Fig. Feynman diagram of each production model

- Main production model and its cross section at 13TeV and Higgs mass of 125GeV
- Gluon-Gluon Fusion: 48.58 pb
- VBF: 3.782pb
- VH: 1.373pb(WH); 0.8839pb(ZH)
- ttH: 0.5071pb

Higgs decay at LHC

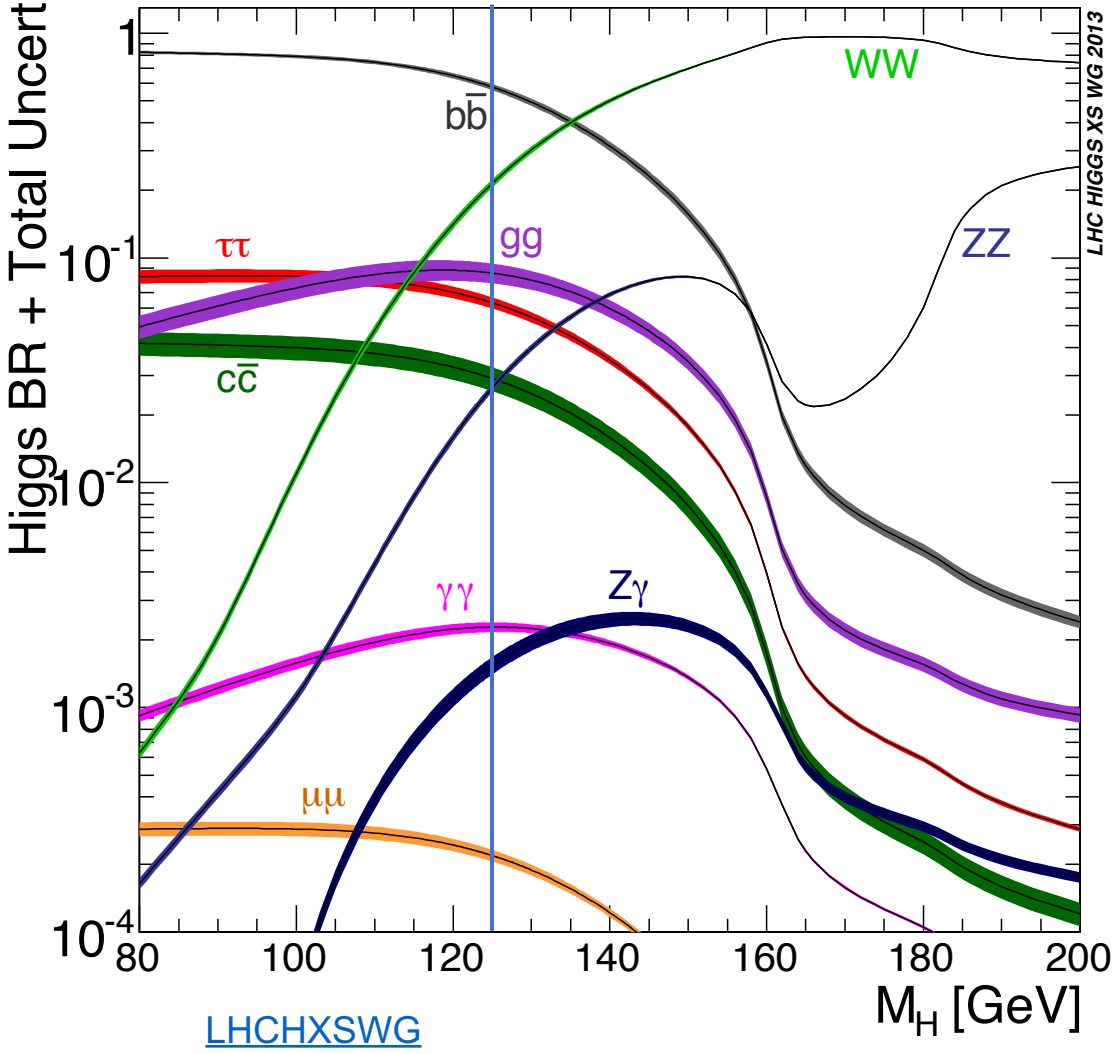

LHCHXSWG

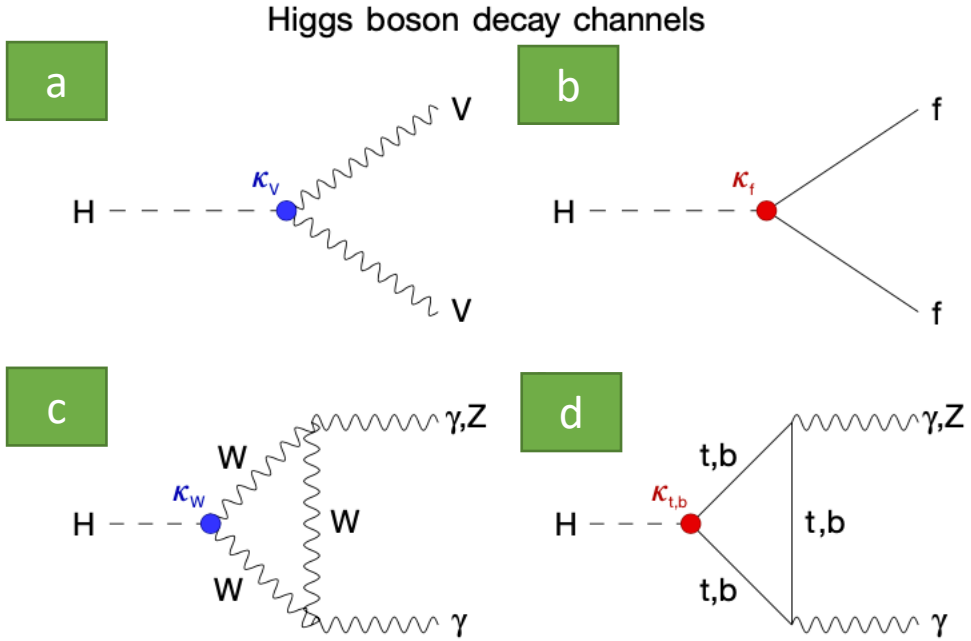

- Higgs boson decays into [Nature 607 (2022) 60–68]
  - Heavy vector boson pairs (**a**)
  - Fermion–antifermion pairs (**b**)
  - Photon pairs or Zγ (**c**,**d**)

Higgs decay

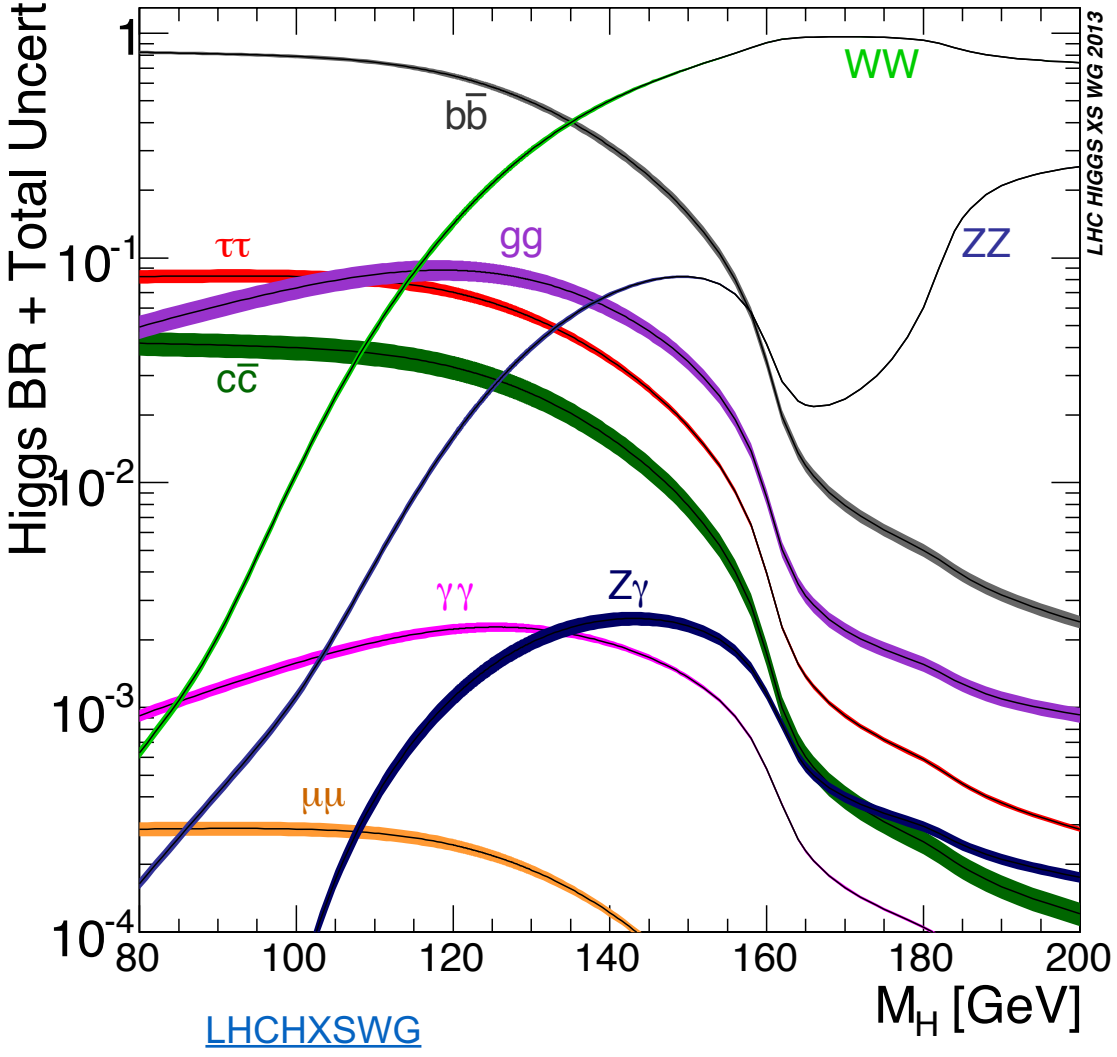

LHCHXSWG

- 4l channel is one of the most important channel for Higgs boson property measurements.
- A large signal-to-background ratio (> 2:1)
- Complete reconstruction of final state decay products
- Excellent lepton momentum reconstruction (1-2%)

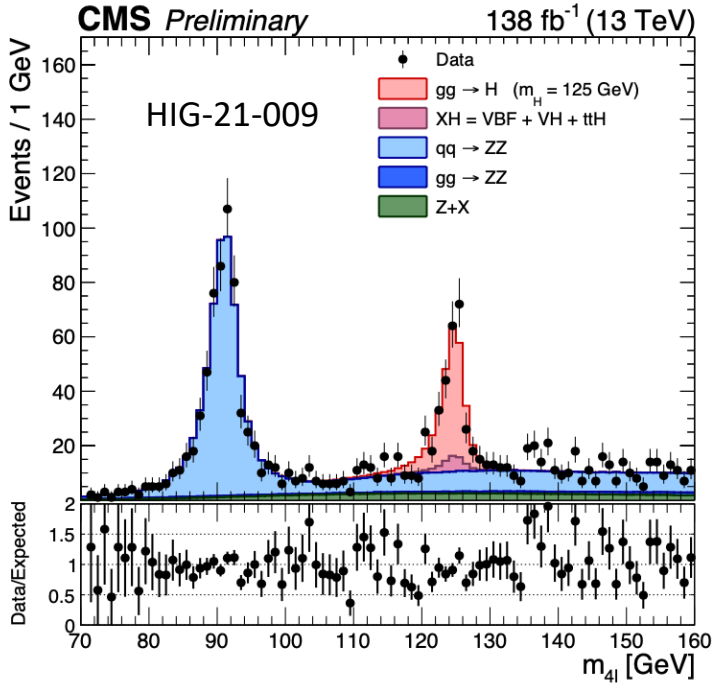

Dataset and simulation samples

- Data recorded in 2016-2018 for physics analyses: 138 fb^{-1}
  - DoubleMuon, MuonEG, EGamma and Single-Muon
  - Use of dedicated collections of HLT paths, combined in a logical “OR” to avoid duplication of events
- Simulation samples
  - Signal: POWHEG V2 generator for the five main production modes
  - Backgrounds: qqZZ, ggZZ and additional MC samples of WZ, Drell-Yan+jets…

Process	MC Generator(s)	$\sigma \times BR(\times\epsilon_{\text{filter}})$
$gg \to H \to ZZ \to 4\ell$	Standard	13.34 fb
$qq \to Hqq \to ZZqq \to 4\ell qq$	Standard	1.038 fb
$q\bar{q} \to ZH \to ZZZ \to 4\ell + X$	POWHEG 2.0 (minlo HZJ)	0.618 fb
$q\bar{q} \to W^+H \to W^+ZZ \to 4\ell + X$	POWHEG 2.0 (minlo HWJ)	0.232 fb
$q\bar{q} \to W^-H \to W^-ZZ \to 4\ell + X$	POWHEG 2.0 (minlo HWJ)	0.147 fb
$gg \to ttH \to ttZZ \to 4\ell + X$	Standard	0.139 fb

Process	Dataset Name	$\sigma \cdot BR$
$qq \to ZZ \to 4\ell$	/ZZTo4L_TuneCP5_13TeV_powheg_pythia8/	1.256 pb
$qq \to ZZ \to 4\ell$	/ZZTo4L_TuneCP5_13TeV-amcatnloFXFX-pythia8/	1.212 pb
$gg \to ZZ \to 4e$	/GluGluToContinToZZTo4e_13TeV_MCFM701/	0.00159 pb
$gg \to ZZ \to 4\mu$	/GluGluToContinToZZTo4mu_13TeV_MCFM701/	0.00159 pb
$gg \to ZZ \to 2e2\mu$	/GluGluToContinToZZTo2e2mu_13TeV_MCFM701/	0.00319 pb
$Z \to \ell\ell$ + jets	/DYJetsToLL_M-50_TuneCP5_13TeV-amcatnloFXFX-pythia8/	6225.4 pb
$Z \to \ell\ell$ + jets	/DYJetsToLL_M-10to50_TuneCP5_13TeV-amcatnloFXFX-pythia8/	18610 pb
$WZ \to 3\ell\nu$	/WZTo3LNu_TuneCP5_13TeV-powheg-pythia8/	4.67 pb

HIG-21-009

OBJECTS

- **Electrons**
  - Loose electrons
    - $P_T > 7$GeV; $|\eta| < 2.5$
    - $d_{xy} < 0.5\ cm$; $d_z < 1\ cm$; $SIP_{3D} < 4$
  - BDT cut based on ID+Iso in 6 ($|\eta|$, P_T)bins

- **Muons**
  - Loose muons
    - $P_T > 5$GeV; $|\eta| < 2.4$
    - $d_{xy} < 0.5\ cm$; $d_z < 1\ cm$; $SIP_{3D} < 4$
  - PF muon ID if $P_T < 200$ GeV, PF muon ID or High-pT muon ID if $P_T > 200$ GeV,
  - RelPFIso($\Delta R = 0.3$) < 0.35

$$\mathcal{I}^{\ell} \equiv \left(\sum p_{\mathrm{T}}^{\mathrm{charged}} + \max\left[0, \sum p_{\mathrm{T}}^{\mathrm{neutral}} + \sum p_{\mathrm{T}}^{\gamma} - p_{\mathrm{T}}^{\mathrm{PU}}(\ell)\right] \right) / p_{\mathrm{T}}^{\ell}$$

$$\Delta R(i,j) = \sqrt{(\eta^i - \eta^j)^2 + (\phi^i - \phi^j)^2}$$

- **FSR photon**
  - $P_{T,\gamma} > 2$ GeV;$|\eta^{\gamma}| < 2.4$;relPFIso<1.8
  - Associated γ to the closest loose lepton
  - $\Delta R(\gamma, l) < 0.5$; $\frac{\Delta R(\gamma,l)}{E_{T,\gamma}^2} < 0.012$; choose photon with lowest $\frac{\Delta R(\gamma,l)}{E_{T,\gamma}^2}$
  - Remove selected FSRs from lepton isolation cone for all loose leptons

- **Jets**
  - AK4 PFCHs jets
  - $P_T > 30$ GeV; $|\eta| < 4.7$; Tight PF jet ID
  - Cleaned $\Delta R(jet, l/\gamma) > 0.4$
  - Cut-based jet ID (tight WP); Jet pileup ID (tight WP)

HIG-21-009

Event reconstruction and selections

- Loose e (μ) passing selections $p_T > 7(5)$GeV; $|\eta| < 2.5(2.4)$; vertex cut $d_{xy} < 0.5\ cm$; $d_z < 1\ cm$;$SIP_{3D} < 4$; Tight Selections based on BDT method for e (PF μ RelPFIso< 0.35);
- Z candidate
  - Any OS-SF pair that satisfy $12 < m_{ll(\gamma)} < 120$ GeV
- Build all possible ZZ candidates defined as pairs of non-overlapping Z candidate; define Z_1 candidate with $m_{ll(\gamma)}$ closest to the POG m(Z) mass
  - $m_{Z1} > 40$ GeV; $p_T(l1) > 20$ GeV; $p_T(l2) > 10$ GeV
  - $\Delta R > 0.02$ between each of the four leptons
  - $m_{ll} > 4$ GeV for OS pairs (regardless of flavour)
  - Reject 4μ and 4e candidates where the alternative pair Z_aZ_b satisfies $|m_{Z_a} - m_Z| < |m_{Z_1} - m_Z|$ and $m_{Z_b} < 12$ GeV
  - $m_{4l} > 70$ GeV
- If more than one ZZ candidate is left, take the one with Z_1 mass closest to m_Z and the Z_2 from the candidates whose lepton give higher p_T sum

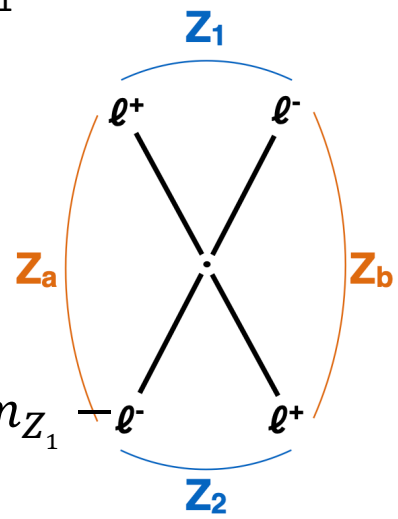

Background estimation

- Irreducible background
  - $q\bar{q} \rightarrow ZZ$
  - $gg \rightarrow ZZ$
  - Estimated using simulation

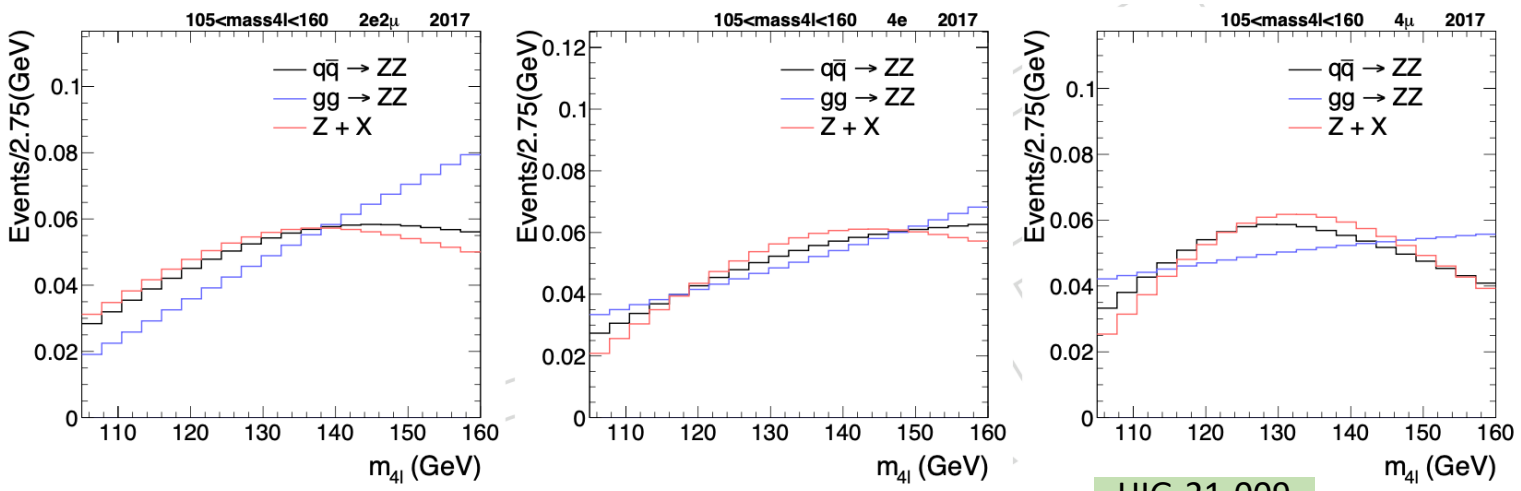

HIG-21-009

- Reducible background
  - Misidentified leptons
  - Secondary produced leptons
  - Two independent methods used to estimated Z+X background: OS and SS
    - Fake rates calculated in Z+l control region
    - Z+X yields estimated in orthogonal regions of Z+ll control region
    - Final estimate combination of 2 methods
  - Templates are built from the control regions in data

Background normalization

- In previous HIG-19-001, ZZ background from MC predictions
  - Both shape and normalization
  - Mass4l [105, 140]
- Several studies carried out to assess the measurement's precision
  - Its ZZ normalization from data sidebands
  - Improvement of estimation as well as **reduction in uncertainties** because luminosity and other theoretical uncertainties no longer contribute to the normalization.
  - **ZZ floating approach**:

      --- inclusive normalization for qqZZ and ggZZ process profiled in the fit

---- only applied in inclusive cross section measurement due to statistics

Systematics Uncertainties

- Experimental uncertainties
  - Integrated luminosity
  - Lepton identification and reconstruction efficiency
  - Reducible background
  - Lepton scale and resolution
  - Jet energy scale

- Theoretical uncertainties
  - **QCD uncertainty**
  - Uncertainty on the Choice of **PDF set**
  - Uncertainty of 2% on H → 4l **branching ratio**

Common experimental uncertainties			
	2016	2017	2018
Luminosity uncorrelated	1 %	2 %	1.5 %
Luminosity correlated 2016–2018	0.6 %	0.9 %	2 %
Luminosity correlated 2017–2018	—	0.6 %	0.2 %
Lepton id/reco efficiencies	0.7–10 %	0.6–8.5 %	0.6–9.5 %
Jet energy scale	0.1%–27%	0.1%–33%	0.1%–33%
Background related uncertainties			
Reducible background (Z+X)	25–43 %	23–36 %	24–36 %
Signal related uncertainties			
Lepton energy scale	0.06% (e)–0.01% (μ)	0.06% (e)–0.01% (μ)	0.06% (e)–0.01% (μ)
Lepton energy resolution	10% (e)–3% (μ)	10% (e)–3% (μ)	10% (e)–3% (μ)

JHEP08(2023)040

Fiducial/Differential Cross Section

- An alternative approach to study the properties of the Higgs boson
- Cross section of bin i is defined as:

$$\sigma_i = \frac{N_{reco,i}}{C_i * A_i * L * B}$$

- **Fiducial cross section** = cross section in fiducial volume (cuts applied to generated events)

$$\sigma_{fid,i} * B = \frac{N_{reco,i}}{C_i * L}$$

- **Higgs boson kinematics**:
  - P_T^H: probes the perturbative QCD modelling of this production mechanism
  - $|\eta^H|$: sensitive to the gluon fusion production mechanism and PDFs
- **Jet activity:** N_{jets}; P_T and η of leading (sub) jet; $\mathcal{T}_B, \mathcal{T}_C$ …
  - sensitive to the theoretical modelling and relative Higgs production.
- **Spin and CP quantum numbers:** Angular observables, such as $\Phi, \Phi_1, \cos\theta_1, \cos\theta_2, |cos\theta^*|$:
  - sensitive to the spin and charge conjugation and parity properties of the Higgs
- **Higgs boson production mechanisms**
  - specific fiducial regions may be constructed

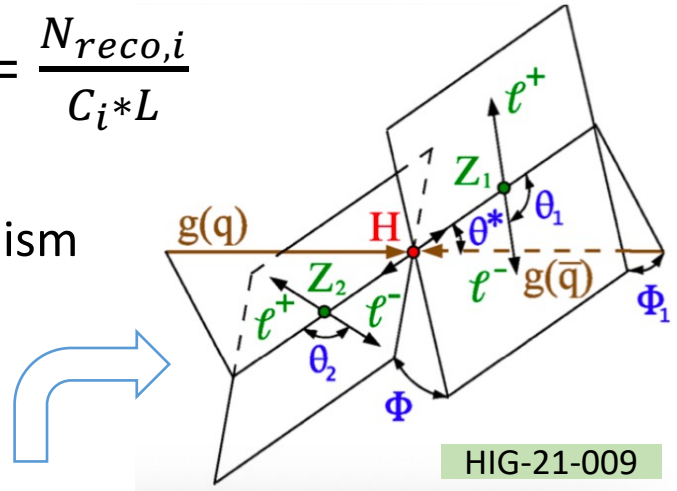

HIG-21-009

Distribution of m_{4l} of Run-2 data

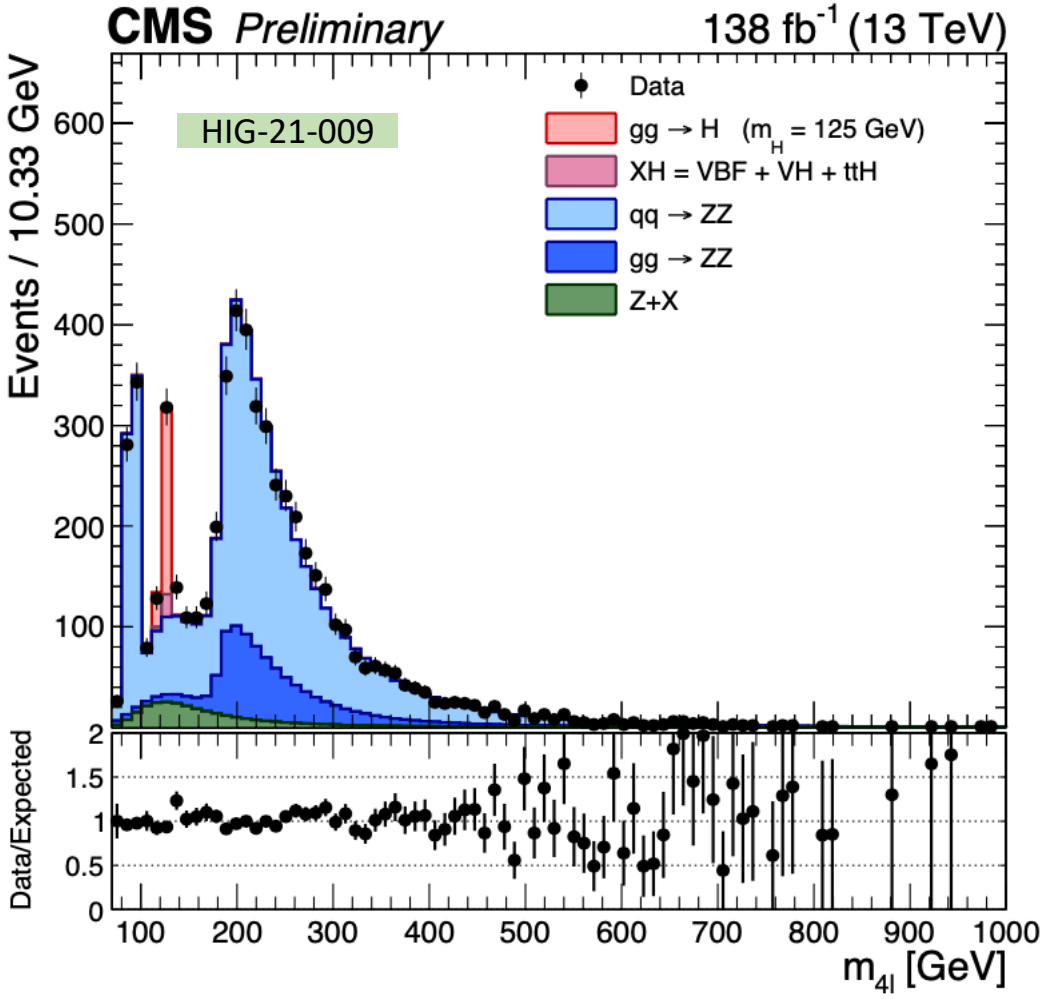

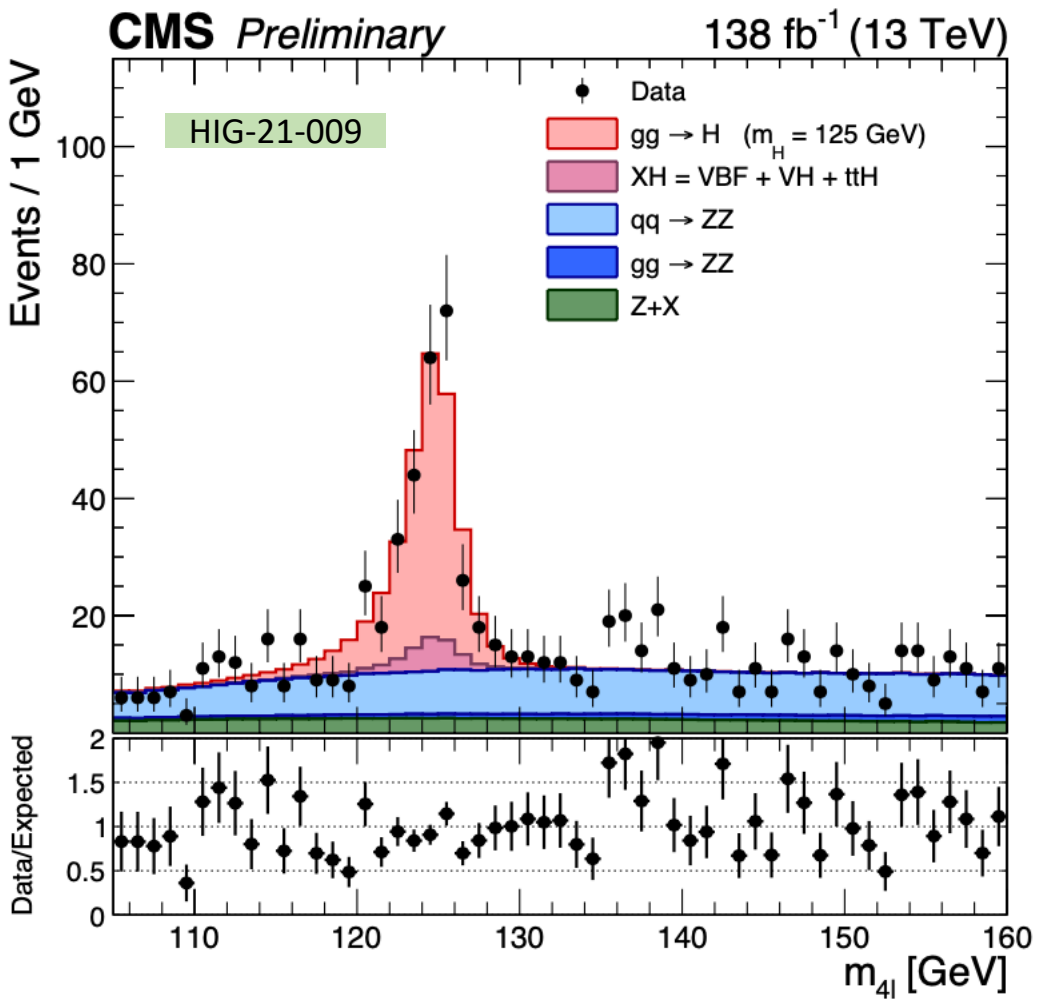

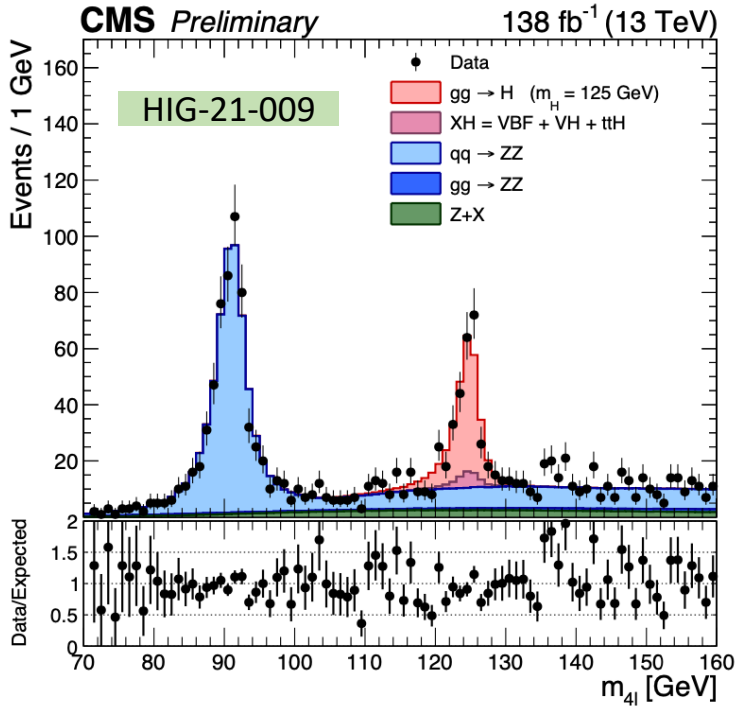

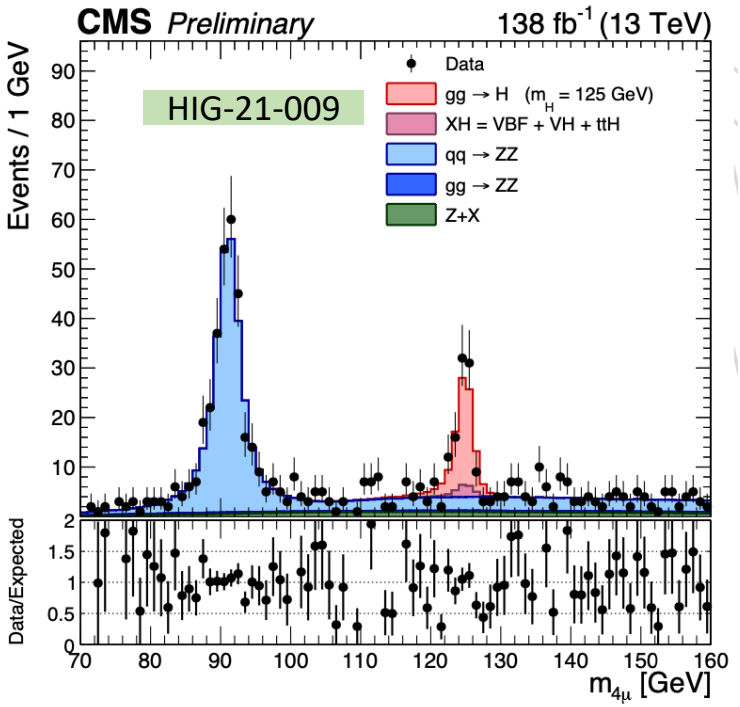

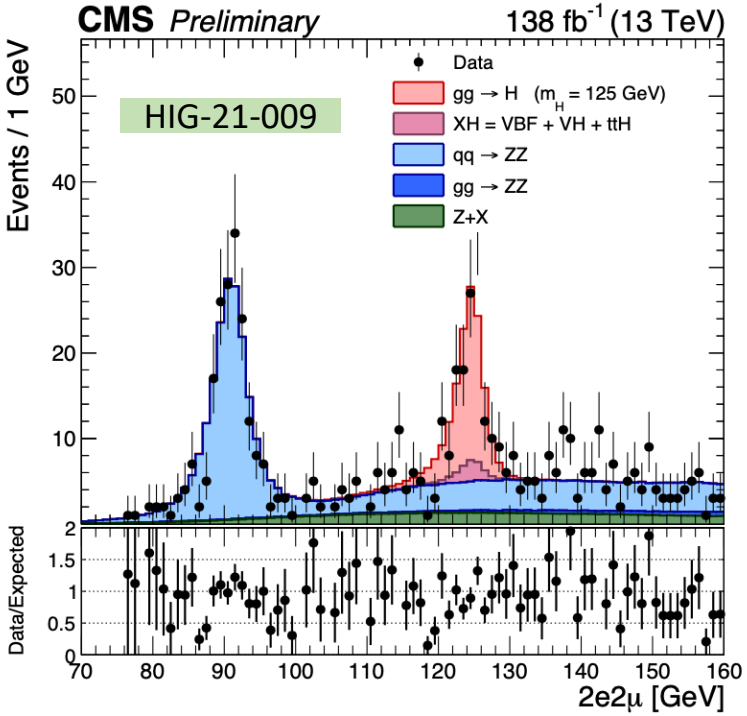

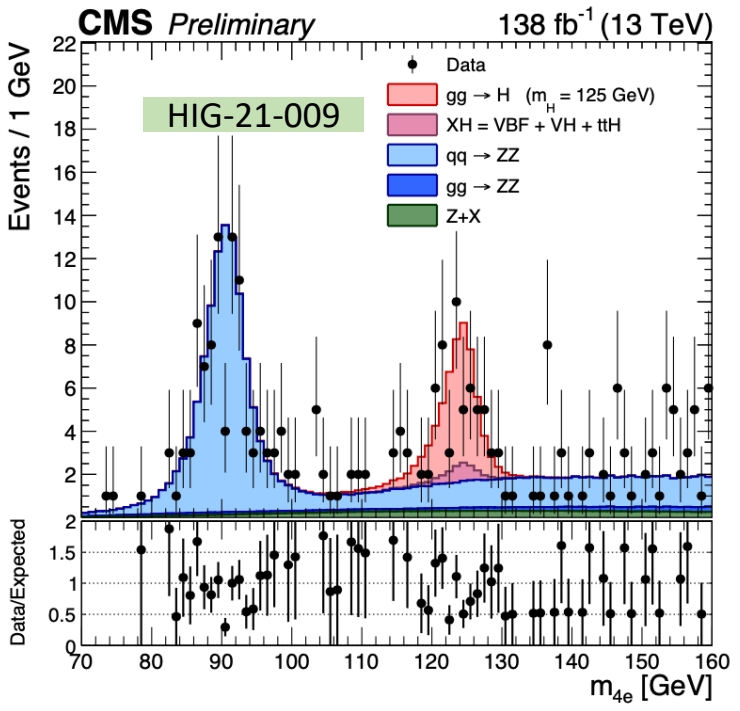

Distribution of m_{4l} of Run-2 data of different final states

1D Observables and bin boundaries of 4l --- production

Observable	Definition	Bin boundaries
$p_{\mathrm{T}}^{\mathrm{H}}$	Transverse momentum of the 4ℓ system	[0,10,20,30,45,60,80,120,200,∞[GeV
$\lvert y_{\mathrm{H}}\rvert$	Rapidity of the 4ℓ system	[0,0.15,0.3,0.45,0.6,0.75,0.9,1.2,1.6,2.5]
N_{jets}	Number of associated jets in the event	$=0$,$=1$,$=2$,$=3$,≥ 4
$p_{\mathrm{T}}^{\mathrm{j}_1}$	Transverse momentum of the leading jet	[0-jet,30,55,95,200,∞[GeV
$p_{\mathrm{T}}^{\mathrm{j}_2}$	Transverse momentum of the subleading jet	[0/1-jet,30,40,65,90,∞[GeV
$\mathcal{T}_{\mathrm{C}}^{\mathrm{max}}$	Rapidity-weighted jet veto	[0-jet|$\mathcal{T}_{\mathrm{C}}^{\mathrm{max}}$,15,20,30,50,80,$\infty$[GeV
$\mathcal{T}_{\mathrm{B}}^{\mathrm{max}}$	Rapidity-weighted jet veto	[0-jet|$\mathcal{T}_{\mathrm{B}}^{\mathrm{max}}$,30,45,75,150,$\infty$[GeV
m_{jj}	Invariant mass of the leading and subleading jets system	[0/1-jet,0,120,300,∞[GeV
$\lvert\Delta\eta_{\mathrm{jj}}\rvert$	Difference in pseudorapidities of the leading and subleading jets	[0/1-jet,0.0,1.6,3.0,10.0]
$\Delta\phi_{\mathrm{jj}}$	Azimuthal angle difference between the leading and subleading jets	[0/1-jet,$-\pi$, $-\pi/2$, 0, $\pi/2$, π]
$p_{\mathrm{T}}^{\mathrm{Hj}}$	Transverse momentum of the 4ℓ and leading jet system	[0-jet,0,30,50,110,∞[GeV
m_{Hj}	Invariant mass of the 4ℓ and leading jet system	[0-jet,110,180,220,300,400,600,∞[GeV
$p_{\mathrm{T}}^{\mathrm{Hjj}}$	Transverse momentum of the 4ℓ, leading and subleading jets system	[0/1-jet,0,20,60,∞[GeV

JHEP08(2023)040

- The variables in green circle are new observables compared with presented in HIG-19-001.

1D Observables and bin boundaries of 4l --- decay

Observable	Definition	Bin boundaries
$\cos\theta^*$	Cosine of the decay angle of the leading lepton pair in the 4ℓ rest frame	[-1.0,-0.75,-0.50,-0.25,0.0,0.25,0.50,0.75,1.0]
$\cos\theta_1$, $\cos\theta_2$	Cosine of the production angle, relative to the Z vector, of the antileptons from the two Z bosons	[-1.0,-0.75,-0.50,-0.25,0.0,0.25,0.50,0.75,1.0]
Φ, Φ_1	Azimuthal angles between the decay planes	$[-\pi, -3\pi/4, -\pi/2, -\pi/4, 0, \pi/4, \pi/2, 3\pi/4, \pi]$
m_{Z_1}	Invariant mass of the two leading leptons	[40,65,75,85,92,120] GeV
m_{Z_2}	Invariant mass of the two subleading leptons	[12,20,25,28,32,40,50,65] GeV
$\mathcal{D}^{\text{dec}}_{0-}$	Matrix element discriminant targeting a_3 coupling	[0.0,0.4,0.5,0.6,0.7,0.8,0.9,1.0]
$\mathcal{D}^{\text{dec}}_{0h+}$	Matrix element discriminant targeting a_2 coupling	[0.0,0.35,0.4,0.45,0.55,0.65,0.75,1.0]
$\mathcal{D}^{\text{dec}}_{\Lambda 1}$	Matrix element discriminant targeting k_1 coupling	[0.0,0.45,0.5,0.6,0.7,1.0]
$\mathcal{D}^{\text{Z}\gamma,\text{dec}}_{\Lambda 1}$	Matrix element discriminant targeting $k_2^{Z\gamma}$ coupling	[0.0,0.35,0.45,0.5,0.55,0.65,1.0]
$\mathcal{D}^{\text{dec}}_{\text{CP}}$	Interference matrix element discriminant targeting a_3 coupling	[-0.75,-0.25,-0.1,0.0,0.1,0.25,0.75]
$\mathcal{D}^{\text{dec}}_{\text{int}}$	Interference matrix element discriminant targeting a_2 coupling	[0.0,0.7,0.8,0.9,0.95,1.0]

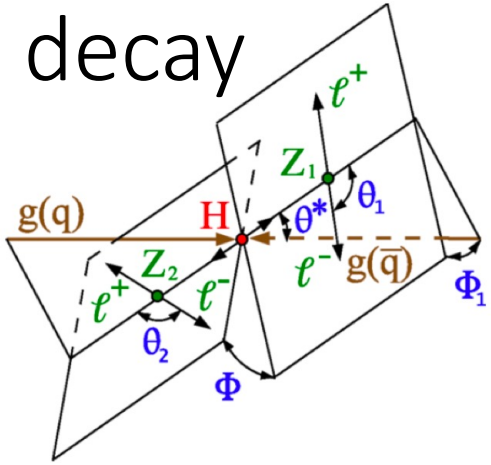

Since the final state is sensitive to interference effects, differential cross sections of ***decay*** are also measured in the ***same-flavor*** and ***different flavor*** final states.

JHEP08(2023)040

- The variables in green circle are new observables compared with presented in HIG-19-001.

Bin boundaries for 2D differential measurement

Observable	Bin 1	Bin 2	Bin 3	Bin 4	Bin 5	Bin 6	Bin 7	Bin 8	Bin 9	Bin 10	Bin 11	Bin 12
m_{Z_1}(GeV)	[40,85]	[40,70]	[70,120]	[85,120]	[85,120]	[85,120]						
m_{Z_2}(GeV)	[12,35]	[35,65]	[35,65]	[30,35]	[24,30]	[12,24]						
$\lvert y_H \rvert$	[0,0.5]	[0,0.5]	[0,0.5]	[0,0.5]	[0.5,1.0]	[0.5,1.0]	[0.5,1.0]	[1.0,2.5]	[1.0,2.5]	[1.0,2.5]		
p_T^H(GeV)	[0,40]	[40,80]	[80,150]	[150,∞[	[0,45]	[45,120]	[120,∞[	[0,45]	[45,120]	[120,∞[		
N_{jets}	0	0	0	1	1	1	1	>= 2	>= 2	>= 2	>= 2	
p_T^H(GeV)	[0,15]	[15,30]	[30,∞[	[0,60]	[60,80]	[80,120]	[120,∞[	[0,100]	[100,170]	[170,250]	[250,∞[	
$p_T^{j_1}$(GeV)	$N_{jets} < 2$	[30,60]	[60,350]	[60,350]								
$p_T^{j_2}$(GeV)		[30,60]	[30,60]	[60,350]								
p_T^{Hj}(GeV)	$N_{jets} < 1$	[0,30]	[0,45]	[30,350]	[45,350]							
p_T^H(GeV)		[0,85]	[85,350]	[0,85]	[85,350]							
$\mathcal{T}_C^{max}$(GeV)	0-jet|$\mathcal{T}_C^{max}$	0-jet|$\mathcal{T}_C^{max}$	0-jet|$\mathcal{T}_C^{max}$	0-jet|$\mathcal{T}_C^{max}$	0-jet|$\mathcal{T}_C^{max}$	0-jet|$\mathcal{T}_C^{max}$	[15,25]	[15,25]	[25,40]	[25,40]	[40,∞[	[40,∞[
p_T^H(GeV)	[0,15]	[15,30]	[30,45]	[45,70]	[70,120]	[120,∞[	[0,120]	[120,∞[	[0,120]	[120,∞[	[0,200]	[200,∞[

JHEP08(2023)040

Distribution of p_T^H and $|y_H|$

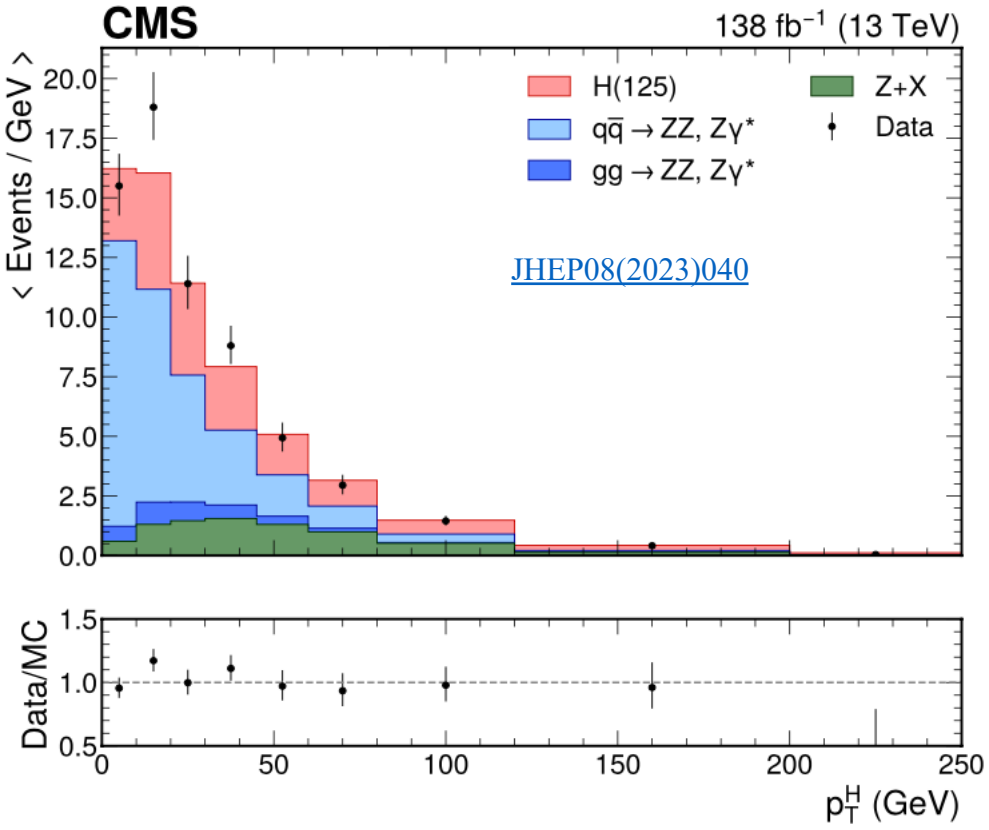

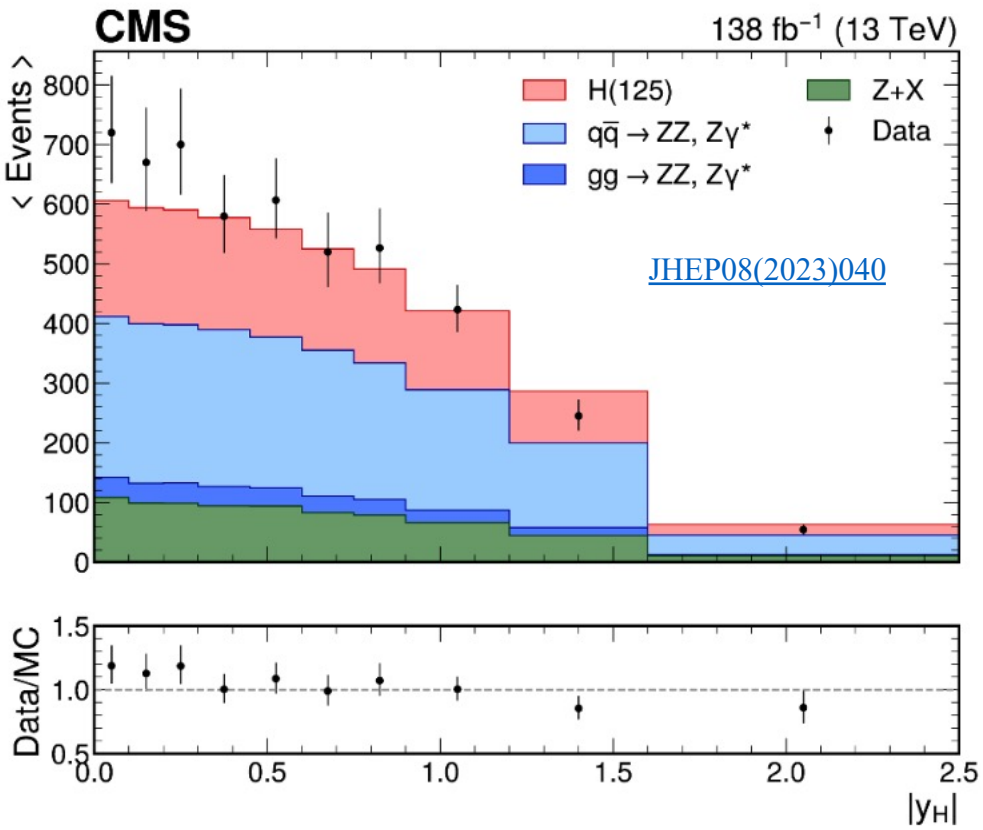

- Points with error bars represent the data, while the solid histograms represent the MC simulation.

Results of inclusive fiducial cross section

	4e	4μ	2e2μ	Inclusive
		Constrained ZZ background		
σ_{fid}	$0.59^{+0.13}_{-0.12}$ fb	$0.75^{+0.10}_{-0.09}$ fb	$1.33^{+0.17}_{-0.16}$ fb	$2.73^{+0.22}_{-0.22}\,(\text{stat})^{+0.15}_{-0.14}\,(\text{syst})$ fb
		Unconstrained ZZ background		
σ_{fid}	$0.57^{+0.15}_{-0.12}$ fb	$0.75^{+0.10}_{-0.09}$ fb	$1.37^{+0.17}_{-0.16}$ fb	$2.74^{+0.24}_{-0.23}\,(\text{stat})^{+0.14}_{-0.11}\,(\text{syst})$ fb
N^{ZZ}	92^{+16}_{-13}	162^{+19}_{-18}	193^{+23}_{-21}	$445^{+27}_{-26}\,(\text{stat})^{+21}_{-19}\,(\text{syst})$
N^{ZZ}_{MC}	74^{+7}_{-8}	152^{+7}_{-8}	188^{+13}_{-14}	414^{+24}_{-28}

- The measured inclusive fiducial cross section and ±1 standard deviation uncertainties for different final states at *m*H = 125.38 GeV.
- The statistical and systematic uncertainties are given separately for the inclusive measurements.
- Comparison of the inclusive fiducial cross section measurement by two methods
  - normalization of the ZZ irreducible background processes taken from MC simulation
  - normalization of the ZZ irreducible background processes as an unconstrained parameter in the fit.

JHEP08(2023)040

Correlation

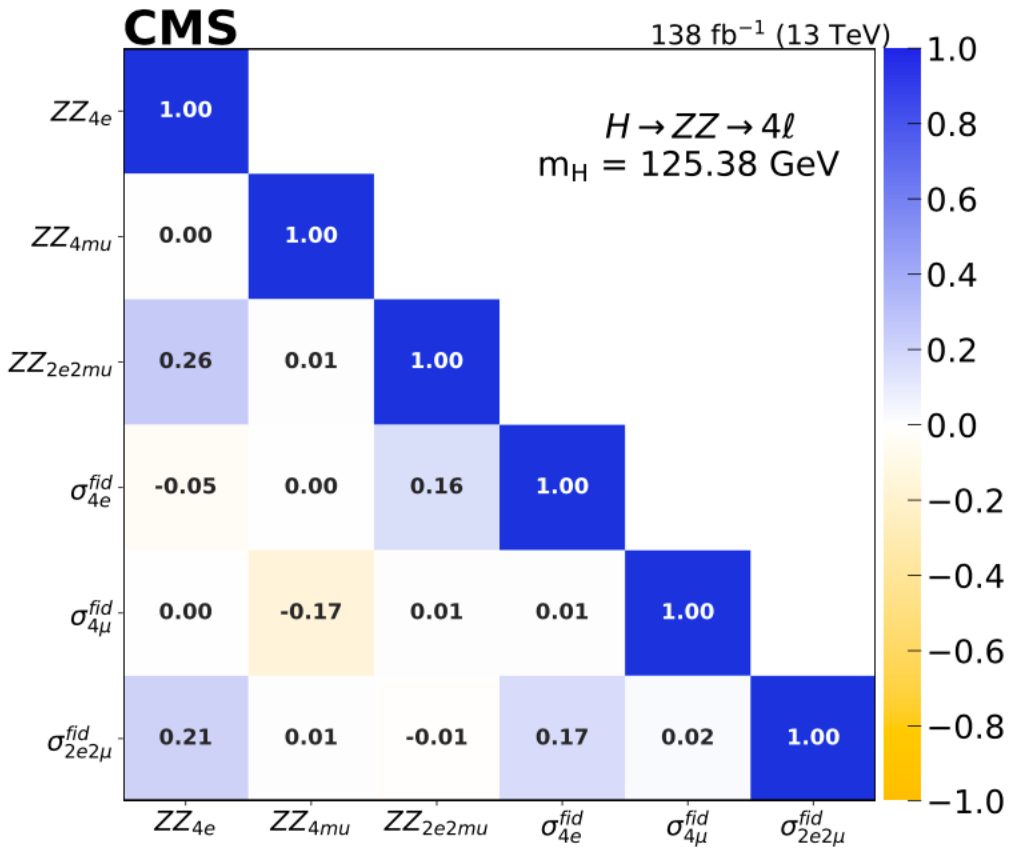

JHEP08(2023)040

- Correlations between the fiducial cross sections in each final state and the ZZ normalization (right).

1D differential cross section measurements

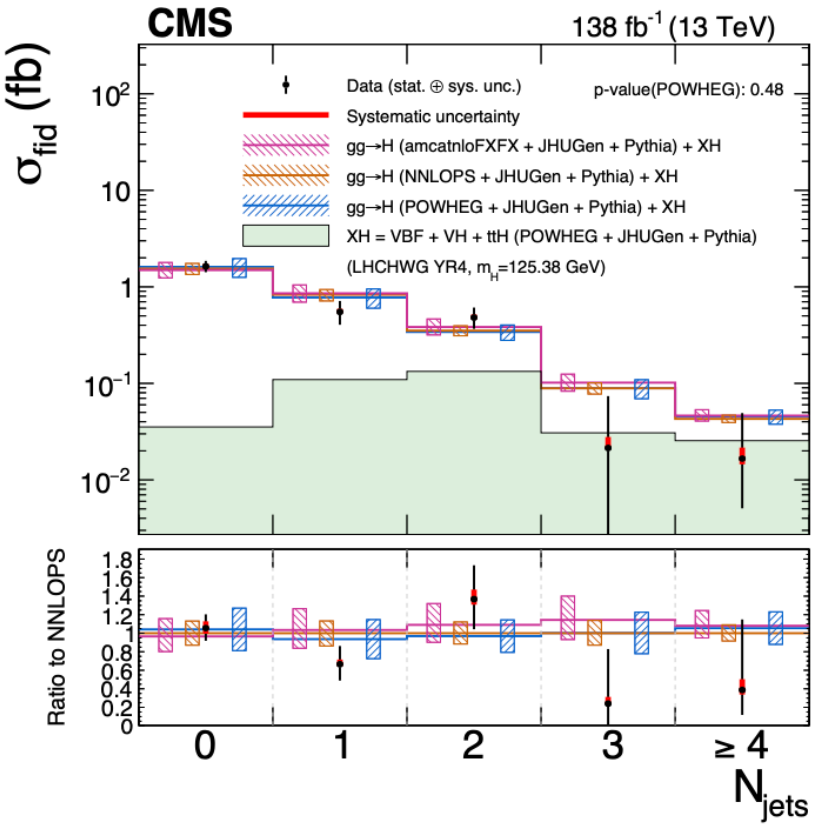

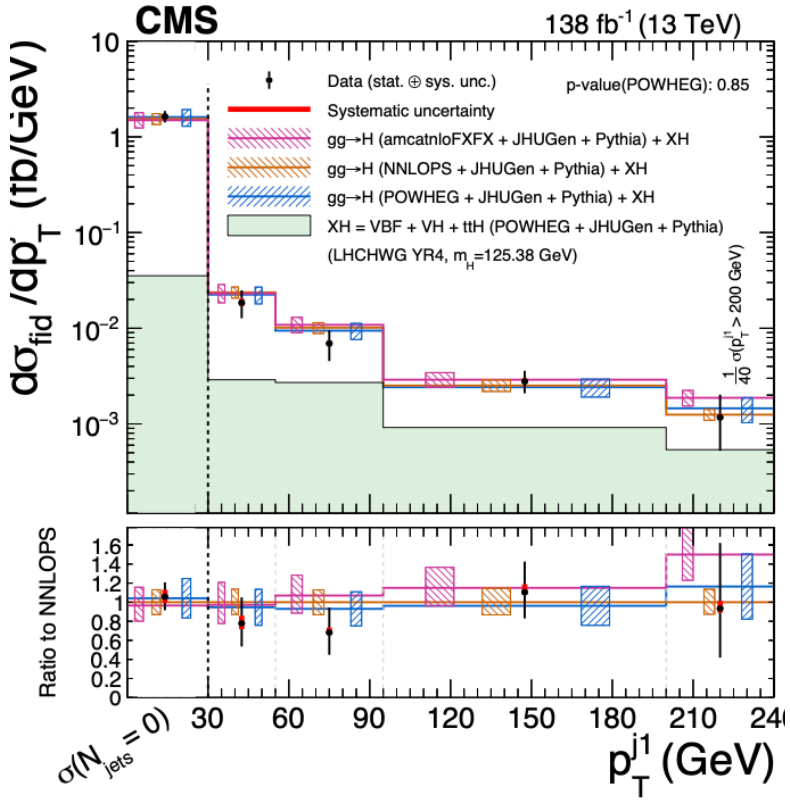

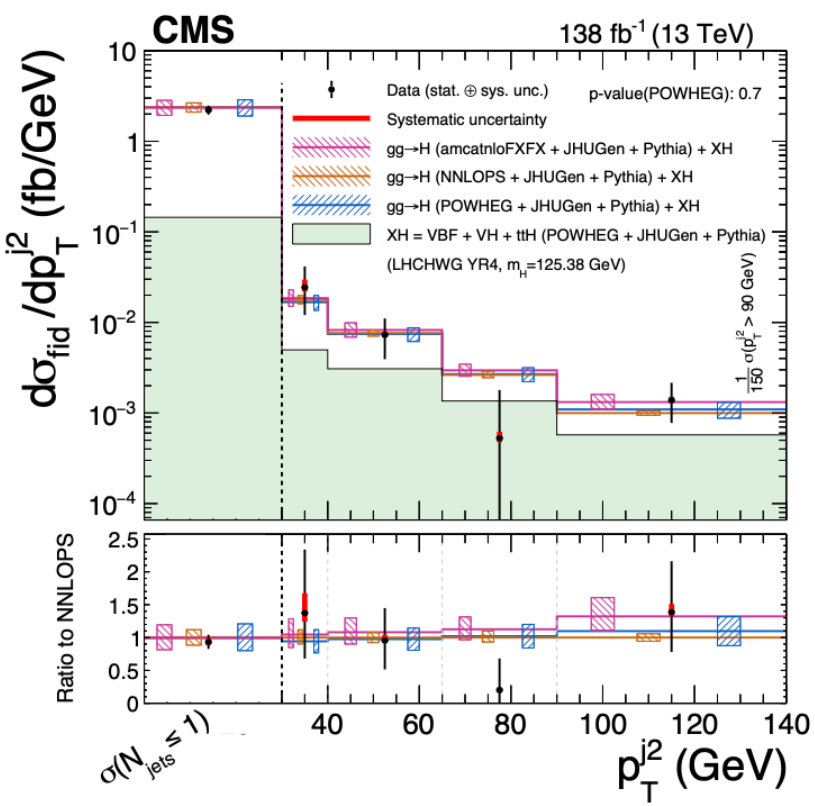

JHEP08(2023)040

1D differential cross section measurements

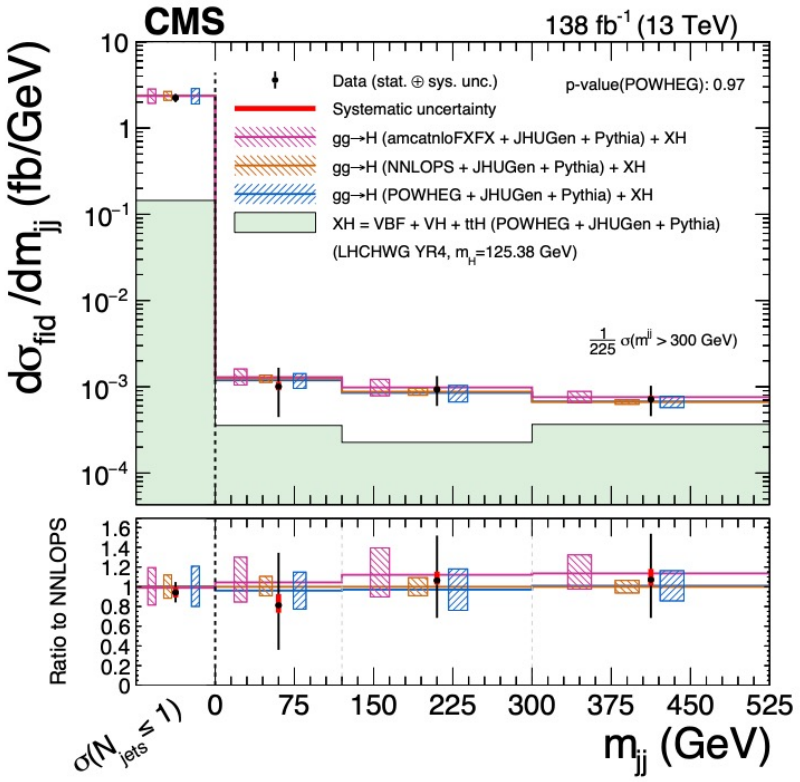

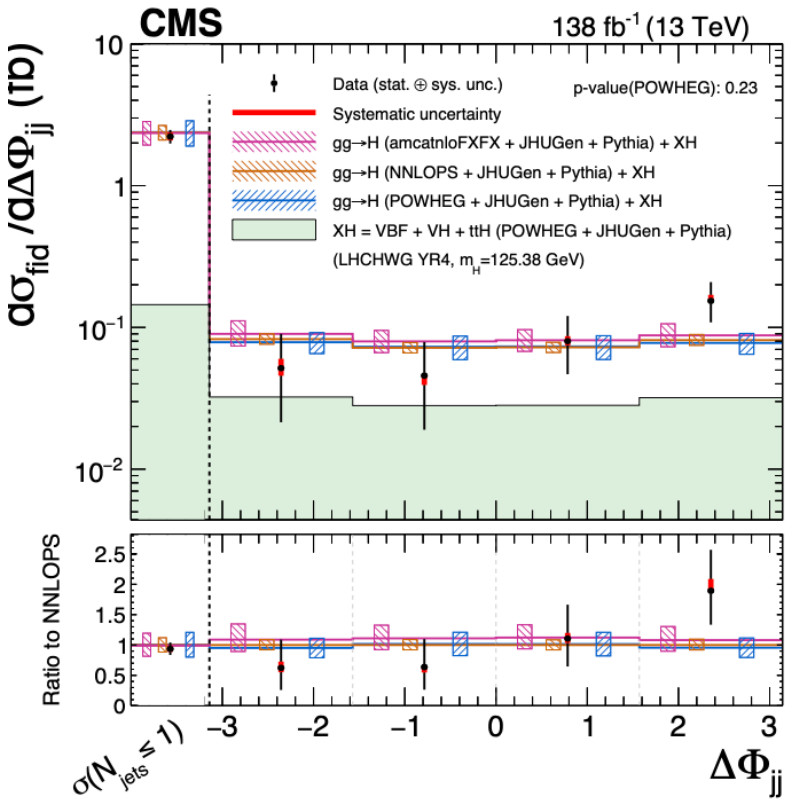

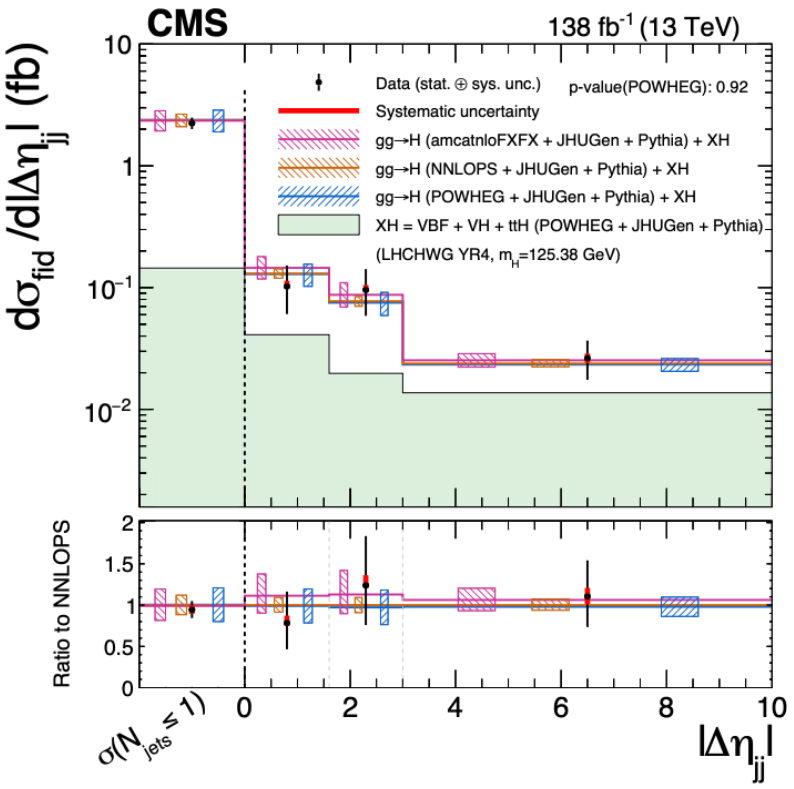

JHEP08(2023)040

1D differential cross section measurements

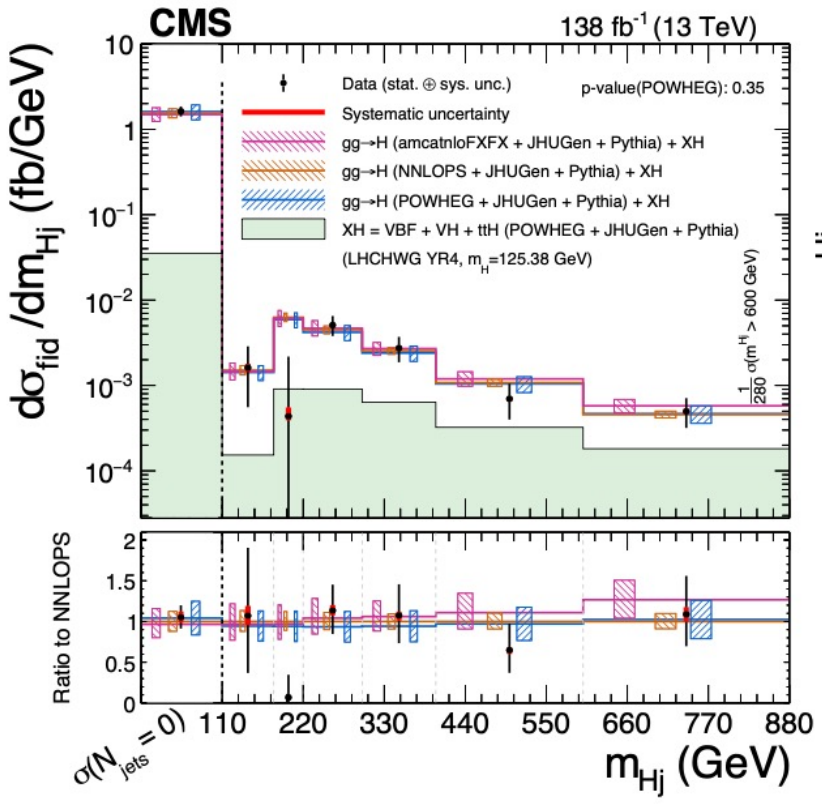

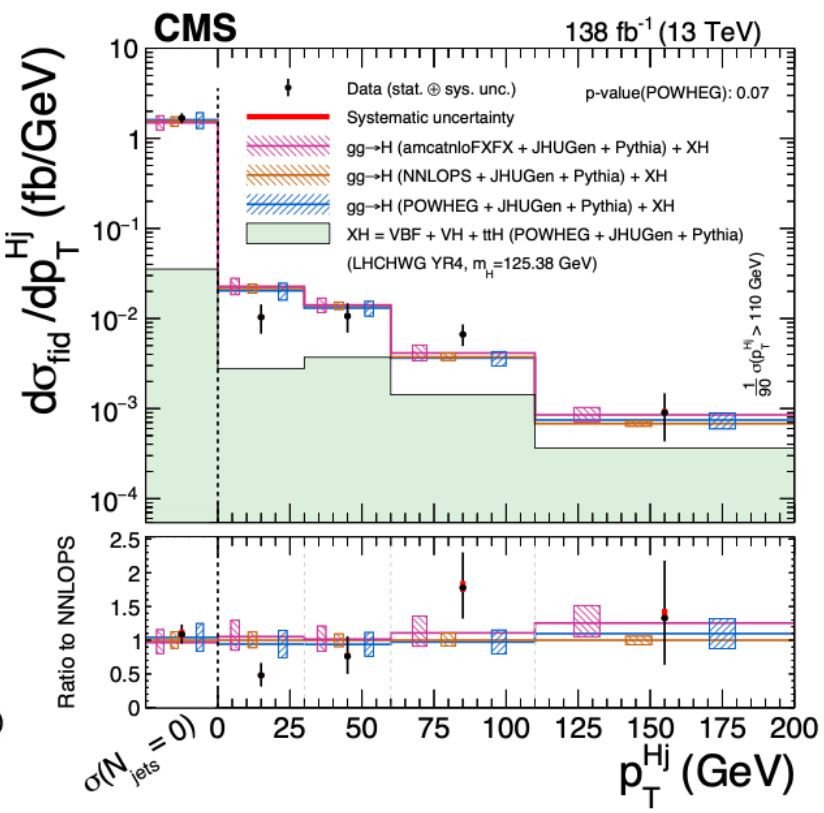

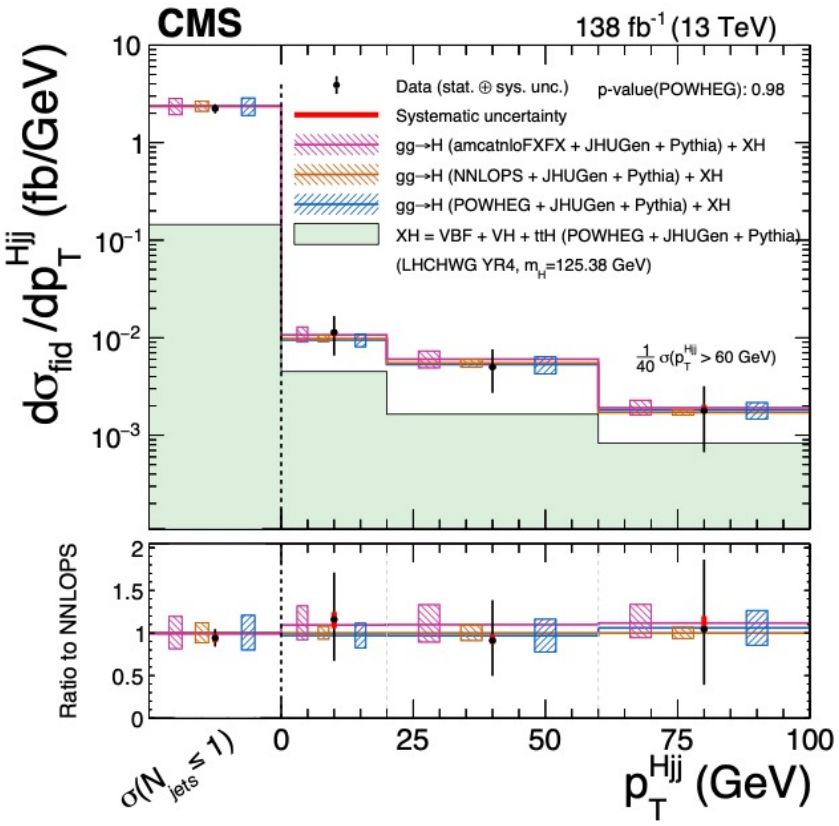

JHEP08(2023)040

1D differential cross section measurements

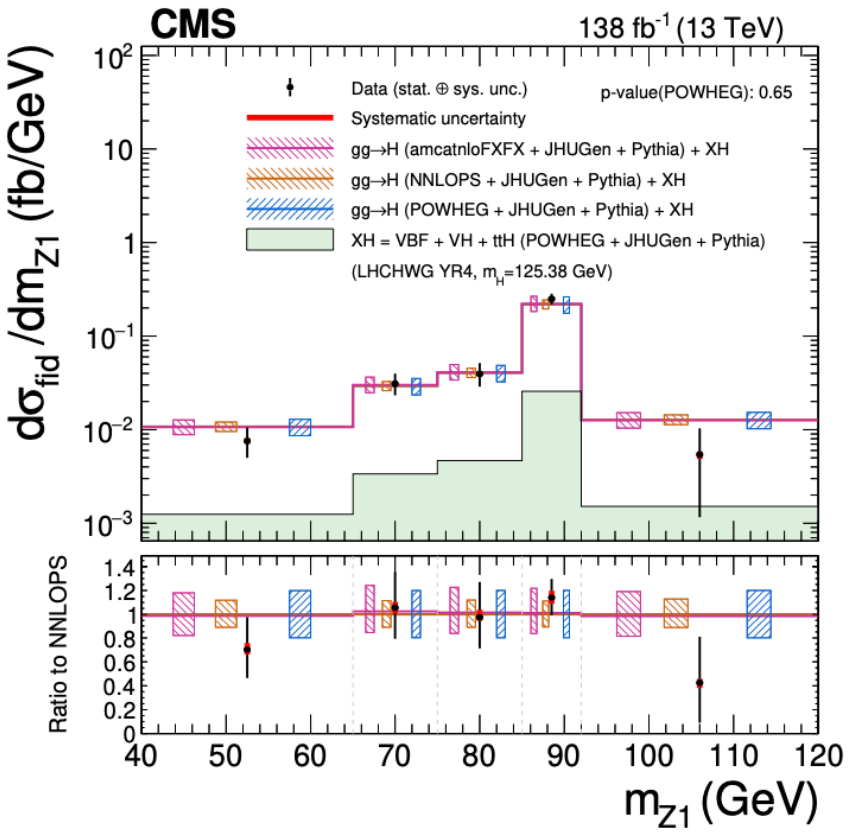

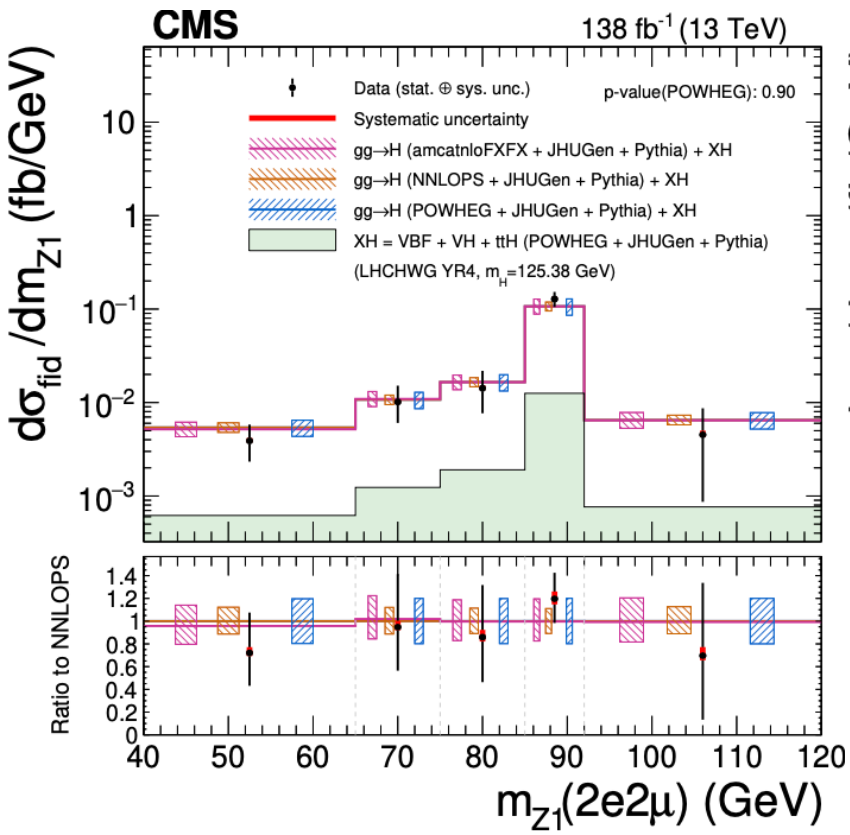

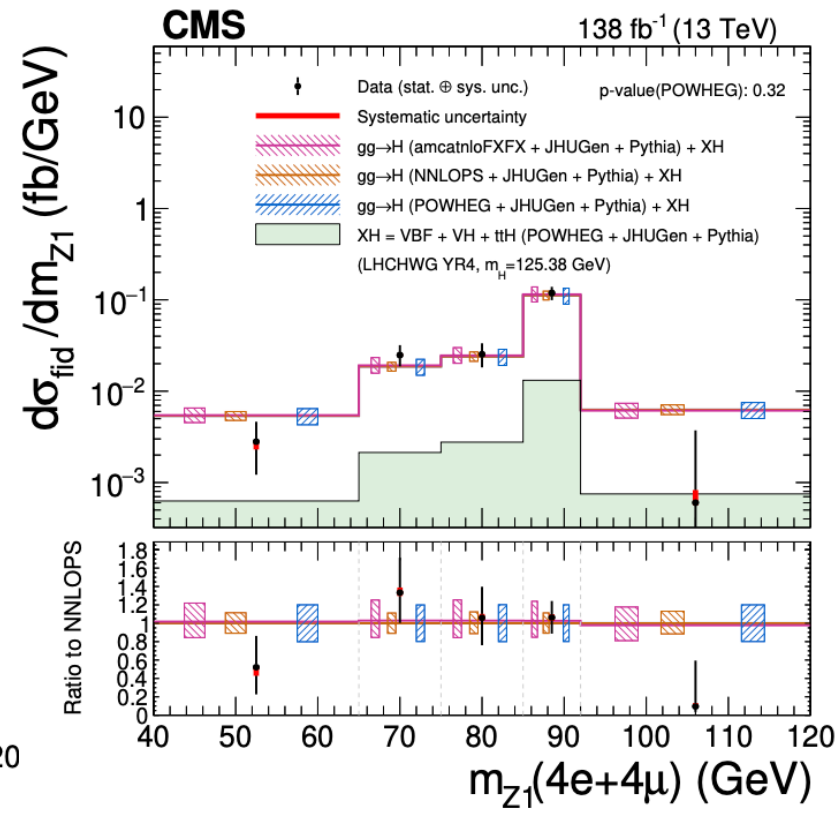

JHEP08(2023)040

1D differential cross section measurements

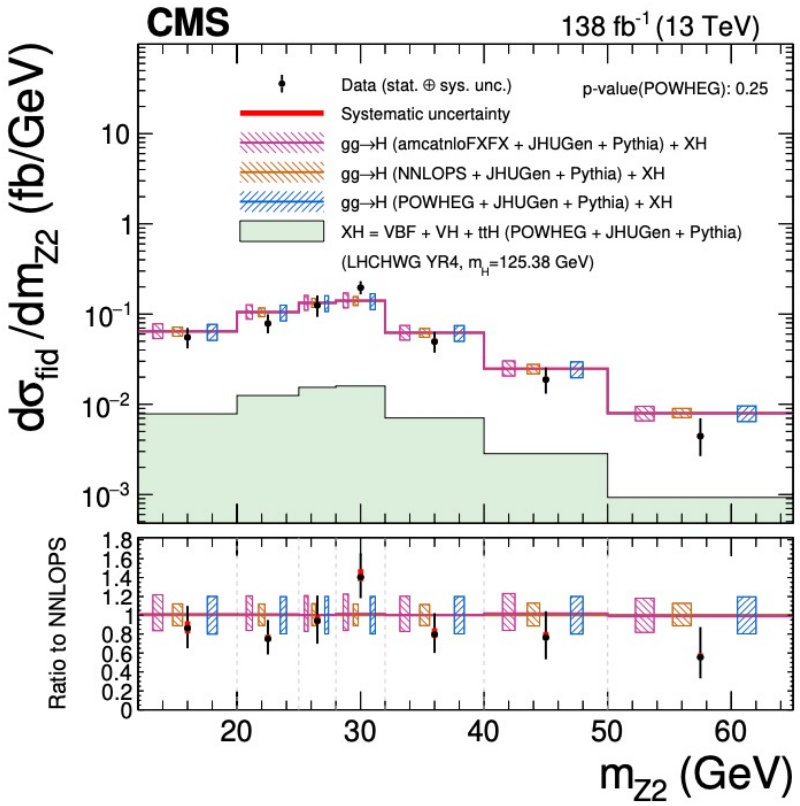

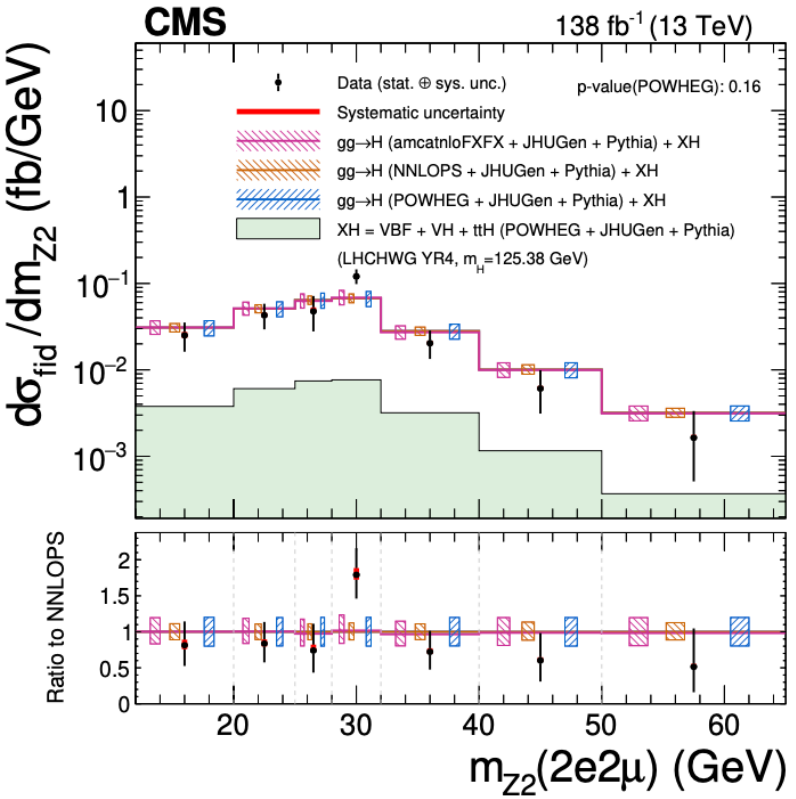

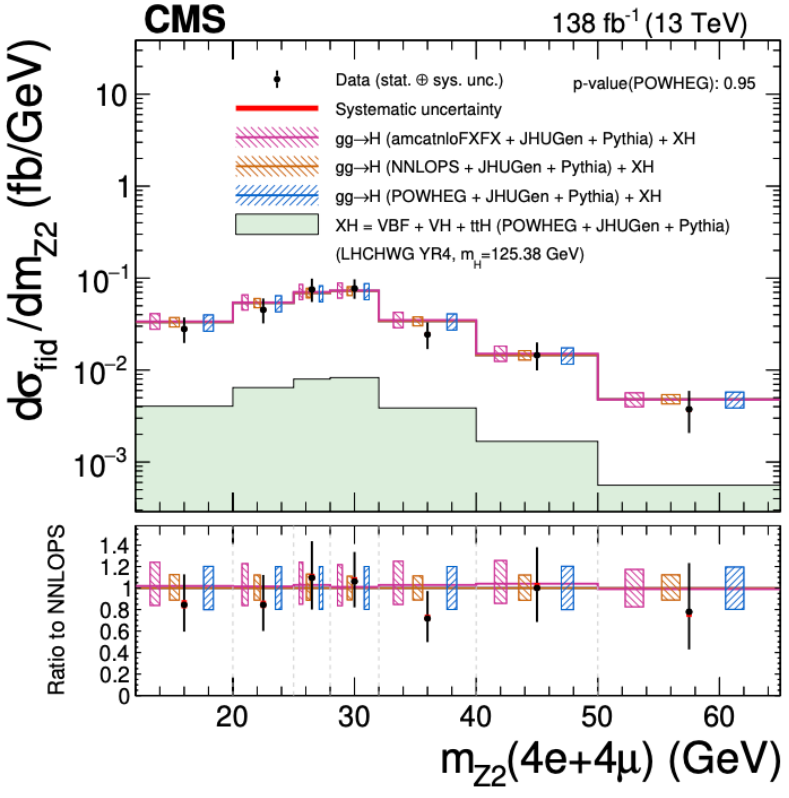

JHEP08(2023)040

1D differential cross section measurements

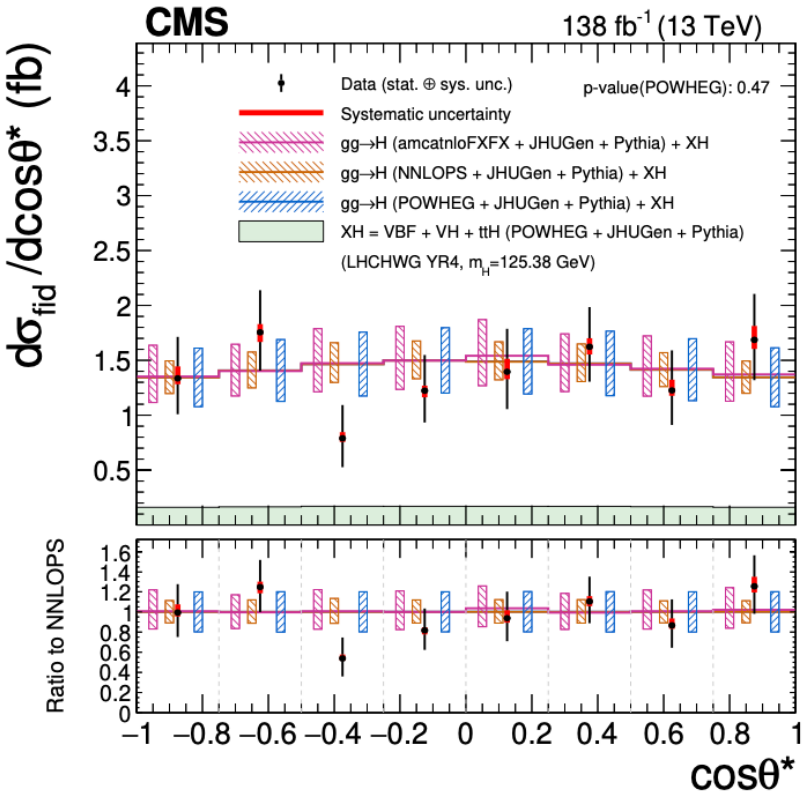

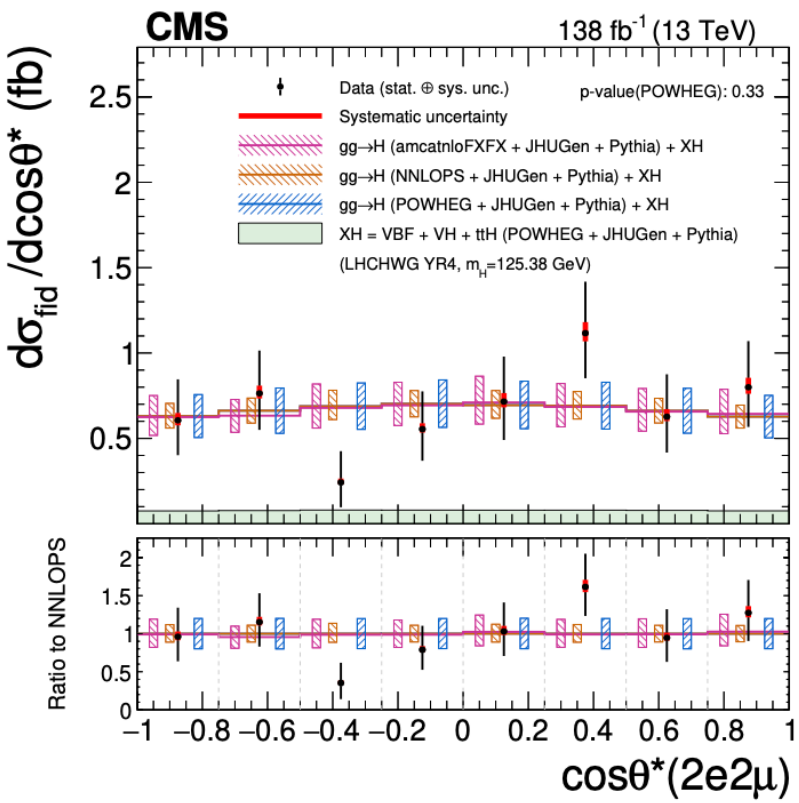

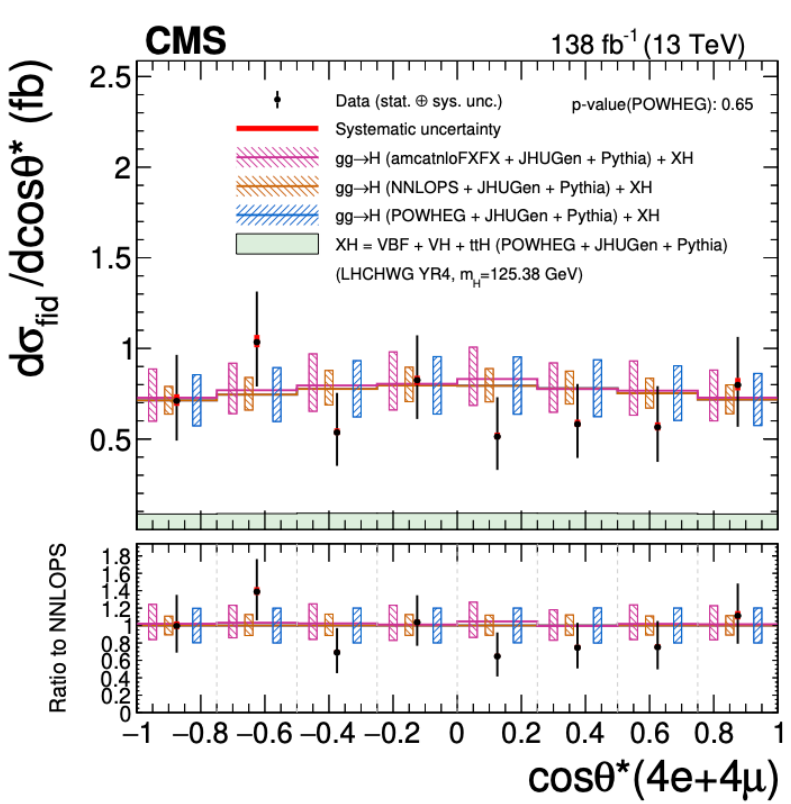

JHEP08(2023)040

1D differential cross section measurements

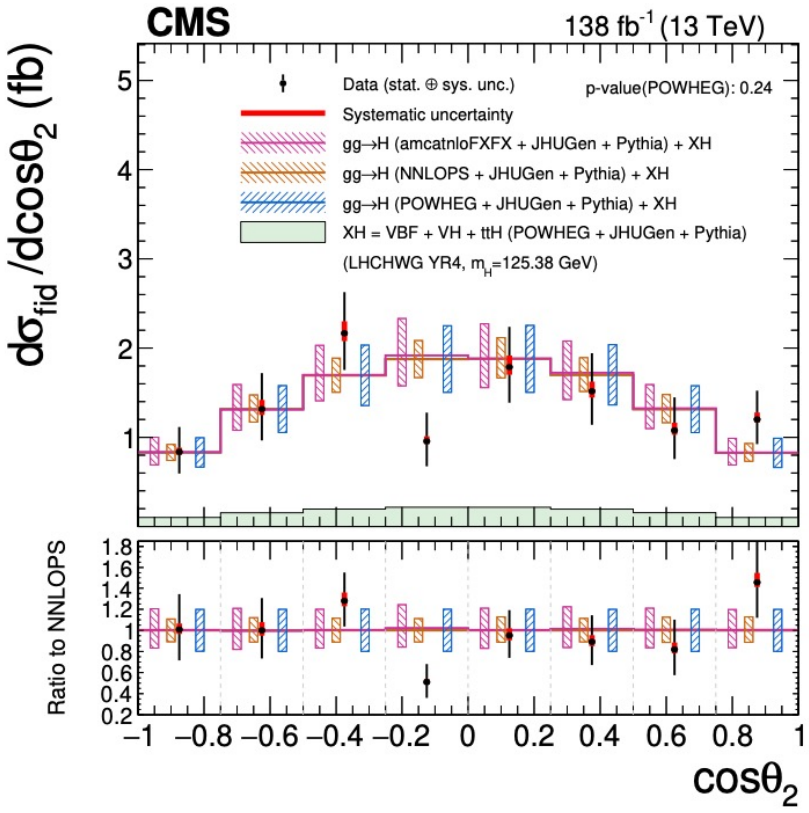

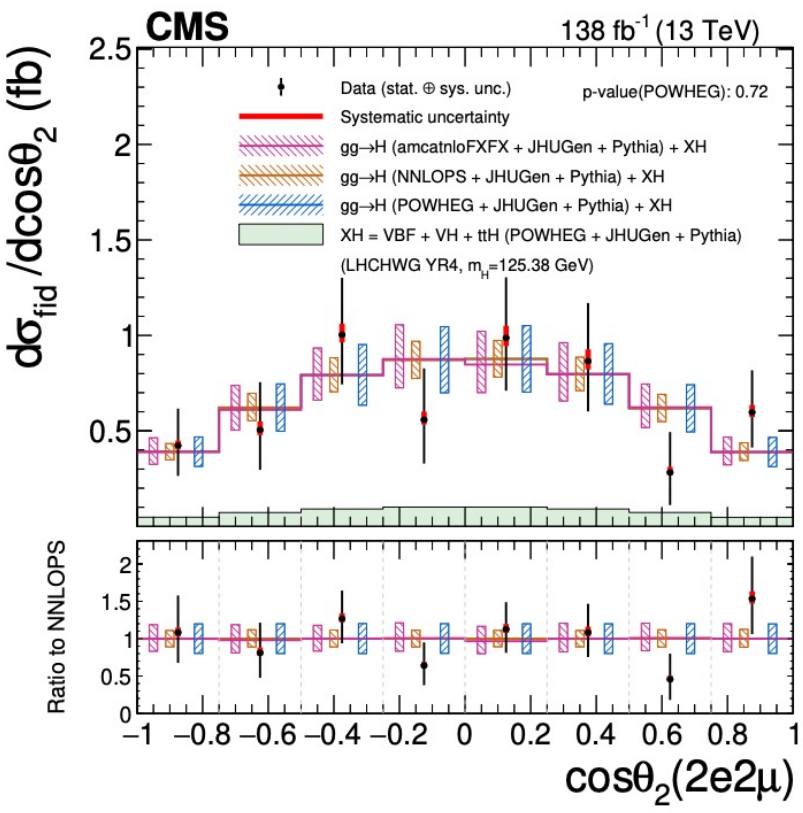

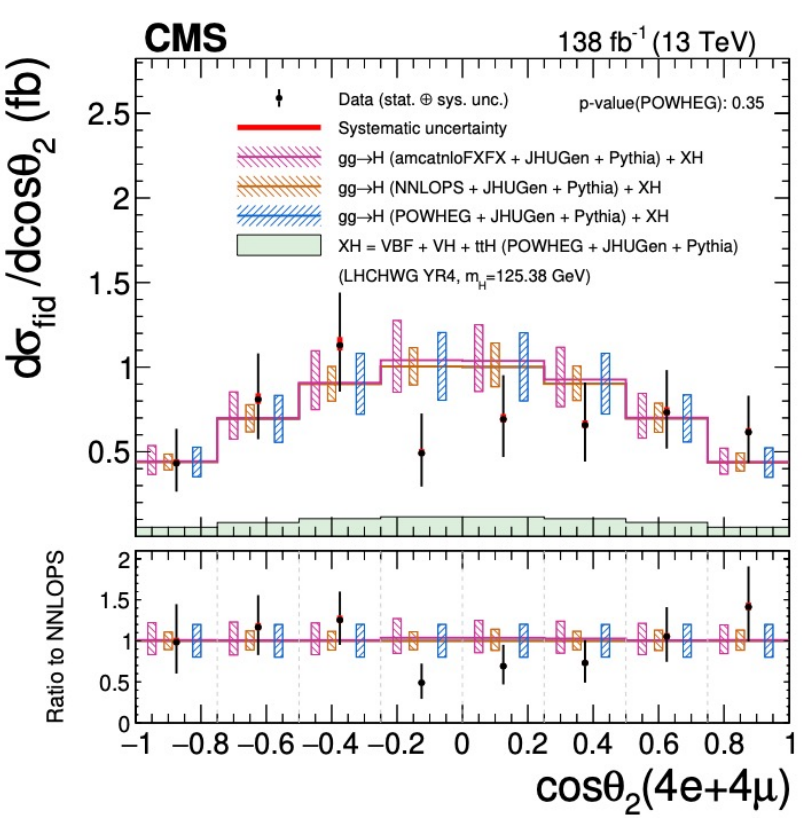

JHEP08(2023)040

1D differential cross section measurements

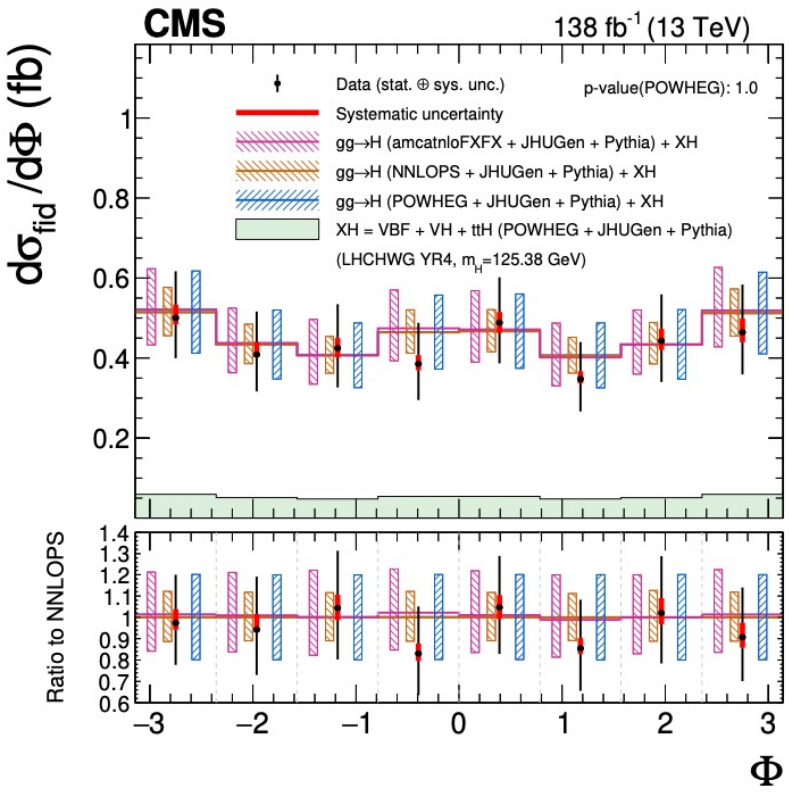

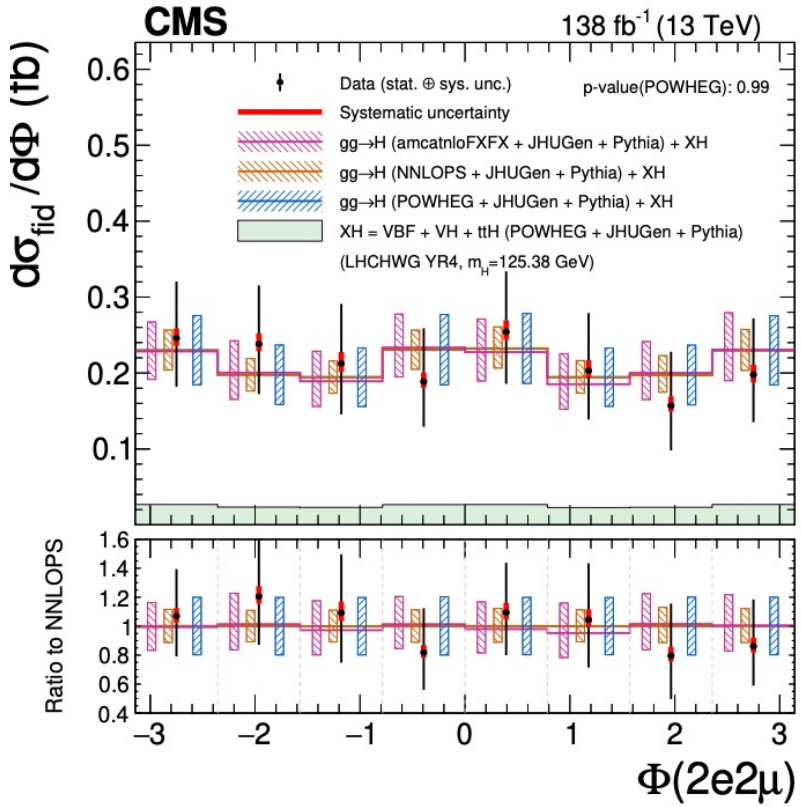

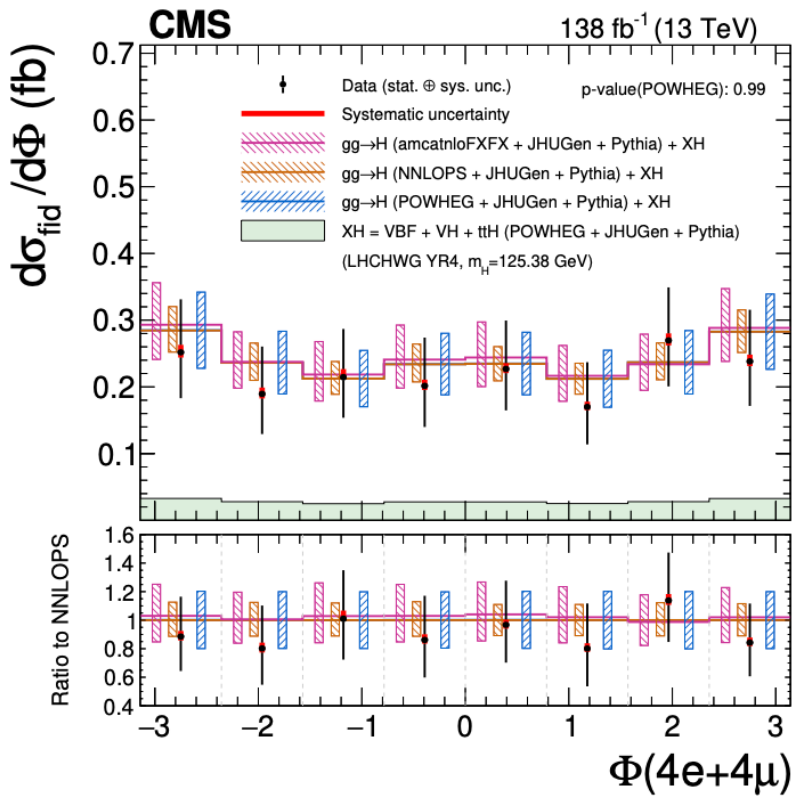

JHEP08(2023)040

1D differential cross section measurements

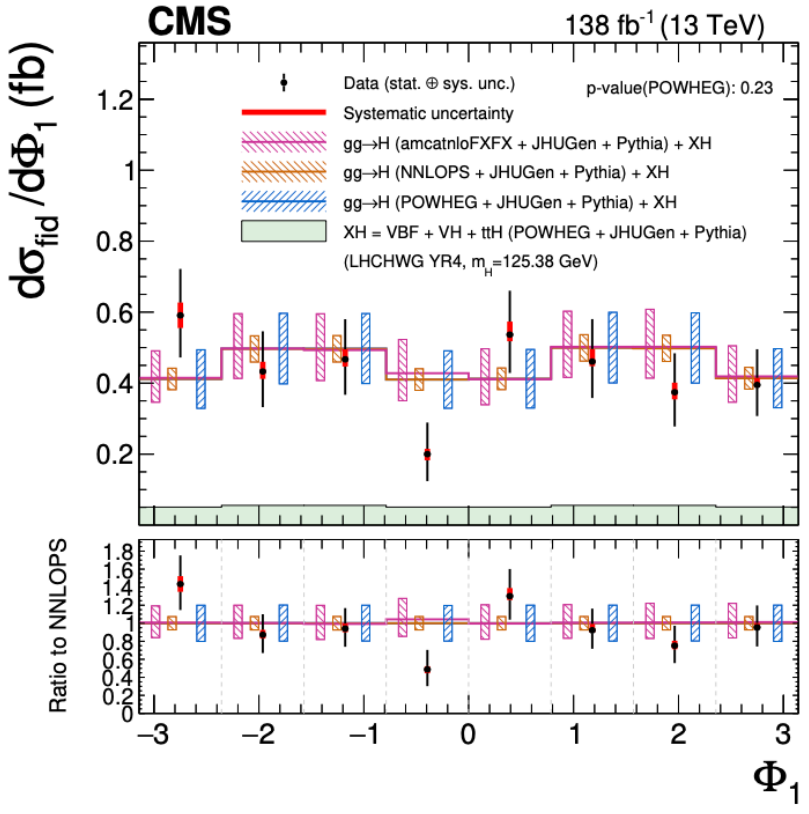

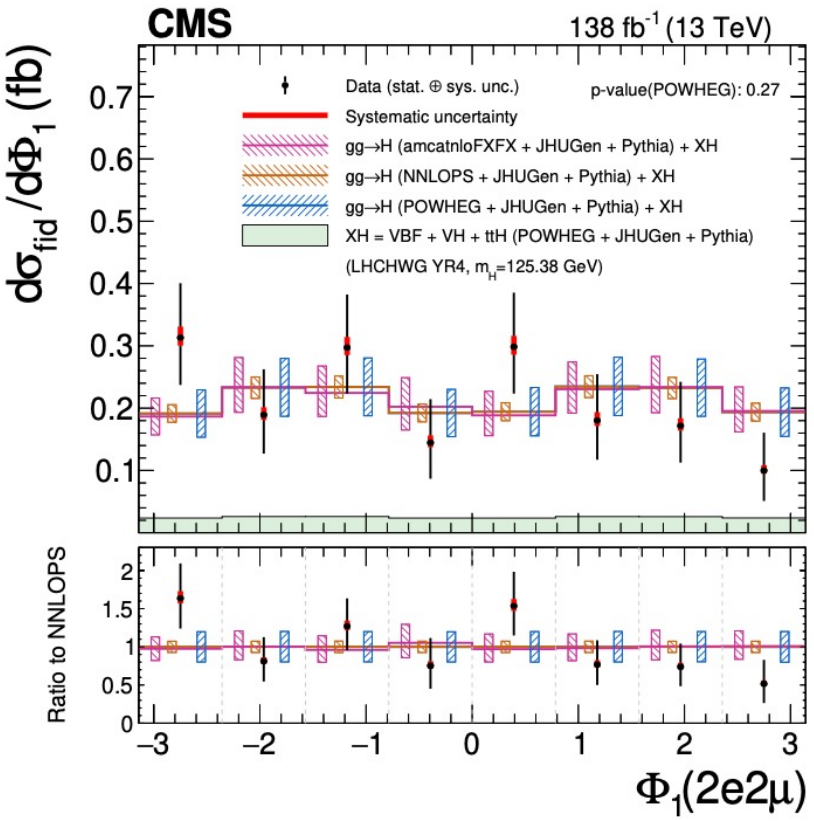

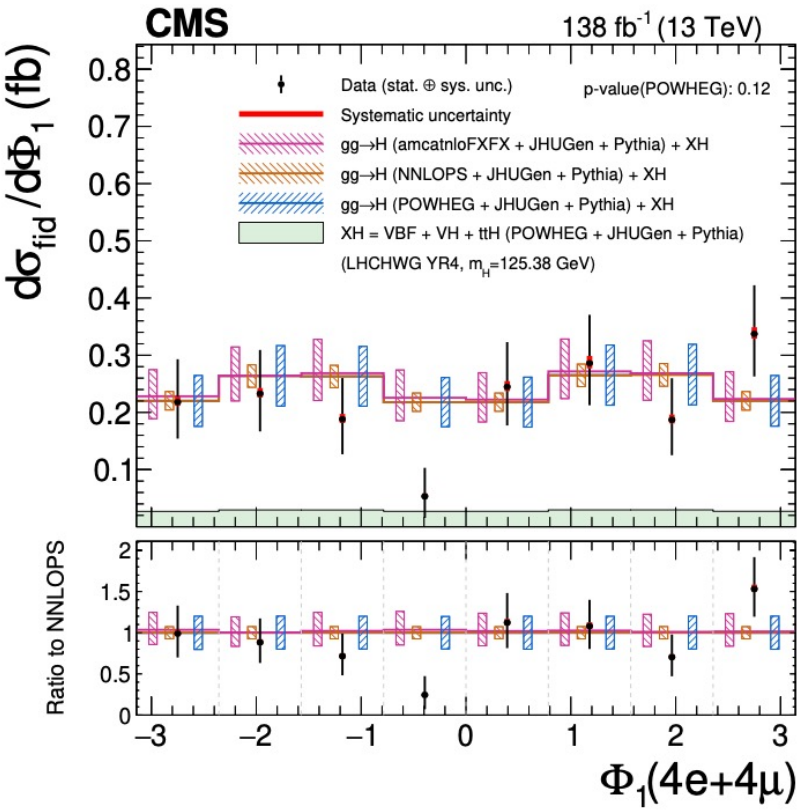

JHEP08(2023)040

1D differential cross section measurements

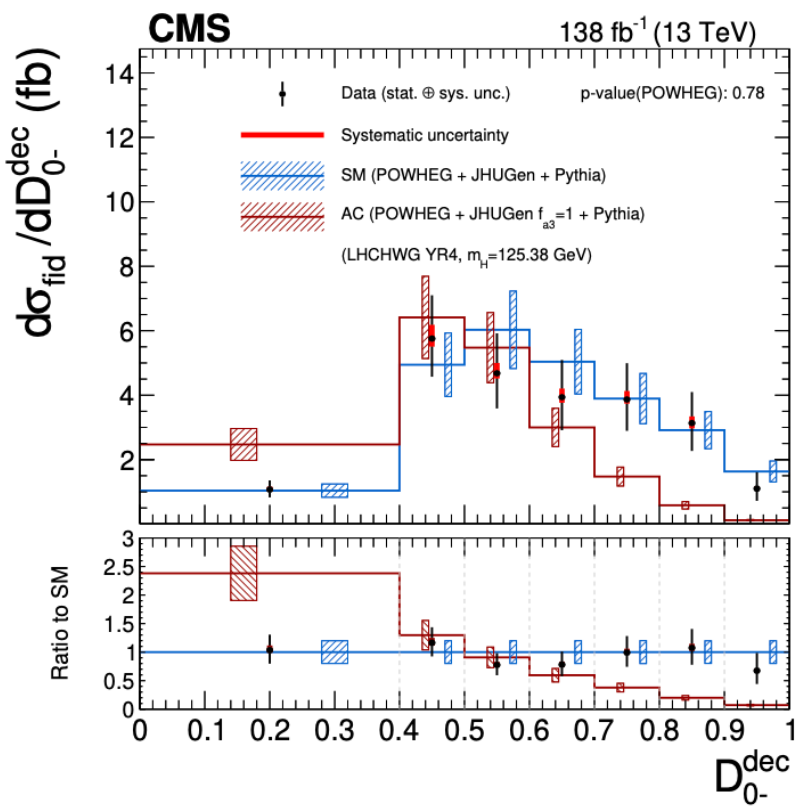

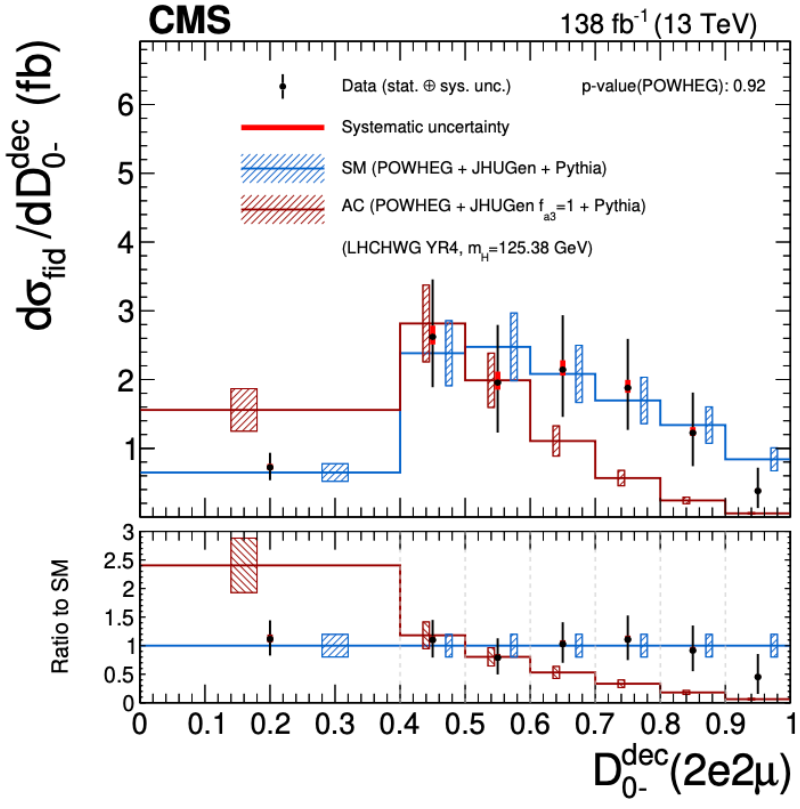

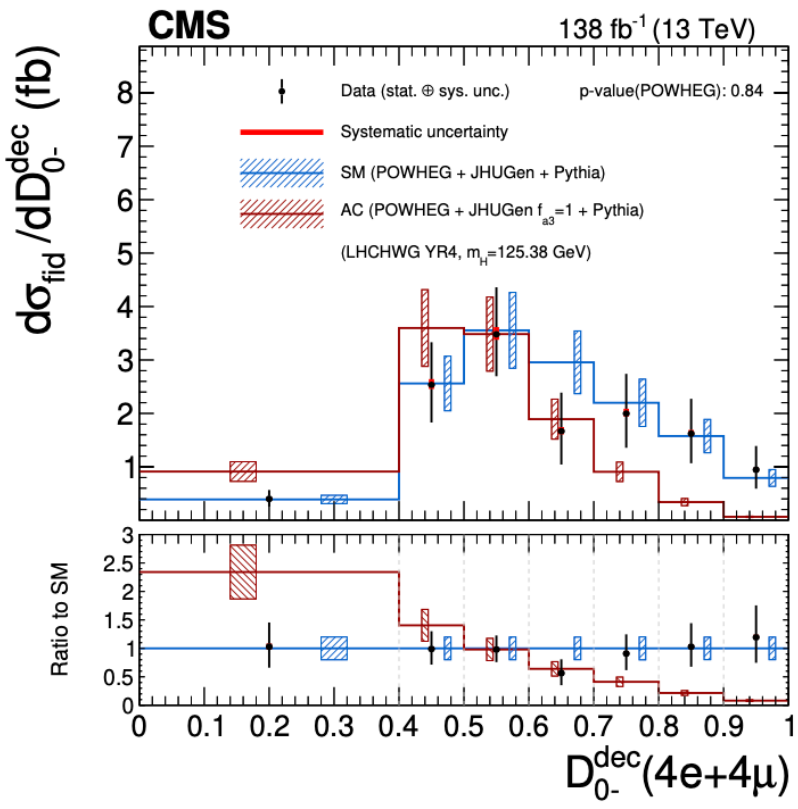

JHEP08(2023)040

1D differential cross section measurements

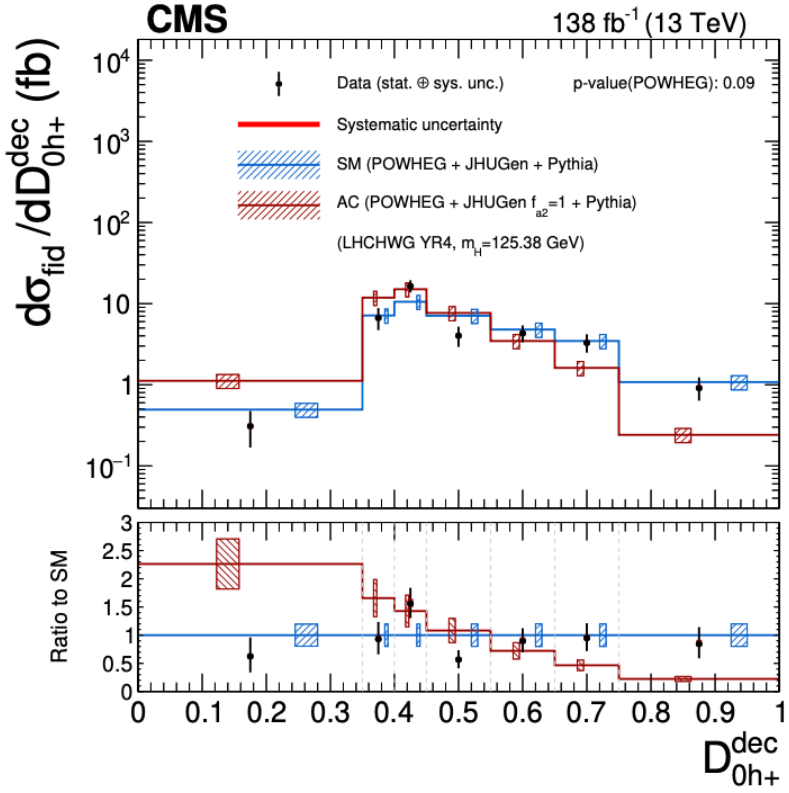

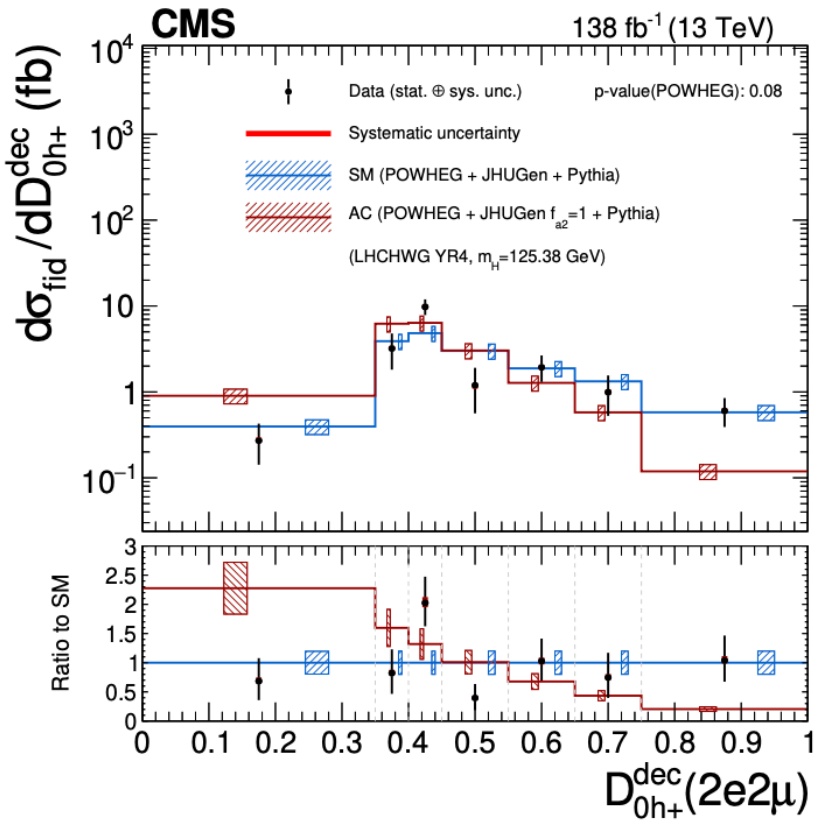

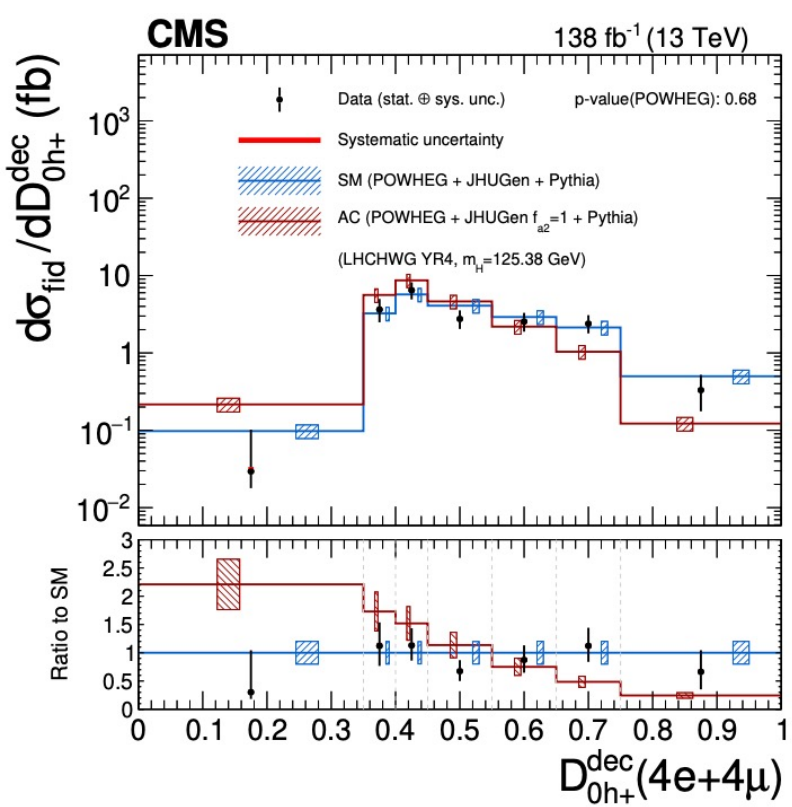

JHEP08(2023)040

1D differential cross section measurements

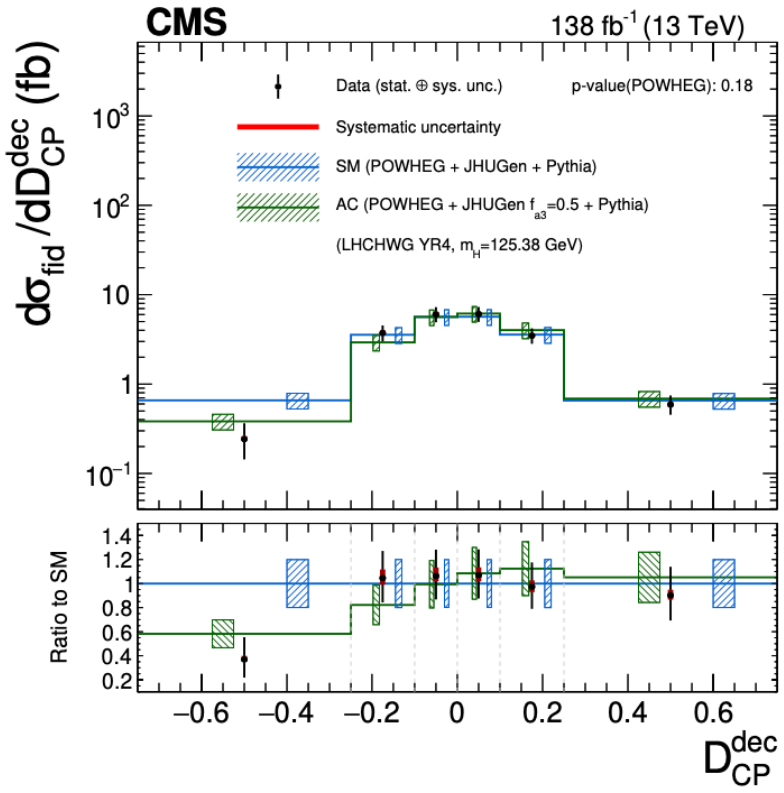

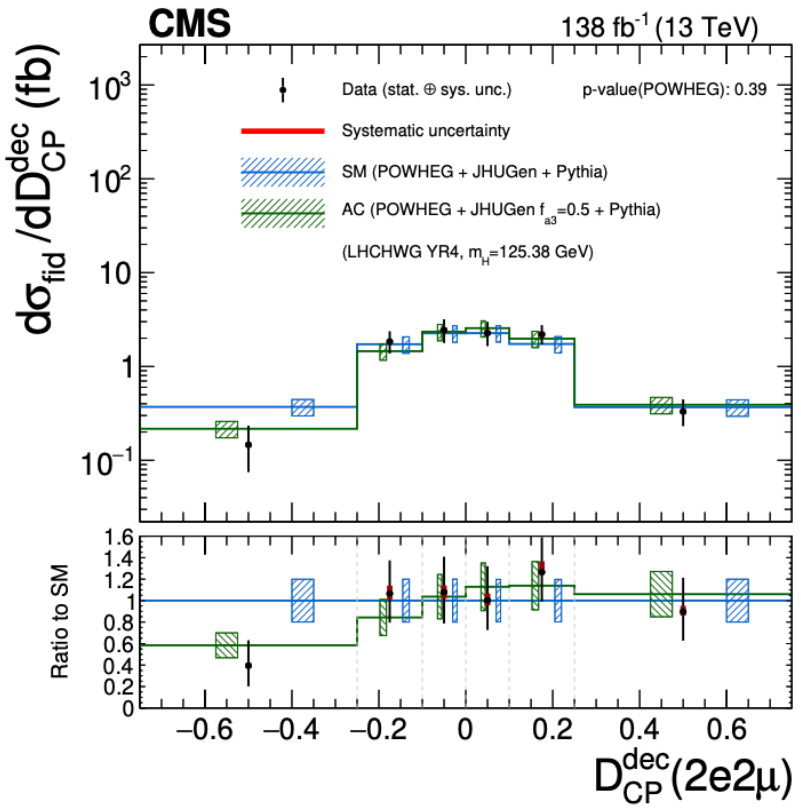

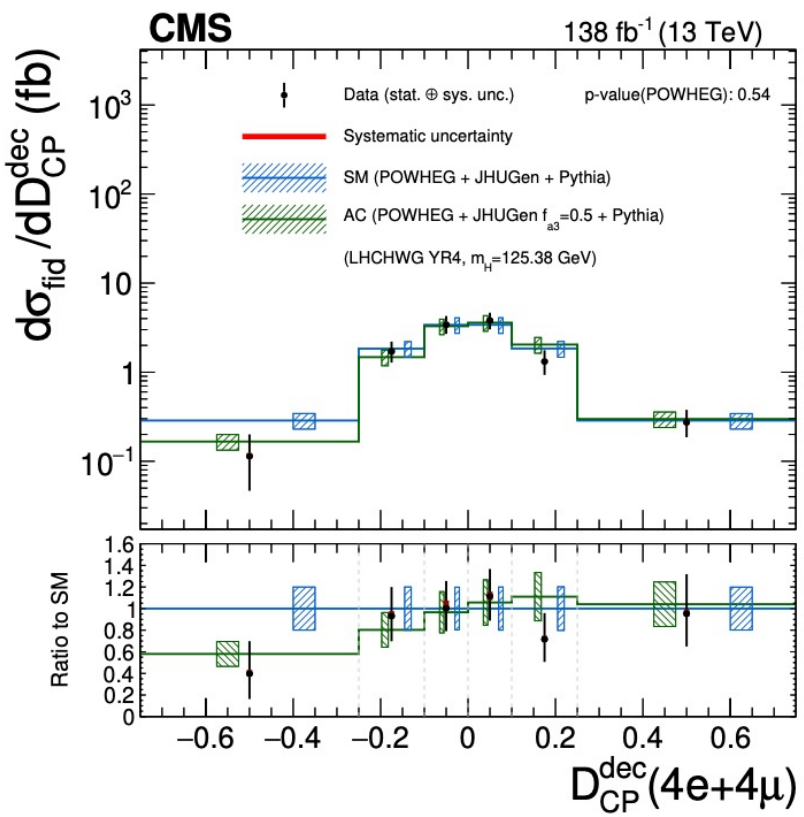

JHEP08(2023)040

1D differential cross section measurements

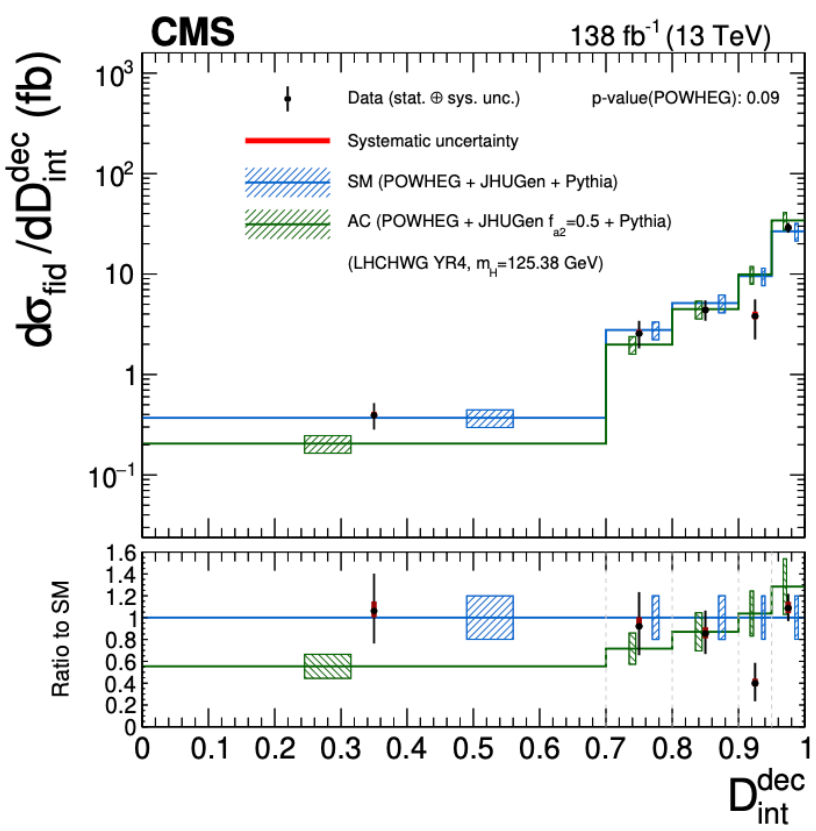

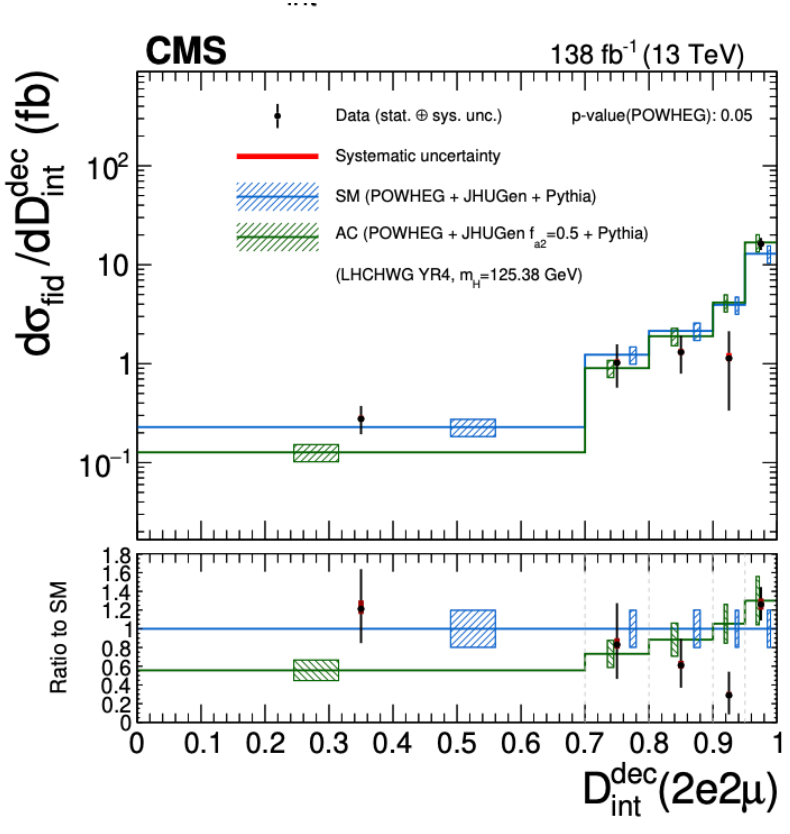

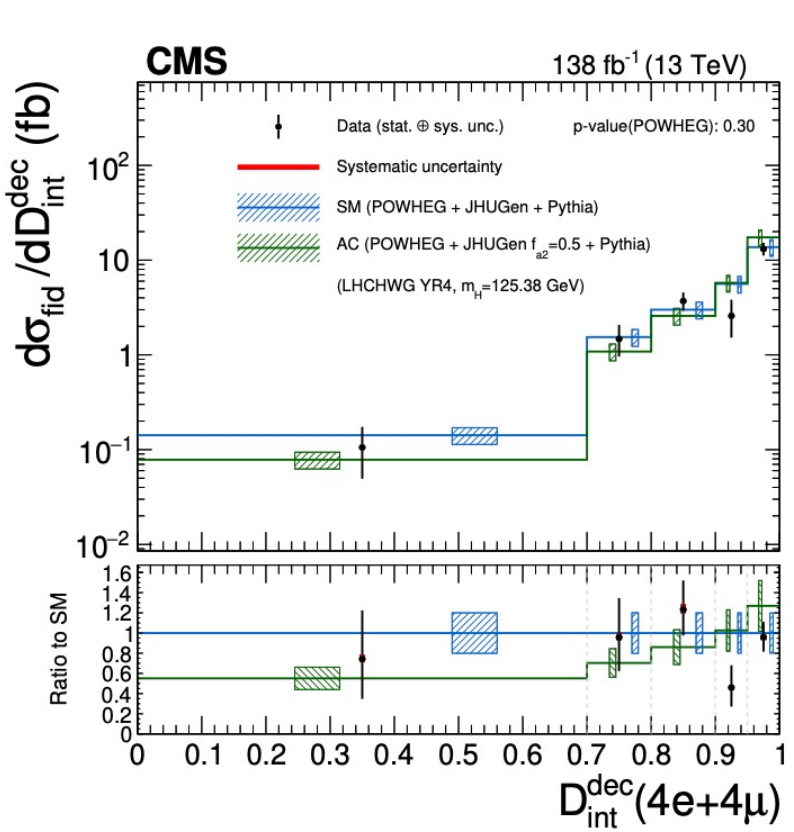

JHEP08(2023)040

1D differential cross section measurements

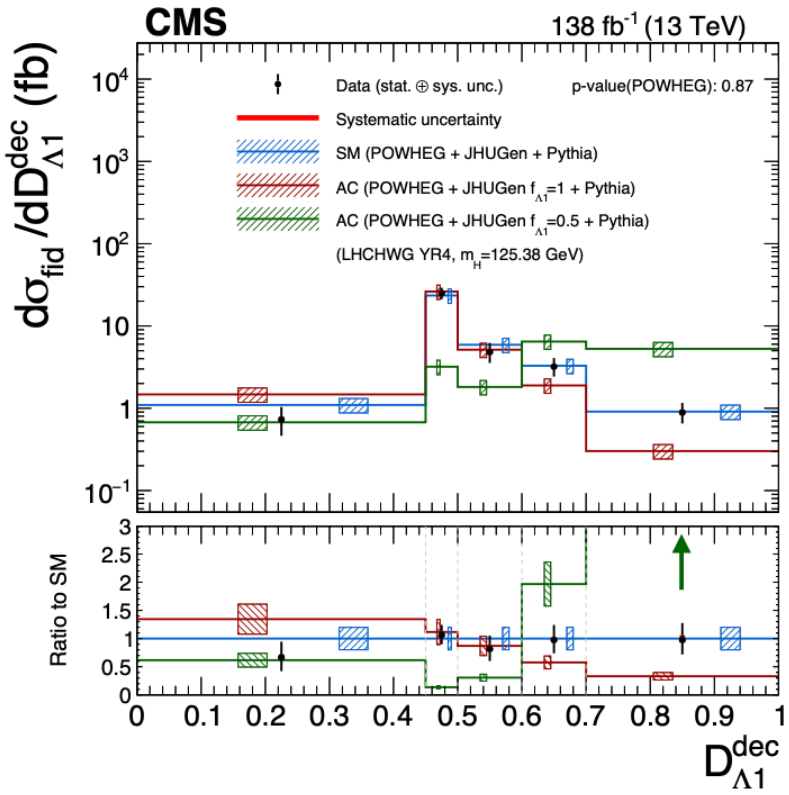

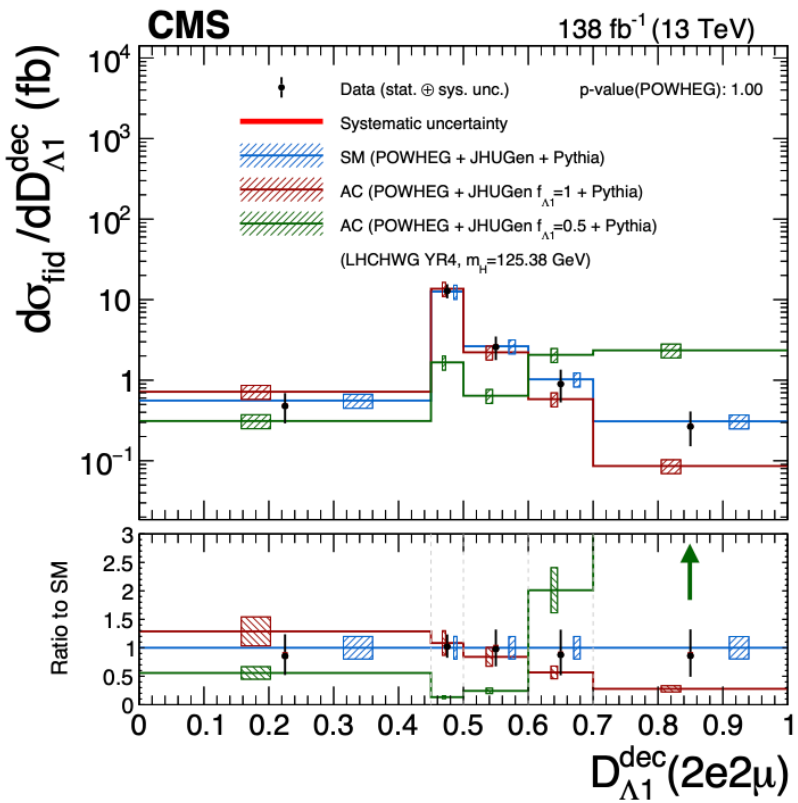

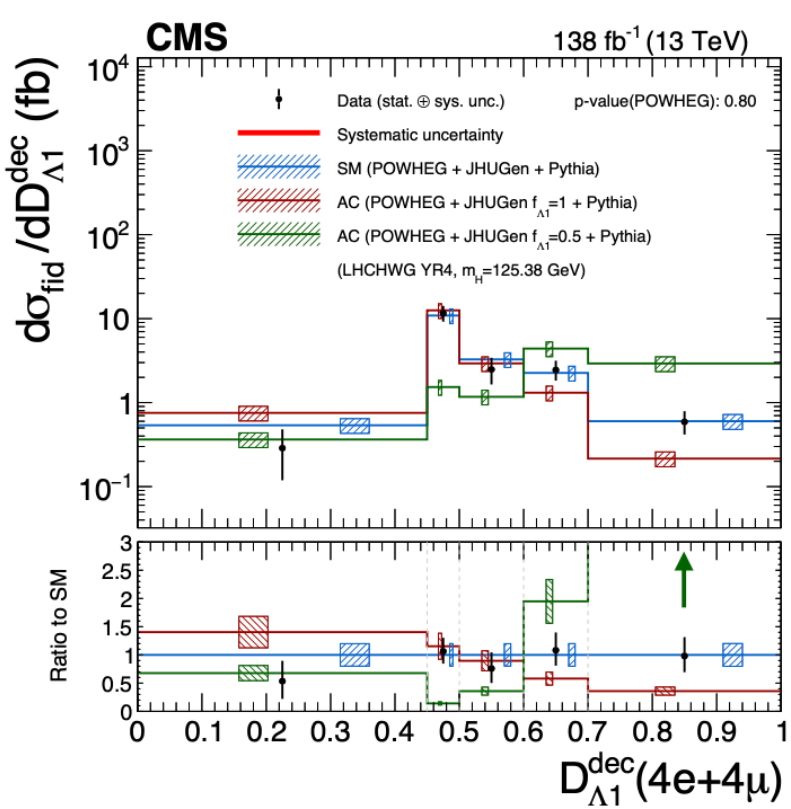

JHEP08(2023)040

1D differential cross section measurements

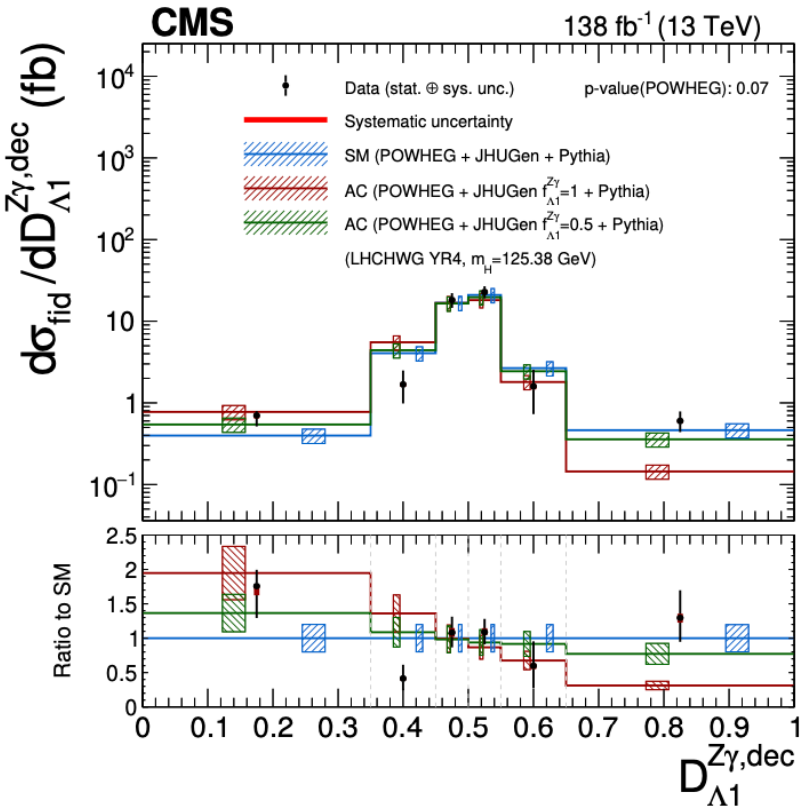

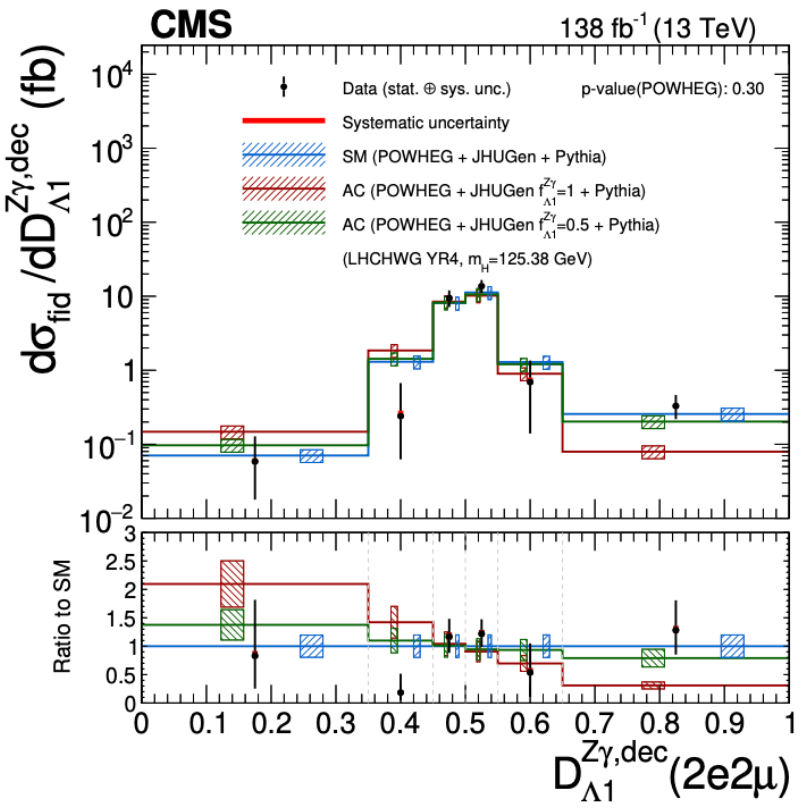

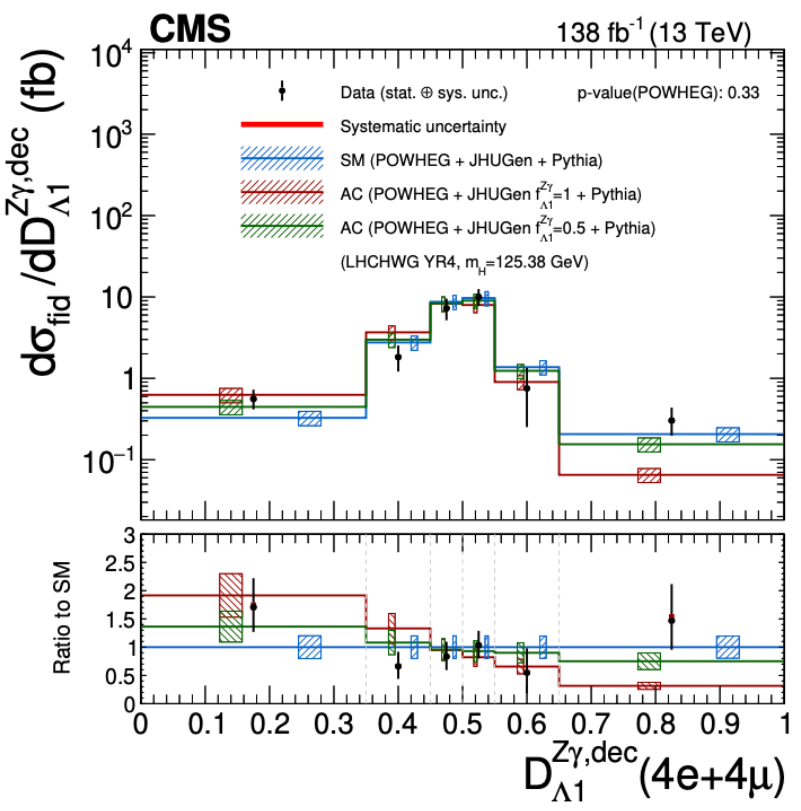

JHEP08(2023)040

1D differential cross section measurements

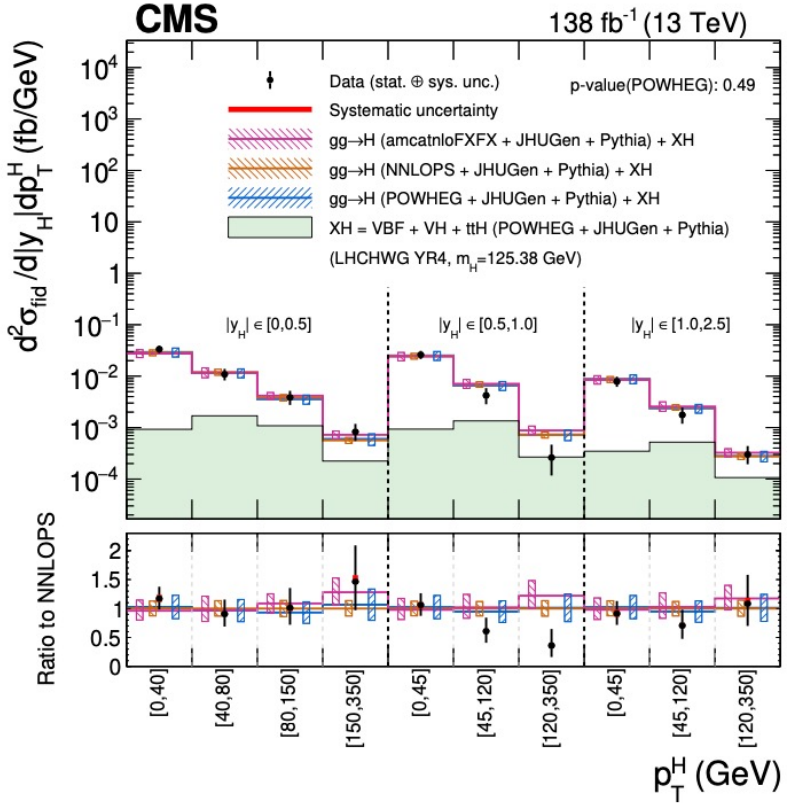

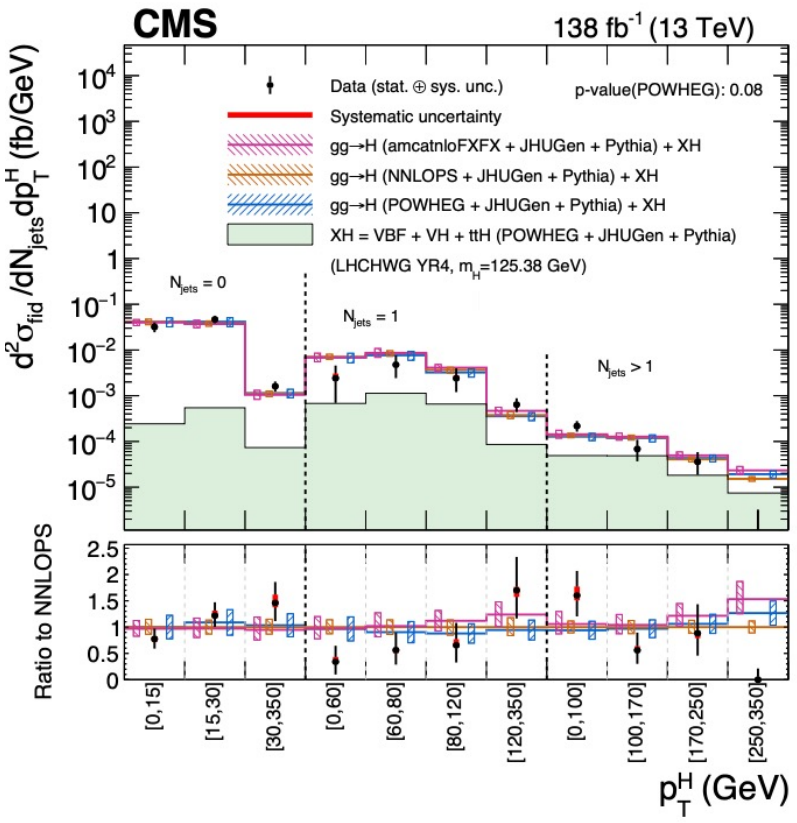

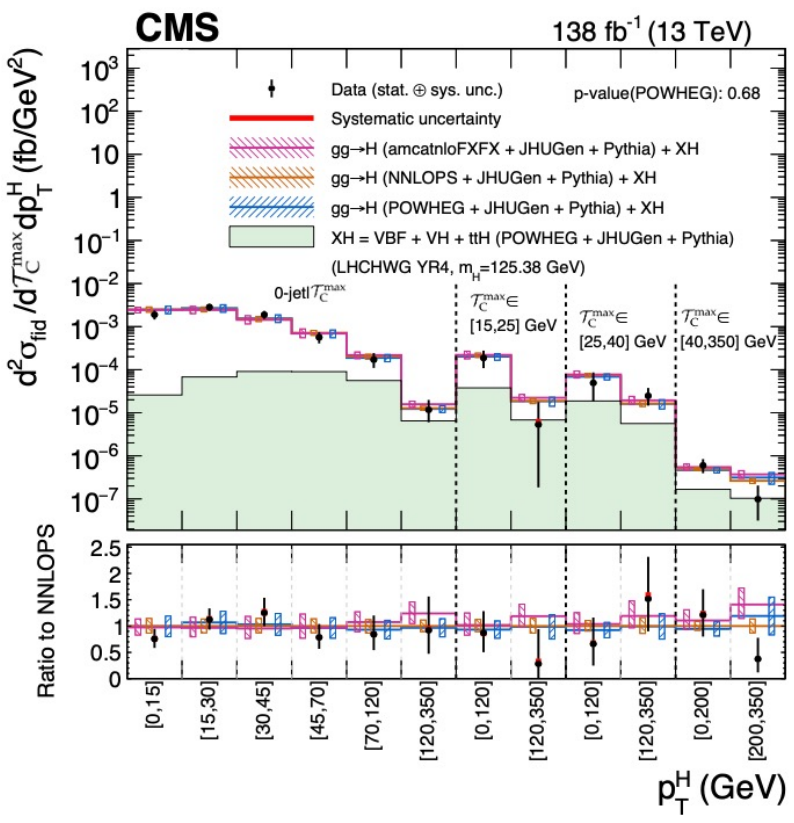

JHEP08(2023)040

1D differential cross section measurements

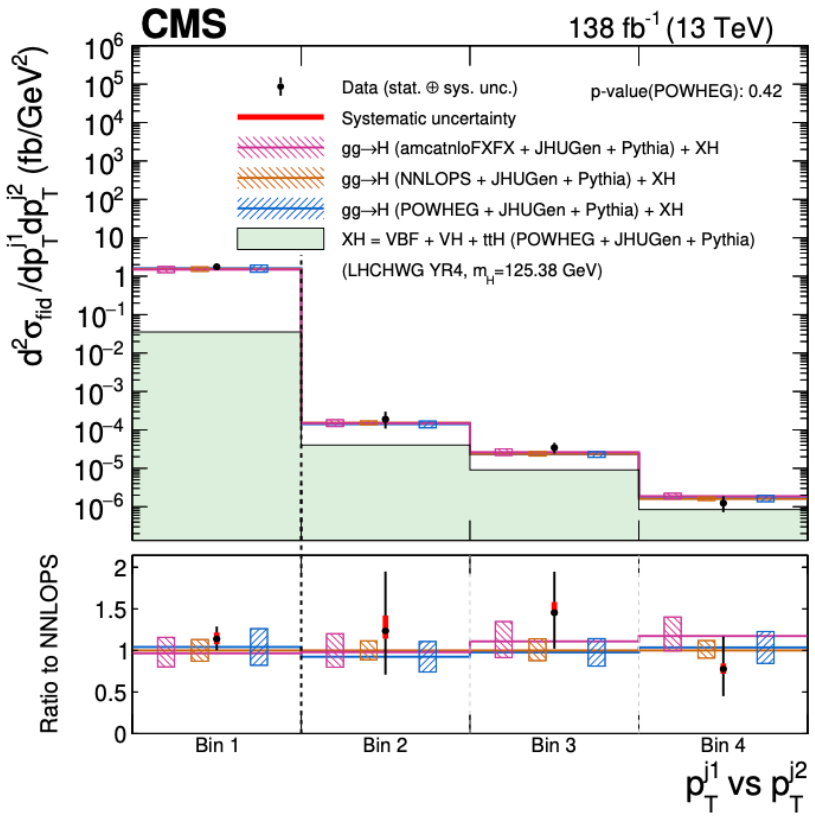

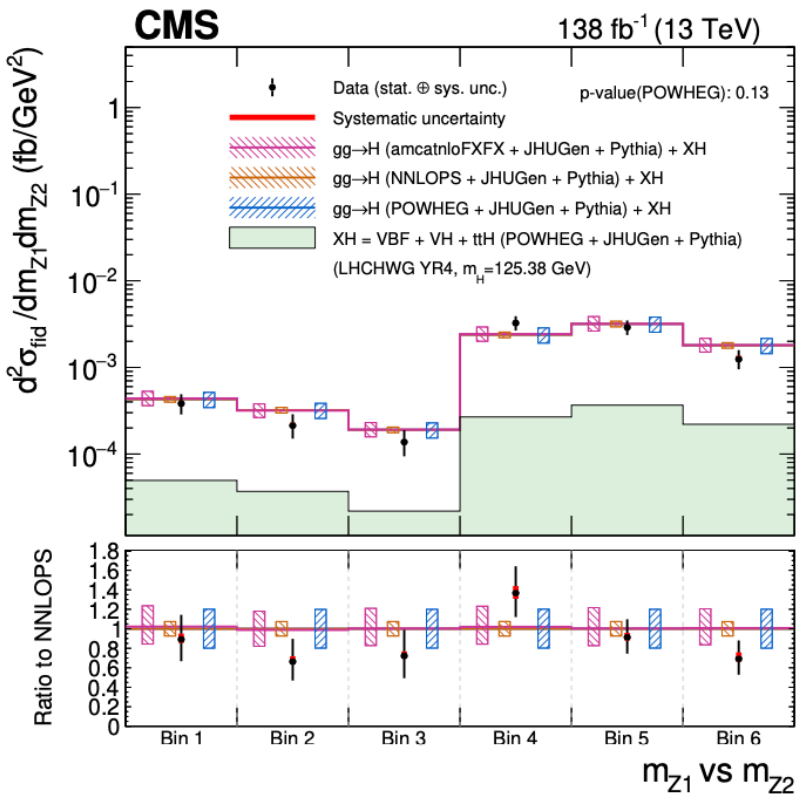

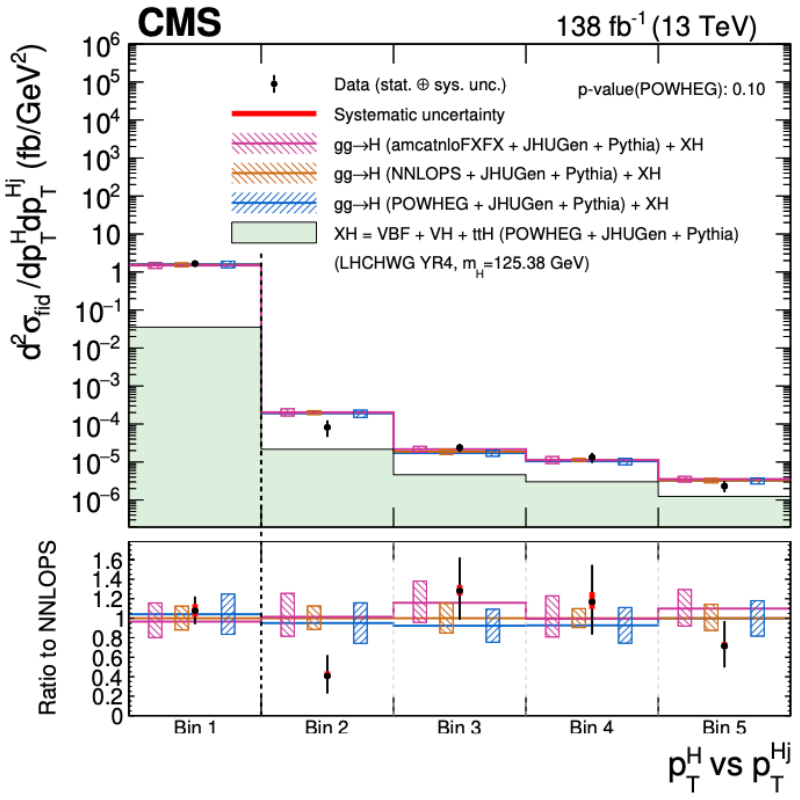

JHEP08(2023)040

RMS method used in electron efficiency measurement

- 4 variables (altSig, altBkg, altMC, altTag)
- choosing the nominal setting to be central value

- The standard way of calculating systematic uncertainty in the Egamma TnP efficiency measurements is done by summing in quadrature 4 variations of the nominal setting.
- The main difference coming from the RMS approach is that we treat all the alternative measurements as variations of the same measurement with equal importance.
- Advantage of RMS method:
  - Sensitive to outliers
  - by adding alternative measurements we increase systematical uncertainty
- The improvement is visible in the reduction of the low pt uncertainty with the RMS approach.

Introduction – Constrains of k_b, k_c

- Precise measurements of Higgs couplings play an important role since the couplings of Higgs boson are sensitive to BSM.
- The couplings to top and bottom are fairly precise while the coupling to charm is measured with large uncertainty.
- ***Direct*** measurement of y_c via:
  - $H \to J/\psi\gamma$ channel is hard due to small signal rate and large continuous background
  - $pp \to W/ZH(H \to c\bar{c})$ and $pp \to Hc$ is dependent of c-tagging performance
- ***Indirect*** method:
  - Interpretation of P_H^T in terms of Higgs boson coupling of light quarks is exploited. Perform the scan of modification $k_c = \frac{y_c}{y_c^{SM}}$ and check its relative formula with P_H^T distribution.

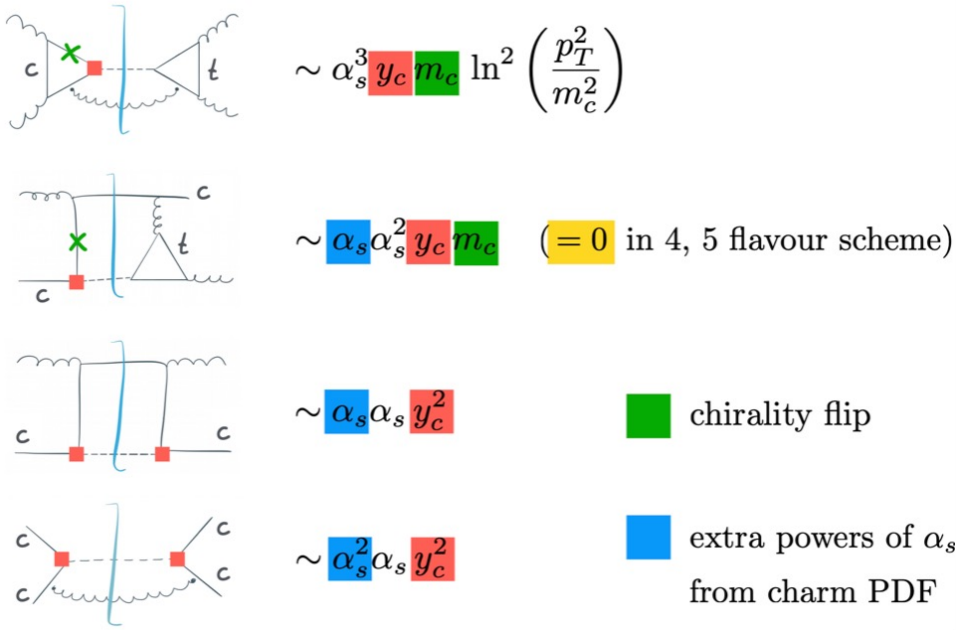

Arxiv: 1606.09253

https://indico.cern.ch/event/783304/contributions/3497890/attachments/1913786/3163217/HC2NP19_Haisch.pdf

Constraints on Higgs boson couplings modifier

Probing k_b, k_c via p_T^H differential cross section

- Interpretation of p_H^T ⇨ extract limits of Higgs boson coupling of light quarks

- Described in κ – framework
  - Coupling modifiers expressed as $\kappa_c = y_c / y_c^{SM}$
  - Scan of modification κ_c
  - Check its relative formula with P_H^T distribution

- The theory predication combined of 2 method
  - Loop-induced ggF production -- Radish
  - Quark-initiated production of Higgs

    -- MadGraph5_aMC@NLO

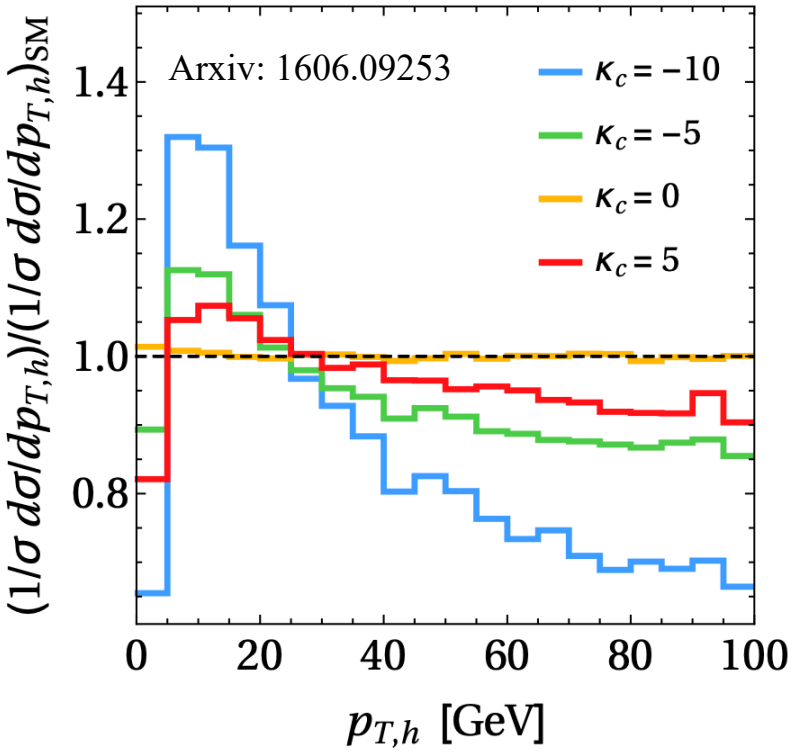

Parameterization of κ_b, κ_c

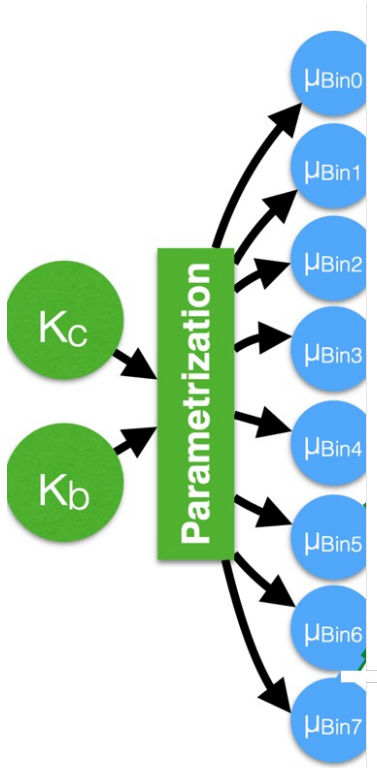

- Obtain 2D likelihood by varying kc and kb: $\vec{\Delta\sigma} \rightarrow \vec{\Delta\sigma}\,(\kappa_b, \kappa_c)$
- Signal model split into ggH and xH processes and the contributions from xH (not ggH) are set to SM
- We assume a parabolic function for the cross section

$$\sigma_{ggH} = \left|\sum_i A_i \kappa_i\right|^2 = A\kappa_b^2 + B\kappa_c^2 + C\kappa_t^2 + D\kappa_b\kappa_c + E\kappa_b\kappa_t + F\kappa_c\kappa_t$$

- Find the cross section for any set of the κ's if we know the coefficients A, …, F
- Use 6 known points: $\sigma_1(\vec{\kappa_1}), \sigma_2(\vec{\kappa_2}), \sigma_3(\vec{\kappa_3}), \sigma_4(\vec{\kappa_4}), \sigma_5(\vec{\kappa_5}), \sigma_6(\vec{\kappa_6})$
- Find values of the coefficients by simple matrix inversion
- κ_t set to 1.0 (SM) for the κ_b, κ_c analysis

$$\begin{bmatrix} \sigma_1 \\ \sigma_2 \\ \sigma_3 \\ \sigma_4 \\ \sigma_5 \\ \sigma_6 \end{bmatrix} = \begin{bmatrix} \kappa_{b,1}^2 & \kappa_{c,1}^2 & \kappa_{t,1}^2 & \kappa_{b,1}\kappa_{c,1} & \kappa_{b,1}\kappa_{t,1} & \kappa_{c,1}\kappa_{t,1} \\ \kappa_{b,2}^2 & \kappa_{c,2}^2 & \kappa_{t,2}^2 & \kappa_{b,2}\kappa_{c,2} & \kappa_{b,2}\kappa_{t,2} & \kappa_{c,2}\kappa_{t,2} \\ \kappa_{b,3}^2 & \kappa_{c,3}^2 & \kappa_{t,3}^2 & \kappa_{b,3}\kappa_{c,3} & \kappa_{b,3}\kappa_{t,3} & \kappa_{c,3}\kappa_{t,3} \\ \kappa_{b,4}^2 & \kappa_{c,4}^2 & \kappa_{t,4}^2 & \kappa_{b,4}\kappa_{c,4} & \kappa_{b,4}\kappa_{t,4} & \kappa_{c,4}\kappa_{t,4} \\ \kappa_{b,5}^2 & \kappa_{c,5}^2 & \kappa_{t,5}^2 & \kappa_{b,5}\kappa_{c,5} & \kappa_{b,5}\kappa_{t,5} & \kappa_{c,5}\kappa_{t,5} \\ \kappa_{b,6}^2 & \kappa_{c,6}^2 & \kappa_{t,6}^2 & \kappa_{b,6}\kappa_{c,6} & \kappa_{b,6}\kappa_{t,6} & \kappa_{c,6}\kappa_{t,6} \end{bmatrix} \begin{bmatrix} A \\ B \\ C \\ D \\ E \\ F \end{bmatrix}$$

Statistical analysis of κ_b, κ_c

- An extended likelihood function is reconstructed by

$$\mathcal{L}(\vec{\Delta\sigma}|\vec{\theta}) = \prod_{i=1}^{n_{bins}^{reco}} \prod_{k=1}^{n_{cat}} \prod_{l=1}^{n_{\mathcal{O}}} (pdf_i^k(\mathcal{O}_l|\vec{\Delta\sigma},\vec{\theta}))^{N_{obs}^{ikl}} \times Poisson(N_{obs}^{ik}|n_i^{sig,k}(\vec{\Delta\sigma}|\vec{\theta}) + n_i^{bkg,k}(\vec{\theta})) \times pdf(\vec{\theta})$$

- n_{bins}^{reco} is the number of reconstructed bins, n_{cat} is the number of categories for decay channel, and $n_{\mathcal{O}}$ is the number of bins for observable $\mathcal{O}$
- $pdf_i^k\left(\mathcal{O}_l|\vec{\Delta\sigma},\vec{\theta}\right)$ describes the probability to find an event measuring observable $\mathcal{O}$ in reconstructed bin i.
- An overall probability distribution function for the observable $\mathcal{O}$ is constructed by summation of the signal and background distributions of the observable.
- In the case of fitting κ , parameter cross section in terms of κ

$\vec{\Delta\sigma} \rightarrow \vec{\Delta\sigma}\,(\kappa_b, \kappa_c)$

Two methods applied in the constrain of κ_b κ_c

- Results vary strongly depending on the assumption of the **branching ratios**.
- **Overall discrimination** power
  - **Shape**
  - **Normalization**
- ***The branching ratios depend on the couplings***
  - Maximum amount of discrimination power
  - Normalization
    - Expected **Cross section**
    - **Branching ratios** scaled with coupling modifications
    - Constrain by the **Higgs decay width**.
- ***Freely floating branching ratios***
  - Normalization of parametrization and coupling dependence of BRs are **eliminated**
  - **Purely the constraints from only the shape**.